NORTHWESTERN UNIVERSITY

Polyvalent Oligonucleotide Gold Nanoparticle Conjugates: Versatile Nanostructures for Biodetection and Chemically Programmable Assembly

A DISSERTATION

SUBMITTED TO THE GRADUATE SCHOOL
IN PARTIAL FULFILLMENT OF THE REQUIREMENTS

for the degree

DOCTOR OF PHILOSOPHY

Field of Chemistry

By

Haley Diana Hill

EVANSTON, ILLINOIS

December 2008

ABSTRACT

Polyvalent Oligonucleotide Gold Nanoparticle Conjugates:

Versatile Nanostructures for Biodetection and Chemically Programmable and Assembly

Haley Diana Hill

Polyvalent oligonucleotide functionalized gold nanoparticle conjugates (DNA-AuNPs) possess unusual properties, which derive from their particle and oligonucleotide subunits as well as their three-dimensional architectures. This dissertation explores the role each chemical component plays in the conjugate's architecture and assembly and recognition capabilities. It also describes their application as probes in novel biodetection assays.

In chapter two, the relationship between AuNP radius of curvature and oligonucleotide packing is investigated. Mathematic relationships are developed, which can predict oligonucleotide loading on anisotropic gold nanomaterials. Additionally, as the AuNPs approach 100 nm in diameter, their loading capacities begin to mimic that of a macroscopically flat surface.

In chapter three, the ability of DNA bases to frame shift or 'slip' when attached to a curved gold nanoparticle surface is shown. This suggests that nucleotide bases, when attached to gold nanoparticles, adapt to form the strongest hybridization arrangements available to them based on their local geometry. This contributes to the increased melting temperature observed for hybridized DNA-AuNPs as compared to free duplex DNA. Consistent with this conclusion, slipping interactions are not observed with DNA-functionalized flat gold nanoprisms.

In chapter four, the role duplex DNA plays in modulating the unit cell parameters of highly ordered face-centered-cubic crystal lattices of DNA-AuNPs is investigated. Nanoparticle

spacing increases linearly with DNA length, yielding maximum unit cell parameters of 77 nm and 0.52 % inorganic-filled space.

In chapter five, the development of a novel oligo-AuNP probe that can be used in the bio-barcode assay is reported. This quantitative assay relies on chemical liberation of adsorbed thiolated oligonucleotides from AuNP surfaces with dithiothreitol yielding a 7 aM assay limit of detection.

In chapter six, a way of using the bar code assay to detect bacterial genomic DNA is reported. A critical step in the assay involves the use of blocking oligonucleotides which bind to specific regions of the target DNA and prevent the strands from re-hybridizing, thus allowing the particle probes to bind. The limit of detection for this assay was 2.5 fM, and the development of the assay represents an important step towards non-enzymatic detection of genomic DNA.

_____

Prof. Chad A. Mirkin

Thesis Advisor

ACKNOWLEDGEMENTS

I would like to acknowledge my advisor Professor Chad A. Mirkin for providing guidance, advice and support during my graduate career. I would also like to thank my committee members, Professor Fredrick Lewis and Professor Amy Rosenzweig for their thoughtful suggestions and constructive criticism throughout my time at Northwestern. Professor George Schatz, though not officially a committee member, has been exceptionally helpful in our discussions and I am exceeding grateful for his efforts. I would be remiss if I did not thank Dr. Sabine Sturm for all of her hard work, career and general life advice, as well as the thoughtfulness and mentoring that she has provided me. The members of the Mirkin group have been the steadfast team that has helped me in more ways than I can possibly list. I would specifically like to thank those Postdocs whose guidance was vital to my study: Dr. Dimitra Georganopoulou, Dr. Wei Wei, Dr. Savka Stoeva, Dr. Byeongdu Lee, Dr. Sungho Park, Dr. Dwight Seferos, Dr. Robert Elghanian, Dr. Jake Cizek, Dr. James Storhoff, Dr. Min Su Han and Dr. Monika Fishler. Those student colleagues whom I owe special thanks are: Dr. Sarah Hurst, Dr. Jill Millstone, Robert Macfarlane, David Giljohann, Dr. Jae-Seung Lee, Dr. Abigail Lytton-Jean, Dr. Chris Oliveri, Dr. Rafael Vega, Dr. C. Shad Thaxton, Matt Banholzer and Weston Daniel. I would also like to thank the Department of Homeland Security for the graduate fellowship which allowed me to pursue this degree.

Prior to my graduate studies, I was privileged to study under the direction of Dr. Michael Hill and Dr. W. Reef Hardy at Occidental College. Without their instruction and guidance I would not be the scientist that I am today. I am also greatly indebted to Dr. Donald Deardorff, Dr. Chris Craney, Dr. Mark Martin and Dr. Tetsuo Otsuki for their support and encouragement.

Additionally, I would like to thank the Beckman Foundation for providing me with my first research fellowship and for their continued support.

Finally I owe an exceptional amount of thanks to my parents, Debbie and Gary Hill. They have been an inspiration to me through their actions and have taught me tenacity, strength and creativity. My brother, 2nd Lt Richard Hill (USMC), has been a great sounding board and motivator, reminding me the school is just like work but with the difference that you get a degree at the end. I owe a great deal of thanks to my Grandparents: Papa, Richie, Grammy, Grandpa and Patu, who taught me the value of a hard day's work, how to fix almost anything and that you can overcome all hardships which come your way in life.

ABBREVIATIONS

Abbreviation	Expansion
DNA	Deoxyribonucleic Acid
RNA	Ribonucleic Acid
DTT	Dithiothreitol
BCA	Bio-Barcode Assay
AuNP	Gold Nanoparticle
Oligo	Oligonucleotide
PBS	Phosphate Buffered Saline
PCR	Polymerase Chain Reaction
ELISA	Enzyme Linked Immunosorbent Assay
A, T, C, G	Adenine, Thymine, Cytosine, Guanine
PEG	Polyethylene Glycol
OD	Optical Density
SDS	Sodium Dodecyl Sulfate
NHS	N-hydroxysuccinimide
RPM	Revolutions per Minute
SAXS	Small Angle X-Ray Scattering

GLOSSARY

Word	Definition
DNA	A polynucleotide having a specific sequence of deoxyribonucleotide units covalently joined through 3′, 5′-phosphodiester bonds. Serves as the carrier of genetic information.
RNA	A polyribonucleotide of a specific sequence linked through 3′, 5′-phosphodiester bonds. Serves as messenger between DNA and protein.
Nanoparticle	A particle that has at least one dimension less than 100 nanometers.
Scanometric	A chip based detection system for nucleic acids which uses the light scattering properties of silver-enhanced gold nanoparticle for readout.
DNase	An enzyme that specifically degrades DNA.
RNase	An enzyme that specifically degrades RNA.
Microbe	A single celled organism; generally bacteria or fungi.
Oligonucleotide	A short single strand of DNA, generally chemically synthesized.

METRIC PREFIXES AND SYMBOLS

Prefix:	Symbol:	Magnitude:	Meaning (multiply by):
Yotta-	Y	10^{24}	1 000 000 000 000 000 000 000 000
Zetta-	Z	10^{21}	1 000 000 000 000 000 000 000
Exa-	E	10^{18}	1 000 000 000 000 000 000
Peta-	P	10^{15}	1 000 000 000 000 000
Tera-	T	10^{12}	1 000 000 000 000
Giga-	G	10^{9}	1 000 000 000
Mega-	M	10^{6}	1 000 000
kilo-	k	10^{3}	1000
hecto-	h	10^{2}	100
deka-	da	10	10
-	-	-	-
deci-	d	10^{-1}	0.1
centi-	c	10^{-2}	0.01
milli-	m	10^{-3}	0.001
micro-	μ	10^{-6}	0.000 001
nano-	n	10^{-9}	0.000 000 001
pico-	p	10^{-12}	0.000 000 000 001
femto-	f	10^{-15}	0.000 000 000 000 001
atto-	a	10^{-18}	0.000 000 000 000 000 001
zepto-	z	10^{-21}	0.000 000 000 000 000 000 001
yocto-	y	10^{-24}	0.000 000 000 000 000 000 000 001

DEDICATION

This work is dedicated to my mother and father,

Debra and Gary

And my great uncle,

Richie

TABLE OF CONTENTS

NANOPARTICLE CURVATURE AND ANISOTROPIC LOADING PREDICTION

CHAPTER THREE

RADIUS OF CURVATURE INDUCED DNA BASE SLIPPAGE

LIST OF TABLES

LIST OF SCHEMES

LIST OF FIGURES

CHAPTER ONE

CHAPTER TWO

CHAPTER THREE

CHAPTER ONE

Introduction

Chapter 1: Introduction

1.1 Background

Gold is perhaps the most widely investigated element of the periodic table if one considers its prevalence beginning in ancient times and continuing into the modern day.[1] Although scientists have been fascinated with gold for millennia, the material is experiencing a renaissance in the early part of the 21st century as scientists are exploring the nanoscale properties of this ancient metal. The field of nanoscience involves the study of objects that have at least one dimension which is less than 100 nm (1 nm is 1 x 10^{-9} meters). Gold nanoparticles are of particular interest as they are the most stable metal nanoparticles and possess a host of interesting chemical and physical properties. This introduction will cover a brief history of gold colloids, their synthesis, unique optical and chemical properties and will introduce the field of oligonucleotide functionalized gold nanoparticles (DNA-AuNPs).

1.1.1 The History of Gold Colloids

The production of bulk gold dates back to the 5th millennium B.C. near current day Bulgaria. It would take an additional 4 millennia for the first indication that "soluble" gold could be produced, which is thought to have first been created between the 5th and 4th Century B.C. in Egypt and China.[1] 'Soluble gold' as it was first known is deep red in color and can be stable indefinitely. In fact, the oldest artifact to demonstrate the presence, stability and use of finely subdivided gold comes from the ancient Romans where it was used to color artwork. The Lycurgus Cup, dated to the late 4th Century A.D. is the only complete ancient example in existence of a type of glass categorized as dichroic, meaning to change color in the light.[2] When light shines on this unique cup from the outside, it appears as opaque green in color due to the

scattering of small gold and silver particles embedded in the glass (Figure 1.1A). However, when illuminated from within, the Lycurgus Cup appears red to the observer, as the metallic particles absorb the visible light and the transmitted light is red (Figure 1.1B). The Romans may have been the first to use such finely subdivided gold (also known as sols) to add color and beauty to glass, but they were by no means the last. As Europe emerged from the dark ages, a revival in the art of colored glass making occurred. Craftsmen, by incorporating a variety of metal salts (copper to produce green colors, cobalt for blue and gold for red), created some of the world's most beautiful stained glass pieces. The three large windows in the Notre Dame cathedral in Paris are a prime example of glasses made in the 13th Century using metal nanoparticles to color the panes (Figure 1.2). In the 16th Century, Paracelsus created what he called *Aurum Potabile* or Potable Gold which he

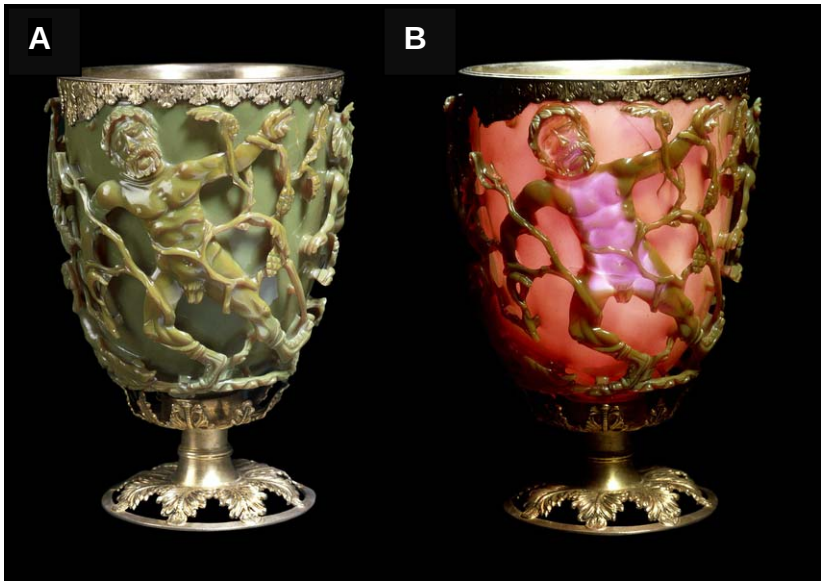

Figure 1.1 The Lycurgus Cup (4th Century A.D. Roman) A) Shows the cup being lit from the outside. B) Shows the cup being lit internally. Reproduced with permission from the British Museum, © Trustees of the British Museum. All rights reserved.

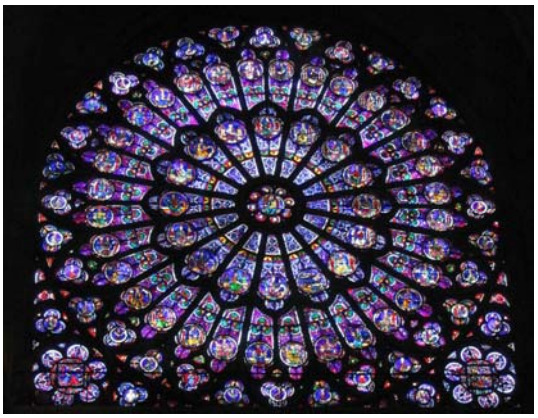

Figure 1.2 The South Rose Window, Notre-Dame Cathedral Paris France. Image courtesy of Richard B. Hill. All rights reserved.

claimed had curative properties.[3] Around that same, time many works were published which enumerated the various curative properties of gold sols, ranging from the treatment of dysentery, epilepsy, tumors and even heart problems.[4,5] Still, it was not until the 1850's that a scientist, Michael Faraday, finally synthesized the first pure sample of colloidal gold from chloroaurate ($AuCl_4^-$) and phosphorus.[6] Faraday also proposed that the intense red color was a direct result of the exceedingly small size of the gold pieces. Additionally, Faraday investigated their unique optical properties by drying them on slides and observing various color changes. Shortly thereafter the term colloid was coined by T. Graham in 1861 which remains the most common modern term for such particles.[7]

1.1.2 The Synthesis of Gold Colloids

Though Michael Faraday developed the first laboratory based chemical synthesis of gold colloids (white phosphorus in diethyl ether combined with $AuCl_4^-$ in water with KOH) he was by far the last. Many other have developed different synthetic routes for generating these interesting materials and by the mid 1950's no less than 10 different synthetic routes had been developed.[8] An electrochemical method using two wires a basic solution of gold salts was pioneered by Bredig in 1898 and generated 3 to 10 nm AuNPs.[9] More commonly used to make gold colloids than the electrochemical reduction methods are the chemical reducing agent such as acetone,[10] tannin, [11, 12, 13] hydroxyl amine,[14] carbon monoxide,[15] acetylene,[8] oxalic acid,[8] citric acid and sodium citrate.[16] These reactions generate gold nanoparticles with sizes that fall between 15 to 200 nm and generally have an average standard deviation around 40%.[8] Emerging from this vast group of techniques as the most widely used method was one pioneered by John Turkevitch and coworkers in 1951. The Turkevitch method uses sodium citrate and $AuCl_4^-$ in water yield very

stable and monodisperse solutions of gold colloids (20 ± 1.5 nm). A modification of this method published by Frens *et al*. in 1973 allows for the formation of particles ranging in size from 13 to 150 nm simply by systematically varying the ratios of reducing agent and gold precursor.[17]

The mechanism of gold nanoparticle formation was elucidated by the Turkevitch laboratory in the 1950's and involves the formation of Au (I) and the oxidation of citrate, (Figure 1.3). Initially the aqueous solution of Au (III) is brought to a vigorous reflux before the addition of sodium citrate. Sodium citrate reduces the Au (III) to Au (I) while itself being oxidized to acetone dicarboxylic acid, (Step 1, Scheme 1.1). This first step is by no means rapid takes approximately 30 seconds for between 10 and 20% of the Au (III) to be reduced to Au (I). However, once enough Au(I) has built up in the solution, a tridentate complex of gold ions form resulting in two Au(I) ions being reduced to Au° (Step 1, Scheme 1.1) and one Au(I) being oxidized back to Au(III) where it re-enters the reduction cycle (Step 3, Scheme 1.1). This process continues until all of the Au (III) has been reduced, at which point the remaining citrate in solution acts as a stabilizing agent for the newly formed particles. It is believed that the slow rate of this reaction allows for the formation of uniform

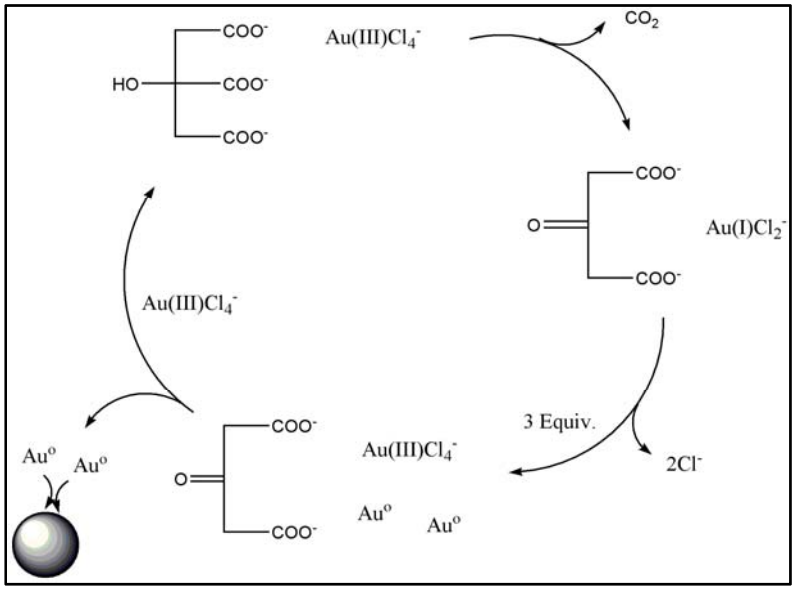

Scheme 1.1 Nanoparticle Synthesis via Citrate Reduction. This image explains the cyclic nature of the oxidation and reduction of Au (III) to form AuNPs via the Turkevitch method.

spherical particles, as stronger reducing agents ($NaBH_4$) produce particles that are more polydisperse. [8]

1.1.3 Optical Properties of Gold Colloids

The deep red color associated with AuNPs in water stems from the interaction of incident light with the surface plasmon band of the AuNPs; it is this interaction which results in a broad absorption in the visible spectrum. The spectrum has three main characteristics: one, a strong absorption band centered around 520 nm, two, a sharp decrease in intensity for particles less than 3 nm, and three, significant red shifting of the surface plasmon band for particles larger than 60 nm. The surface plasmon band or surface plasmon resonance (SPR) is due to the collective oscillation of the conduction band electrons confined to the nanoparticle surface and was explained by Mie in 1908.[18] The free electrons in the conduction band occupy the energy level just above the Fermi level and oscillate in dipole mode in the case of spherical gold nanoparticle. This surface plasmon band is affected by the proximity of AuNPs to each other such that as interparticle distance decreases the absorption band red shifts to longer wavelengths of electromagnetic radiation and the particles appear purple or blue to the observer. Additionally, the stabilizing ligands on the AuNP surface has an effect on the surface plasmon due to a change in the refractive index of the surrounding materials in much the same way that various solvents change the AuNP spectra.[1] This distance dependent change in the optical properties of AuNPs is utilized for investigations presented in chapters three and four.

1.2 Oligonucleotide-Functionalized Gold Nanoparticles (DNA-Au NPs)

DNA-AuNPs are a two-component system which use the AuNPs discussed above as a scaffold for the assembly of thiol-capped oligonucleotides. Oligonucleotides were first

covalently bound to gold nanoparticles using thiols in 1996 by members of the Mirkin laboratory at Northwestern University.[19] By replacing the citrate layer on the AuNP surface with DNA the negative charge needed to keep the particles separated is maintained while introducing many new properties. In order to synthesize these materials, thiol terminated oligonucleotides are added to the citrate stabilized gold colloids and allowed to form a self assembled monolayers overnight. Sodium chloride is then added in a stepwise manner helping to screen some of the charge carried by the oligonucleotides and allowing for the formation of dense oligonucleotide monolayer. These hybrid materials combine the optical features of the AuNPs with the bio-recognition capabilities of oligonucleotides, while producing additional properties unique to the conjugates. The simplicity with which oligonucleotides can be synthesized and modified has imparted a high degree of tailorability on the material. In the decade since their development, numerous research laboratories and companies interested in nanoscience have begun using this unique material for assembly, screening, sensing and therapeutic applications.

1.2.1 General Properties of DNA-AuNPs

In the years preceding the functionalization of AuNPs with oligonucleotides, they had been conjugated with other biomaterials such as antibodies and used for the detection of proteins, viruses and to localize organelles within animal cells using electron microscopy.[20-24] The renewed interest from researchers looking to use gold nanoparticles in biological applications stems from their numerous and versatile properties. AuNPs are easily functionalized,[1] possess catalytic activity,[31] have extended stability and environmental benignancy,[1] and can be routinely fabricated with a high degree of control over their sizes.[17] Importantly in biological applications, AuNPs (5 nm and larger) do not exhibit cytotoxicity like semiconductor (CdSe) nanoparticles

when used for intracellular applications.[25, 26, 27]

Oligonucleotides are of special interest to researchers due to their chemical tailorability, ease of synthesis (phosphoramidite chemistry), structural rigidity in duplex form, and recognition capabilities. Moreover, as AuNPs are exceedingly sensitive to local dielectric, the net negative charge of oligonucleotides (due to PO_4^- in the backbone) maintains the charge repulsion required to keep AuNPs dispersed in solution, resulting in versatile and stable hybrid bio-inorganic nanomaterials. In addition to the properties brought to the oligonucleotide gold nanoparticle conjugates by the components individually, the dense functionalization of the oligonucleotides on the nanoparticle surface imparts the material with new properties unique to the conjugates. For this reason, the term polyvalent oligonucleotide gold nanoparticle conjugates; (DNA-AuNPs) is used to describe the material.

In solution, monodisperse 13 nm DNA-AuNPs exhibit a characteristic red color with a relatively narrow surface plasmon absorption band centered at 520 nm in the UV-visible spectrum (Figure 1.3). In contrast, solutions containing assembled DNA-AuNPs appear purple in color, corresponding to a red shift in the SPR of the AuNPs to approximately 600 nm (Figure 1.3). This assembly can be induced by using DNA-AuNPs which are complementary to a target nucleic acid (Figure 1.3A). Systems have been designed such that, in the presence of a complementary DNA target, nanoparticle aggregation occurs resulting in a subsequence color change. This type of detection system is generally known as a colorimetric detection assay.[19] Moreover, this change of SPR of DNA-AuNPs is amplified when AuNPs are close to the noble metal surface film after the binding of a targeted analyte.[27, 28] This optical property can also be used for surface-based protein and DNA detection assays. With such great versatility, AuNPs

have been used by many researchers who have in turn increased the sensitivity of SPR-based bio-molecule sensing techniques used extensively for studying biomolecular interactions.[29-31]

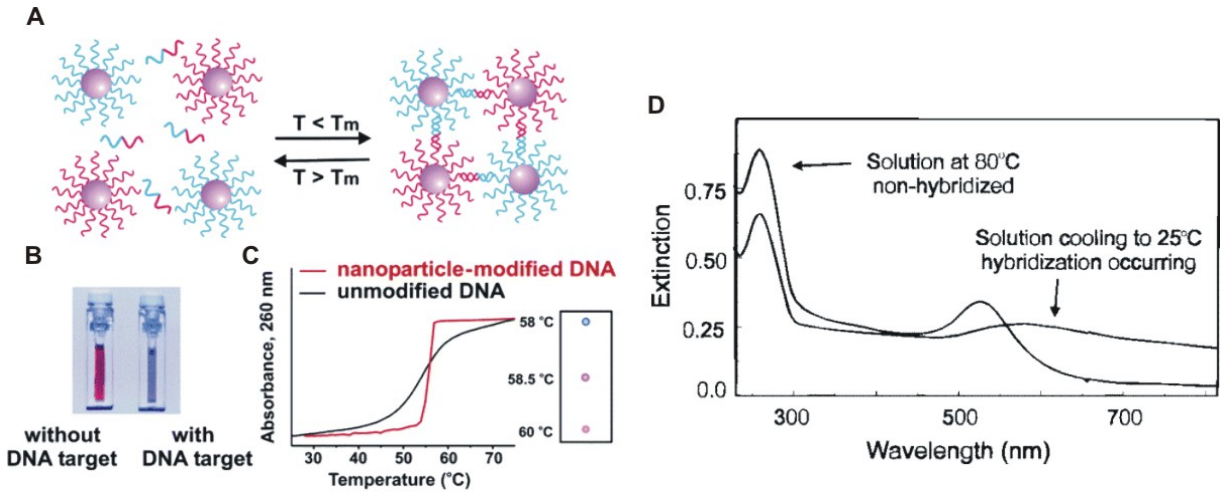

Figure 1.3 Optical Properties of DNA-Functionalized Gold Nanoparticles. A) Two types of DNA-AuNPs (a and b) are linked by a complementary DNA target strand (a′b′) and their assembly is temperature dependent. **B)** DNA-AuNPs with and without linking target. **C)** Thermal dehybridization profiles of DNA-gold nanoparticle aggregates exhibit substantially sharper melting transitions when compared to unmodified DNA as followed by UV-visible spectroscopy at 260 nm. **D)** Complete UV-visible spectra of DNA-AuNPs before melting (25 °C) and after dehybridization (80 °C). Reproduced with permission from the American Chemical Society, 2000, all rights reserved.

Additionally, the melting profiles for DNA-AuNPs are considerably sharper than for the same DNA strand free in solution, which is a result of the cooperative binding properties of the DNA-AuNPs (Figure 1.3C).

1.2.2 Binding Properties of DNA-AuNPs

Though the sharpened and elevated melting transitions for oligonucleotide functionalized gold nanoparticles had been known since the late 1990's, a thermodynamic investigation aimed at comparing the binding properties of these gold probes with those of free DNA in solution was only reported in 2005.[32] Experiments to elucidate the equilibrium binding constants for the two systems were obtained by measuring the increase in fluorescence as the DNA hybrids melted away from their complement attached to a quencher or gold nanoparticle (Figure 1.4). The work

showed that the oligonucleotide functionalized gold nanoparticle exhibited a two-fold increase in binding strength as compared to the same sequence in solution with a quencher.[32] It was also noted that utilizing a poly-$(dA)_{10}$ spacer was required for the enhanced binding, but that extending the spacer did not further enhance the equilibrium. Conversely, if the spacer was removed the increase in binding strength from the nanoparticle was lost. Additionally, it should be noted that the initial experiments were conducted with a 15 base pair (bp) sequence, but when the experiment was repeated using a 21 bp sequence the increase in binding strength was only one order of magnitude above that for the free DNA. The study concluded that when designing oligonucleotide probes for detection systems it was important to consider the length of the probe in relation to specificity and enhanced binding. This increase in effective binding constant gives the DNA-AuNP a selectivity advantage in a

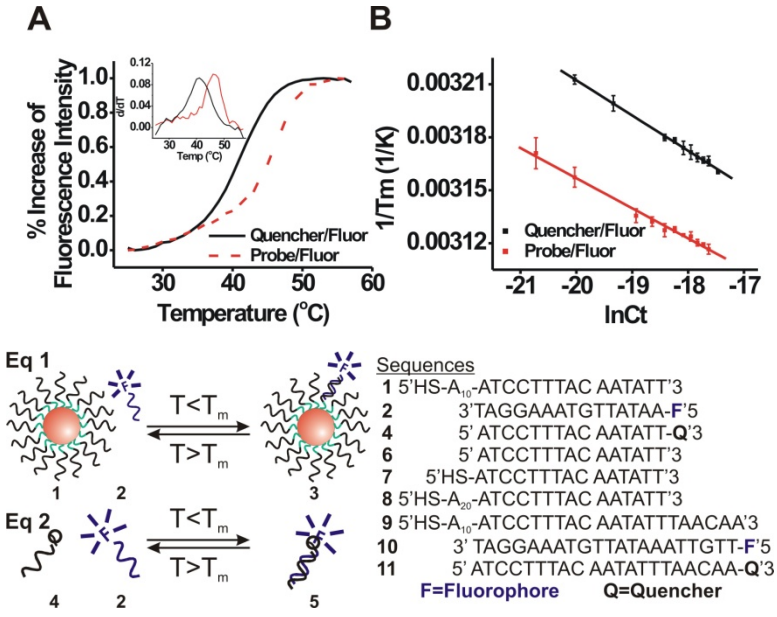

Figure 1.4 Experimental Scheme for Elucidating the Binding Constants for DNA-Au NPs versus their Counterparts in solution. **A)** Representative melting curves for the two duplex sets, as well as the first derivative of those melts [Concentration 3 nM]. **B)** Thermodynamic analysis of the concentration dependant melting data for the DNA-Au NPs versus the quencher/fluorophore pair. Eq. 1 shows the fluorescently labeled oligonucleotide binding to the gold nanoparticle, while Eq. 2 shows the fluorescently labeled oligonucleotide binding to the complementary strand with a quencher. Both systems effectively eliminate fluorescence when in the bound state. Reproduced with permission from the American Chemical Society, 2005, all rights reserved.

variety of applications ranging from bio-diagnostics to intracellular gene regulation.[20, 31]

Another study examined the thermodynamic effects of multiple duplex formations on an oligonucleotide functionalized gold nanoparticle.[33] These experiments utilized dynamic light scattering to look at the hydrodynamic radius formed by a 8 bp "sticky end" extending from the duplexes. Xu *et al.* found that as the number of duplexes formed on the particle surface increased, the individual stability of each duplex was lessened as compared to that of a free duplex in solution. This is not unexpected however, as the nanoparticles are densely functionalized and it stands to reason that when complementary strands hybridize they may have to overcome significant amount of steric repulsion. Furthermore, the research demonstrated that longer stands attached to the gold nanoparticle were destabilized faster than their shorter counterparts attached to the same size nanoparticle.[33]

1.3 DNA-AuNP Assembly and Crystallization

In 1996, when the concept of programmable materials synthesis from oligonucleotide nanoparticle conjugates was first introduced, a goal was to be able to use DNA to direct the three-dimensional assembly of nanoparticles into discrete preconceived structures.[19] Early demonstrations focused primarily on the formation of amorphous polymers, where rough

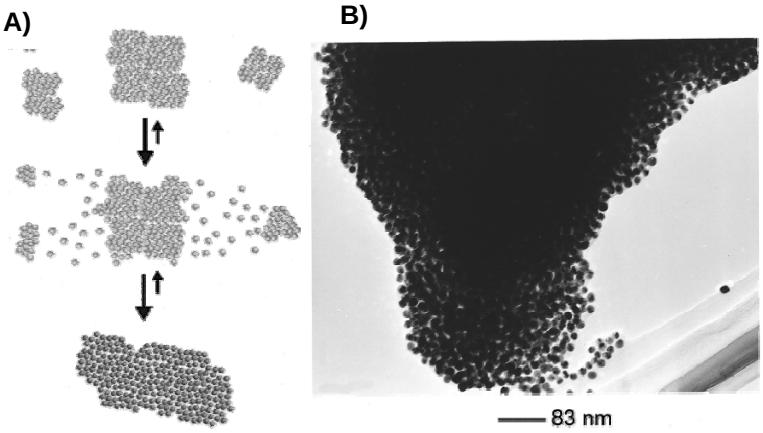

Figure 1.5 Early Attempts at Nanoparticle Crystallization. A) Model of aggregate formation is thought to begin with the formation of smaller aggregates which over time fuse to form larger organized structures. **B)** Transmission Electron Micrograph (TEM) of an assembled structure held together through DNA connections. Reproduced with permission from the American Chemical Society, 2001, all rights reserved.

placement and periodicity of the particles was controllable (Figure 1.5).[19, 35] Later advances showed that crystallization might be possible and suggested that it might be viable to form different crystal structures from one type of nanoparticle building block but different sequences of oligonculeotides.[36, 37] Recently, both our group and the Gang group independently discovered different but related routes for using DNA linkers to effect the crystallization of polyvalent oligonucleotide gold nanoparticle conjugates.[38, 39] Both groups have shown that with different

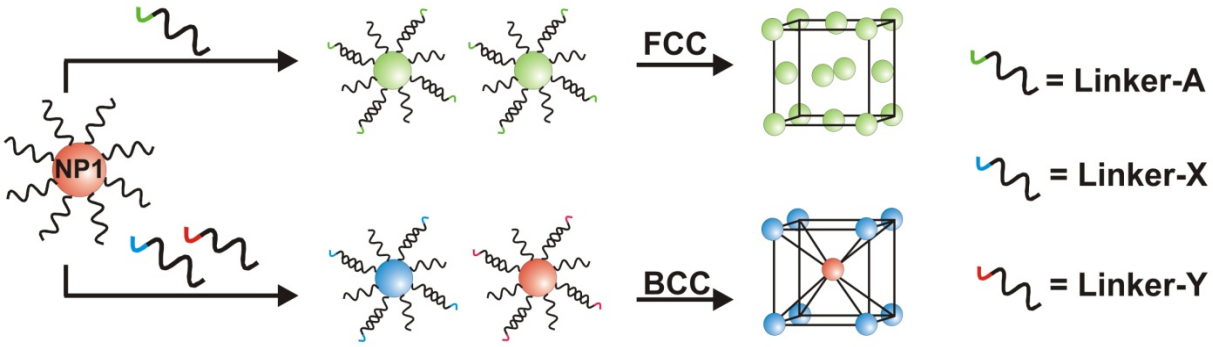

Figure 1.6 Synthetic Route to Forming FCC and BCC Gold Nanoparticle Crystals

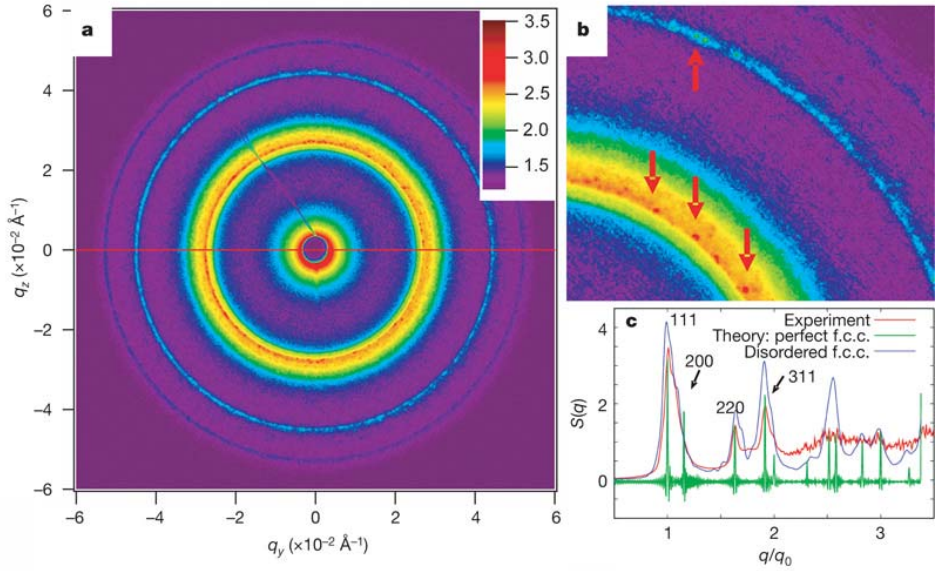

Figure 1.7 FCC DNA -AuNP crystals. A) 2D SAXS Image. **B)** Red arrows indicating scattering spots in the rings from crystals. **C)** Averaged 2D data comparing the crystal pattern formed to perfect FCC patterns and a modeled AuNP system confirms FCC structures. Reproduced with permission from the Nature Publishing Group, 2008, all rights reserved.

types of linkers, one can form either face-centered cubic (FCC) or body-

centered cubic (BCC) unit cells (Figure 1.6) with edge lengths as long as 38 nanometers (nm) and as little as 3% inorganic matter by volume (Figure 1.7).[38, 39] Chapters five and six will explore the versatility of oligonucleotides in controlling nanoparticle crystals.

1.4 DNA-AuNP Based Detection Assays

In addition to the structure directing capabilities of oligonucleotides attached to the AuNPs, they possess the ability to recognize targets and act as a signal transduction agent. The surface plasmon resonance and the enhanced binding properties of this hybrid nanomaterial make it versatile in a large number of assays. This section will cover the past applications of DNA-AuNPs to biological sensing and the sensing of complex genomic DNA detection will be covered in chapters seven and eight.

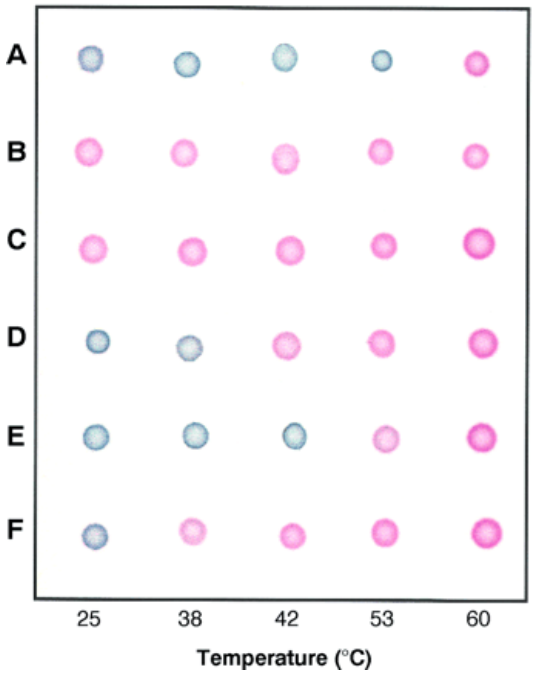

Figure 1.8 Selective Polynucleotide Detection for Target Probes A) complementary target B) no target C) complementary to one probe D) a 6 bp deletion E) a 1 bp mismatch F) a 2 bp mismatch. The sharp thermal dehybridization transitions for such probe aggregates allows for SNP detection. The 'Northwestern spot test' is shown in which samples of the aggregate mixture are spotted to a reverse-phase silica plate at a given temperature permanently recording the hybridization status. Reproduced with permission from the American Chemical Society, 2001, all rights reserved.

1.4.1 Homogeneous DNA Detection

The deep red color exhibited by gold nanoparticle sols in aqueous media shows a broad absorption in the visible range around 520 nm. In contrast, the effective shift of the plasmon band when the gold nanoparticles form aggregates, can result in shifts of 50 nm or more.[1] The use of DNA-

AuNPs has generated a large number of detection assays, which make use of the shift in the SPR between the monodisperse state and the aggregated states. These detection schemes are known as colorimetric detection methods. In 1997, Mirkin and co-workers reported the synthesis of DNA-AuNP probes for the colorimetric detection of complementary target sequences.[34] In a typical assay, single-stranded oligonucleotide targets were detected using DNA-AuNP probes. Two types of probes, each functionalized with DNA sequences complementary to one half of a given target sequence are mixed with the target strands resulting in particle aggregations of DNA-Au NPs with a concomitant red-to-purple color change. (Figure 1.3) This hybridization behavior affects the optical properties of the nanoparticles as discussed previously. Importantly, melting analyses of the hybridized particle aggregates showed sharp melting transitions [full width at half maximum (FWHM) as low as 1 ℃] while free DNA duplex shows very broad one. The fundamental of this sharp melting transition is explained by a cooperative mechanism that originates from the presence of heavily loaded multiple DNA linkages between each pair of DNA-AuNPs and a decrease in the aggregate melting temperature as DNA strands melt due to the concomitant reduction in local salt concentration.[40, 41] Transfer of the hybridization mixture to a reverse-phase silica plate resulted in a permanent and easily readable record of the hybridization state at any given temperature (Figure 1.8). Researchers later demonstrated that one could selectively detect target DNA sequences with single base imperfections, regardless of position, using DNA-AuNP probes oriented in a tail-to-tail arrangement.[41] Li and Rothberg have shown that Au NPs functionalized with non-thiolated oligonucleotides can also be used to detect oligonucleotides in solution[42] as well as PCR fragments.[43] These initial studies were very important because they revealed the versatility of DNA-AuNP and that they can be taken

advantage of for biomolecule detection assays.

Using DNA-AuNPs to detect complementary DNA targets was only the beginning of the colorimetric detection arena, as new colorimetric schemes using gold nanoparticle probes with oligonucleotides have been developed to detect metals, proteins, and small molecules. Furthermore, colorimetric sensing has been used to screen libraries of intercalating agents in a high throughput manner. Liu *et al* first used DNAzyme (catalytic DNA strand) functionalized gold nanoparticles to detect lead in a reverse colorimetric manner (blue to red).[44] The method works by first linking the particles together with the substrate strand and then adding the enzyme strand to form an aggregate system (Figure 1.9). The substrate strand has a ribose base near the stem loop formed by the enzyme strand, which in the presence of lead catalyzes the cleavage of the substrate strand, and the destruction of the aggregate. A similar methodology was used to detect adenosine.[45] Aptamer functionalized AuNPs have been used by Huang and coworkers to detect platelet-derived growth factors in the low nanomolar (nM) range.[46]

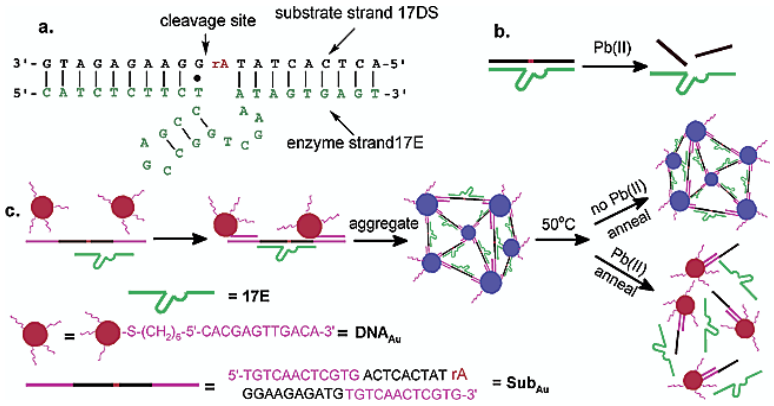

Figure 1.9 DNAzyme Based Colorimetric Pb Sensor A) Secondary structure of the DNAzyme system that consists of an enzyme strand and a substrate strand. Except for a ribonucleoside adenosine at the cleavage site (rA), all other nucleosides are deoxyribonucleosides. **B)** Cleavage of substrate strand by the enzyme strand in the presence of Pb (II). **C)** Schematics of DNAzyme-directed assembly of gold nanoparticles and their application as biosensors for metal ions such as Pb (II). In this system, the DNAzyme strand has been extended on both the 3' and 5' ends for 12 bases, which are complementary to the 12-mer DNA attached to the 13 nm Au NPs. Reproduced with permission from the American Chemical Society, 2005, all rights reserved.

Storhoff and coworkers used the distance dependant

relationship between gold nanoparticles to detect genomic DNA from the bacterium *Staphylococcus aureus.*[47] In the method the two sets of 50 nm particles were functionalized with different capture sequences that were spatially close to each other, so that when probe binding to the target occurred, a shift in the wavelength of the scattered light for the bound and unbound probes.

Recently Han *et al.* used a colorimetric screening method to investigate the binding affinities between DNA binding molecules and duplex DNA. Two sets of partially complementary DNA-AuNPs were prepared and mixed together to form aggregates. Then to separate aliquots of aggregates, DNA binding molecules were added and the DNA-Au NPs were put through a thermal analysis. It was seen that the molecules that bound to the duplex DNA stronger melted at a higher temperature.[48] The assay was able to see non-binders, weak binders, moderate binders, and strong binders. In general DNA-AuNPs have proven to be rapid and cost effect way to detect targets without the need of sophisticated equipment.

1.4.2 Heterogeneous DNA Detection Assays

Recently, major advances in genomic studies have been achieved using commercialized chip-based quantitative DNA assays known as “gene-chips” or “DNA-microarrays” originally developed by Brown and co-workers in 1995.[49] With such arrays, DNA labeling is typically carried out with organic fluorophore label. As will be pointed out later in this chapter, fluorophore labeling has several drawbacks, many of which can be overcome by using DNA-NP conjugate labels.

Currently numerous research groups have been utilizing AuNP probes for chip-based detection schemes. Keating and co-workers used Au NP probes to amplify changes in the SPR of

gold films during DNA hybridization to capture strands.[50] In addition, Genicon offers a commercially available DNA chip-based assay in which AuNPs functionalized with anti-biotin IgG are used to label biotinylated DNA targets of interest in chip-based format whereupon the light-scattering properties of Au NPs with different sizes and shapes are used as the readout.[51,52] Furthermore, Mirkin and co-workers demonstrated the direct labeling of DNA target strands using DNA-Au NP probes. In their work, a sandwich assay was devised such that DNA "capture" strands, replacing the probe stands from their homogeneous solution-based experiments, were covalently attached to the surface of a glass slide in microarray fashion. Subsequently, DNA target strands and complementary DNA-Au NP probes were added in a stepwise manner to the chip surface for hybridization (Figure 1.10). Since the Au NPs catalyze the reduction of silver ions to silver metal, a silver-developing solution was added onto the chip surface for amplification of probe signal and visualization of the surface bound capture-target-probe complex. Results visible to the naked eye could be recorded with a conventional flatbed scanner. As discussed below, light scattering can also be used as a readout mechanism, in some cases obviating the need for silver enhancement of surface immobilized DNA-Au NP probes.[31, 51, 52] The light-scattering method is more sensitive than the analogous fluorescence-based assay by a couple of orders of magnitude, but it is difficult to calibrate due to the background and

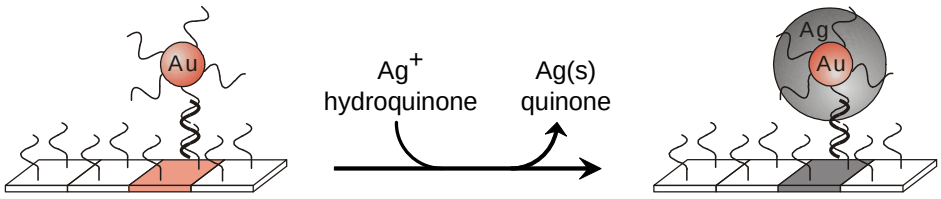

Figure 1.10 The Scanometric Method for DNA Detection

complexity of the scattering response. Indeed, the signal from nanoparticles and assemblies of nanoparticles on the detection surface are often overlapping and must be deconvoluted in any assay based upon such structures.[51] Finally, using stringency washes of increasing temperature, it was demonstrated that single-base imperfections could be detected with increased selectivity (factor of 4) and sensitivity (10,000 times) when compared to fluorophore labeling methods.[31, 53, 54, 55]

Mirkin et al. have also demonstrated that two-color labeling can be accomplished using the size-dependent light-scattering properties of Au NPs of two different sizes. AuNP probes of different size and shape have light scattering at different wavelengths. Therefore, instead of using two different organic fluorophore labels, one can use Au NPs with different size dimensions to achieve multi-color capabilities. DNA-Au NP probes of different sizes allow for the direct labeling of DNA targets of interest in multi-color fashion.

As discussed previously the Scanometric method for detecting DNA sequences hybridized to a surface with gold nanoparticle probes has a sensitivity level in the low femtomolar range. Initial studies with this method detected only synthetic single strand oligonucleotides. The applicability of this method has been proven for detecting genomic DNA from bacteria and humans, including single nucleotide polymorphism (SNP) discrimination. The DNA isolated from the cells of interest is sheared mechanically by sonication before hybridization to the slide, and probing by the gold nanoparticles. The data showed the Scanometric methods ability to detect un-amplified genomic DNA down to 50fM concentration.[56] The Scanometric method has also proven efficient at returning a haplotype from human genomic DNA in less than an hour from DNA isolation.[57] The advantages of the

Scanometric method over conventional fluorophore based microarray determinations are that there is no need for enzymatic amplification, increased sensitivity, higher specificity conferred by gold nanoparticles, and total assay time of one hour.

A chip-based detection method for DNA targets using an electrical readout scheme offers several advantages over conventional readout and detection methods. First, massive multiplexing is possible when the chip electronic circuitry can be fabricated such that an individual circuit corresponds to an individual DNA target of interest.

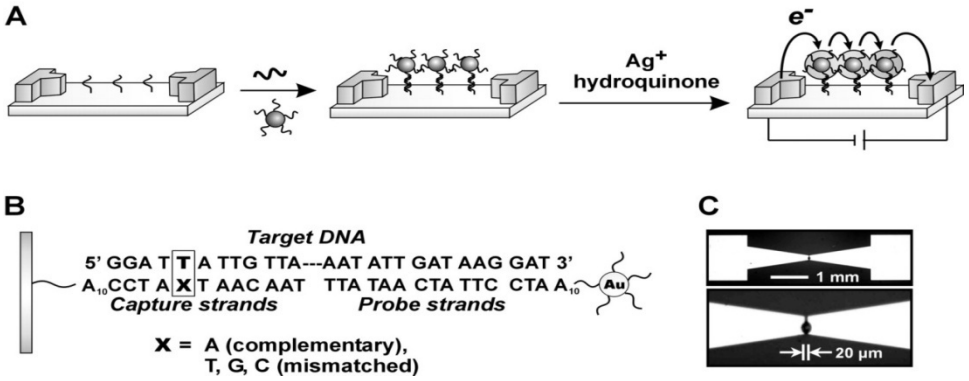

Figure 1.10 Chip-based Electrical Detection of Target DNA Strands Using DNA-Au NP Probes. Immobilized capture strands on the chip are hybridized with the target strands and DNA-Au NP probes followed by the silver staining enhancement, which changes the electric conductance for target detection. Reproduced with permission from Science magazine, 2002, all rights reserved.

Changes in the resistance or conductance in the electrical behavior are monitored for an extremely convenient and straightforward detection readout method. In addition, such an assay can also provide the extraordinarily high sensitivity and the huge variety of target species. In light of such advantages, much progress has been made on the development of such an assay.

Mirkin and co-workers developed the following detection assay based on the ability of surface-bound DNA-Au NPs to conduct electricity, especially when exposed to silver-developing solution. In sandwich assay format, the DNA capture stands were immobilized in the gap between microelectrode, and the capture-target-probe complexes were hybridized in the gap followed by exposure to silver-developing solution. When a target complementary to the capture

and probe strand was present, silver developing resulted in a decrease in the resistance of the gap, an increased conductivity, and subsequent electrical readout (Figure 1.10). As with the previous assays, it was shown that the DNA-Au NP probes had the ability to distinguish perfectly complementary targets from ones with single base mismatches. In order to remove mismatched targets, stringency washes with a buffer solution with decreased salt concentration at room temperature were performed showing better selectivity as compared to the thermal stringency washes with the same-buffered salt concentration. Further, the electrical detection assay was shown to have an un-optimized sensitivity of approximately 500 femtomolar (fM), which can be dramatically decreased through miniaturization of the electrode gap and the number of nanoparticles in the gap.[54]

Willner and co-workers developed a surface-based DNA assay in which microgravimetric measurements or Faradic impedance spectroscopy with Au electrodes and Au quartz crystals were used for target hybridization and detection.[58, 59] Importantly, DNA-functionalized liposomes and biotinylated liposomes showed dendritical amplification of the detection signal whose detection limit is 1 picomolar (pM) with identification of single-base mismatches.[58, 59]

1.5 Summary and Thesis Overview

Polyvalent oligonucleotide functionalized gold nanoparticle conjugates possess distinctive chemical and physical properties stemming from the relationship between their chemical building blocks and three-dimensional architectures. These materials have become widely adopted by chemists and biologists alike looking to take advantage of the properties discussed above. This dissertation explores the intimate role each chemical component plays in the conjugates architecture, assembly and recognition capabilities, and investigates their

applications towards bio-sensing.

In chapter two, the effect of the radius of curvature of the AuNP and the packing of oligonucleotides on the gold surface is investigated. Ultimately, the data confirms that radius of curvature greatly affects oligonucleotide packing, allowing higher surface densities on smaller AuNPs. Also as AuNPs grow larger than 100 nm the local environment around the DNA generally resembles that of a flat surface. Finally, from these experiments it is possible to generate mathematic relationships designed to predict oligonucleotide loading on anisotropic nanomaterials, rods.

In chapter three, the ability of bases attached to AuNPs to frame shift in an aggregate is shown, and confirms that bases adapt to form the strongest arrangement based on their geometry. This ability is not unexpected given the high degree of polyvalency these particles posses, but these experiments clearly show the impact that these slipped interactions have on the overall stability of nanoparticle assemblies. This may be one of the major reasons that the melting temperatures of oligonucleotides on AuNPs are higher than their free counterparts.

In chapter four, the role duplex DNA plays in modulating the unit cell parameters of highly ordered face-centered-cubic crystal lattices of DNA-AuNPs is demonstrated. Nanoparticle spacing increases linearly with DNA length, yielding maximum unit cell parameters of 77 nm and 0.52 % inorganic-filled space. Finally, an equation is derived for calculating unit cell parameters from the number of bases to be used in the crystal linker system.

In chapter five, the development of a new oligo-AuNP probe that can be used in the bio-barcode assay, which requires only *one* thiolated oligonucleotide strand, is reported. This new assay relies on the chemical liberation of adsorbed thiolated oligonucleotides from the AuNP

surface with dithiothreitol and assay yields a sensitivity of 7 aM where quantification can be achieved.

In chapter six, the detection of bacterial genomic DNA through the bio-barcode assay is reported. A critical step in the new assay involves the use of blocking oligonucleotides which bind to specific regions of the target DNA and after heating and upon cooling and prevent the duplex DNA from rehybridizing, allowing the probes to bind. The limit of detection for this assay was determined to be 2.5 fM.

CHAPTER TWO

Nanoparticle Radius of Curvature:

The Key to Predicting Oligonucleotide Loading on Anisotropic Gold Nanostructures

Portions of this chapter appear in: **Hill, H.D.,** Millstone, J.M., Banholzer, M.J., Mirkin, C.A., "Radius of Curvature: The Key to Estimating the loading of ssDNA on Anisotropic Gold Nanostructures" **(2008)** Submitted *ACS Nano***.**

Chapter 2: Nanoparticle Radius of Curvature: The Key to Predicting Oligonucleotide Loading on Anisotropic Gold Nanostructures

2.1 Introduction

Polyvalent oligonucleotide gold nanoparticle conjugates (oligo-AuNPs) are being extensively used in the development of therapeutic, diagnostic, and spectroscopic applications.[1-5] The reasons these structures have found such widespread use is that they can be easily synthesized and chemically modified, exhibit intense surface plasmon resonances ($\varepsilon > 3x10^8$ [L/(mol•cm)]),[2] have catalytic properties distinct from their bulk counterparts, and are generally stable in the context of diagnostic probe and therapeutic applications.[6-8] The surface coverage of oligonucleotides on spherical or highly faceted gold nanoparticles, which is often times much greater than other particle compositions (e.g. silica, polystyrene),[9] leads to unusually high electrostatic and steric stabilization of the particles and their ability to engage in highly cooperative hybridization interactions with complementary nucleic acids.[9, 10] The high loading of oligonucleotides on gold nanoparticles derives from: 1) the substitutionally labile coordination sphere of citrate ions adsorbed onto the surfaces of the particle precursors used to prepare the oligo-AuNPs; 2) the thiol-gold chemistry used to surface immobilize the oligonucleotides; 3) the salt-induced aging procedures used to decrease electrostatic interactions between neighboring oligonucleotides, and 4) the radius of curvature of the particles. The first three factors are constant regardless of particle size, whereas radius of curvature is highly dependent upon the dimensions of the particle.

These observations make one question, when do the surface modification properties and capacity for adsorbate loading of a particle begin to resemble those of a planar surface? This

question has been considered for uncharged hydrophobic alkanethiols on Au clusters by Landman *et al*., but not for chemically more sophisticated structures like oligonucleotides on larger gold nanoparticles (>2 nm).[11, 12] Charged multifunctional adsorbates like oligonucleotides likely will follow a similar trend but have a greater number of variables, which significantly affect their packing behavior. Herein, we present a study of oligo-AuNPs made from Au cores ranging in diameter from 10 to 200 nm, and aimed at determining how the radius of curvature of a particle influences oligonucleotide surface coverage. We compare these results to values obtained from planar gold surfaces and identify the nanoparticle size that begins to mimic the properties of a planar substrate. We then evaluate how these numbers and geometric models can be used to predict the oligonucleotide surface coverage for anisotropic rod-shaped particles.

2.2 Experimental Methods

2.2.1 Materials

Gold nanoparticles (10, 15, 20, 30, 40, 50, 60, 80, 100, 150 and 200 nm diameter) were purchased from Ted Pella, Inc (Redding CA) and used as received. All oligonucleotides were synthesized on an ABI Expedite Nucleic Acid Synthesizer using standard phosphoramidite chemistry [27] with reagents from Glen Research Corporation (Sterling, VA). All oligonucleotides were purified by reverse phase high-pressure liquid chromatography on an Agilent 1100 HPLC (Santa Clara, CA). Sodium Chloride (NaCl), Sodium Phosphate (Na_2HPO_4 and NaH_2PO_4, PB), Sodium Dodecyl Sulfate (SDS) and Dithiothreitol (DTT) were molecular biology grade, purchased from Sigma Aldrich (Milwaukee, WI) and used as received. NAP-5 columns were obtained from GE Healthcare (Piscataway, NJ) and used for all desalting procedures. All experiments were done using Nanopure™ water (Barnstead Int., Dubuque, IA). Anodic

aluminum oxide templates were obtained from Synkera Technologies Inc. Metal plating solutions were obtained from Technic, Inc. and used as received

2.2.2 Gold Nanorod Synthesis and Characterization

Nanorods were fabricated using an electrochemical, template-directed method.[28, 29] Briefly, a 125 nm Ag backing was thermally evaporated onto one side of an anodic aluminum oxide (AAO) membrane (35 nm pore diameter, 13 mm membrane diameter), which served as a working electrode during the electrodeposition growth process. The template was placed in an electrochemical cell with a platinum counter electrode and a Ag/AgCl reference electrode. 1025 Silver RTU solution (Technic Inc.) was diluted by a factor of 3 with water, and used to plate a silver section into the AAO template (-800 mV vs Ag/AgCl). This silver section served as a "buffer layer" to create more uniform electrical contacts, which results in more uniform gold rods (~3 C, 1-3 μm in length depending on contact between evaporated silver backing and AAO membrane). After deposition of this buffer segment the Ag plating solution was removed, and the electrochemical cell was rinsed with water for 3 minutes. Next, a solution of Orotemp 24 Gold RTU plating solution (Technic, Inc., diluted by a factor of 3 with water) was used to grow the gold nanorods at -900 mV vs. Ag/AgCl (485 mC of charge was passed to generate approximately 500 nm-long gold rods). After the electrodeposition was completed, the membrane was placed in concentrated HNO_3 (40 min) to dissolve the silver backing and buffer layer. The mixture was then rinsed and sonicated in NaOH (3 M) to dissolve the AAO template (30 min). The resulting nanorods were rinsed first with water (3x), then ethanol (3x), and finally with water (3x). The resulting rods were then characterized by scanning electron microscopy

(LEO 1525 FE-SEM, 3kV) in order to determine their dimensions (diameter (d) = 35 ± 5.3 nm; length (ℓ) = 475 ± 33 nm).

2.2.3 Oligonucleotide Functionalized Gold Nanoparticle Preparation

Oligonucleotide functionalized gold nanoparticles were prepared following literature procedures.[10] All procedures were conducted in the dark to prevent photobleaching of the fluorescein dye (FITC). Briefly, lyophilized oligonucleotides (5' – HS - AAA AAA AAA AAA TAT TGA TAA GGA T- FITC - 3') were re-suspended in a solution of 0.1 M dithiothreitol in 0.17 M phosphate buffer (PB) at pH 8 in order to deprotect the terminal thiol. After 1 hour in the reducing environment, the oligonucleotides were desalted over a NAP-5 column (GE Healthcare). Freshly deprotected oligonucleotides (4 nmol) in Nanopure™ water (250 μL) were added to 1 mL of gold colloid in a glass EPA vial. The solution was shaken at 120 rpm for 16-20 hours prior to salt stabilization. The oligo-AuNP solution was buffered to a pH of 7.2 with a final concentration of 10 mM PB and 0.01% SDS. The mixture was then allowed to equilibrate for 30 minutes before bringing the NaCl concentration to 1.0 M over an 8 hour period in a stepwise manner. The solutions were sonicated to keep the particles dispersed during the salting procedure. Following salting, the particles were shaken at 120 rpm for an additional 16-20 hours to yield fully functionalized oligo-AuNPs. To verify that the oligo-AuNPs were fully functionalized we measured the loadings[10] on particles stabilized at 0.1, 0.2, 0.3, 0.4, 0.5, 0.6, 0.7, 0.8, 0.9, 1.0, 1.5 and 2.0 M NaCl. Indeed, above 0.9 M NaCl there is no significant increase in oligonucleotide loading (Figure 2.1). Finally, to remove all unbound oligonucleotides from the oligo-AuNPs, the conjugates were washed by sequential centrifugation, supernatant removal and re-suspension (0.01% SDS in water). This procedure was repeated four times. Additionally,

planar thin film gold surfaces[30] were functionalized with oligonucleotides in a manner almost identical to that used for the AuNPs by immersing them in a 1 mL solution of water with 4 nmol of oligonucleotide. The substrates were salted in the same manner as the particles and cleaned by successive dipping into 50 mL of 0.01% SDS in water.

2.2.4 Oligonucleotide Functionalized Gold Nanorod Preparation

Lyophilized oligonucleotides were re-suspended in a solution 0.1 M dithiothreitol in 0.17 M PB at pH 8 in order to reduce the terminal thiols of the modified ssDNA. After 1 hour in the reducing environment, the oligonucleotides were desalted over a NAP-5 column (GE Healthcare). Approximately 2 ODs (~ 6 nmol) of purified oligonucleotides were combined with the rod solution (~ 10 fM). After 30 minutes, the solution was buffered to 0.01% SDS, 10 mM PB, and 1.0 M NaCl over 3 hours. The final solution was shaken for 48 hours at 1000 RPM, at 23 °C on a thermomixer (Eppendorf, Inc.) prior to use.

2.2.5 Measuring Oligonucleotide Loading on Gold Nanoparticles

Freshly cleaned oligo-AuNPs were resuspended in a solution of 10 mM PB, 0.01% SDS, and 0.3 M NaCl and 100 μL of each sample were placed in a 96 well fluorescence compatible microtiter plate. The extinction of each sample was measured on a Thermo UV-Vis plate spectrophotometer at 530 nm. To determine the concentration of each AuNP sample, an extinction coefficient at 530 nm was determined for each particle size. This was done by measuring the absorbance at 530 nm of a 100 μL sample of unfunctionalized gold nanoparticles on the same UV-Vis plate reader and relating it to known particle concentrations. Additionally, known concentrations of fluorophore-labeled DNA (100 μL,) were placed in the microtiter plate and 100 μL of 1.0 M DTT in water were added to each well of the microtiter plate. After

liberation of the thiolated oligonucleotides from the surface of the AuNPs (overnight), the total fluorescence of each well was measured on a fluorescence plate reader (FluorDia T70, Otsuka Electronics) and converted to a concentration by comparison to a standard curve. By measuring the concentration of oligonucleotides and AuNPs in each sample (six times), an average number of oligonucleotides per particle were calculated (Table 2.1). The loading of oligonucleotides on gold nanoparticles was also determined in the same manner as that used for the gold nanorods (see below) to ensure that the error introduced by the measurement techniques was minimized.

2.2.6 Measuring Oligonucleotide Loading on Gold Nanorods

A sample of oligo-functionalized nanorods was prepared as described above. An aliquot of these rods was then washed 3 times in 0.01% SDS, resuspended in 35 μL of 0.1 M aqueous solution of KCN, and allowed to react for 1 hour in order to completely dissolve the gold rod. The resulting sample was analyzed by inductively-coupled plasma mass spectrometry (ICP-MS) to determine the amount of gold. Rod concentration was determined by calculating the average number of gold atoms per nanorod (d = 35 nm, ℓ = 475 nm, 2.43×10^7 atoms) and dividing the total amount of gold present in the dissolved sample by the number of gold atoms per nanorod. The number of oligonucleotides from this aliquot was quantified using the Oligreen® assay (Invitrogen, Inc.) in a manner similar to that described above for the AuNPs. By coupling the rod concentration obtained from ICP-MS with results from the Oligreen® assay, the average number of ssDNA oligonucleotides on a single nanorod could be determined (3330 ± 114 strands per rod).

2.3 Results and Equation Derivations

2.3.1 Surface Oligonucleotide Loading as a Function of Salt Concentration

Previous work by our group and others has shown that the surface loading of oligonucleotides increases with increasing salt concentration.[8, 10] To evaluate the optimum salt concentration for loading oligonucleotides on Au nanoparticle surfaces, we measured surface loading for 20 nm diameter particles as a function of successively increasing salt concentration (Figure 2.1). One observes a steady rise in loading up to about 1 M NaCl concentration, after which loading levels off. Therefore, we chose this salt concentration as a constant for all subsequent measurements.

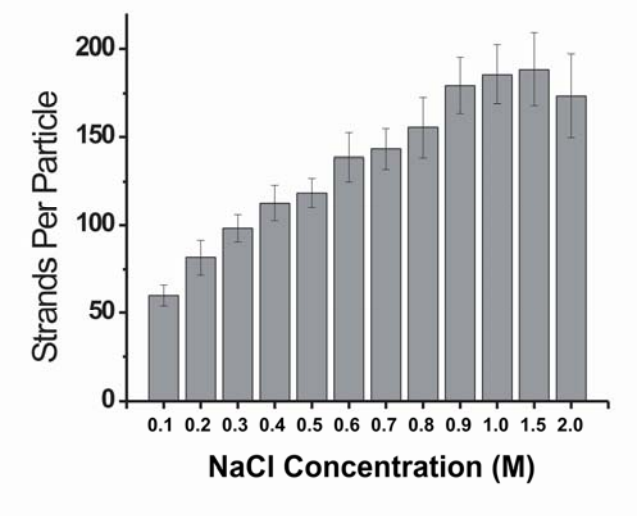

Figure 2.1 Oligonucleotide loading as a function of salt concentration for 20 nm AuNPs.

2.3.2 Surface Density of Oligonucleotides as a Function of Nanoparticle Radius

The surface density of oligonucleotides for each particle size was calculated by dividing the number of oligonucleotides per particle by the calculated surface area (nm^2), (Table 2.1; Column 2). Several assumptions regarding surface area were made. First, the nanoparticles were modeled as perfect spheres. Second, the numbers of particles larger and smaller than the average particle size were assumed to be equal. Third, the oligonucleotides were assumed to be evenly distributed on the nanoparticle surface. As predicted, the surface curvature significantly affects the loading of oligonucleotides with smaller particle sizes exhibiting higher coverages than larger

diameter structures. From these data, one can see that when the particles reach a diameter of approximately 60 nm (and certainly above 100 nm), the surface coverage remains nearly

diameter (nm)	oligos/ particle	coverage (oligos/cm^2)	footprint (nm^2)	deflection (Deg)
10	64 ± 6	2.05E+13	4.9	28.55
15	117 ± 13	1.66E+13	6.0	21.15
20	180 ± 17	1.43E+13	7.0	17.09
30	263 ± 7	9.31E+12	10.7	14.13
40	428 ± 6	8.52E+12	11.7	11.08
50	639 ± 84	8.13E+12	12.3	9.07
60	885 ± 22	7.83E+12	12.8	7.70
80	1426 ± 132	7.09E+12	14.1	6.07
100	2233 ± 185	7.11E+12	14.1	4.85
150	5063 ± 128	7.16E+12	14.0	3.22
200	8476 ± 150	6.75E+12	14.8	2.49
Planar Gold	N/A	5.75E+12	17.5	0

Table 2.1 The average values for particle sizes, absolute number of oligonucleotides per particle, surface coverage, effective footprint and calculated deflection angle.

constant for all particle sizes above this value and is comparable to values determined for a planar gold substrate (Figure 2.2).

The effective DNA footprint (K) is one way to think about the spatial arrangement of oligonucleotides on the nanoparticle surface. Footprint is defined as the average area each oligonucleotide occupies on the nanoparticle surface (Table 2.1, Column 3; eq. 1).

$$footprint: \mathrm{K}\left(\frac{\mathrm{nm}^2}{\mathrm{DNA}}\right) = \left[\frac{4\pi r^2}{N_r}\right] \qquad (1)$$

K represents the average area each oligonucleotide occupies on the nanoparticle surface in nm^2 (footprint), and *N* represents the average number of oligonucleotides per particle for a given radius, *r* (Scheme 2.2A).

2.3.3 Calculating the Deflection Angle between Oligonucleotides:

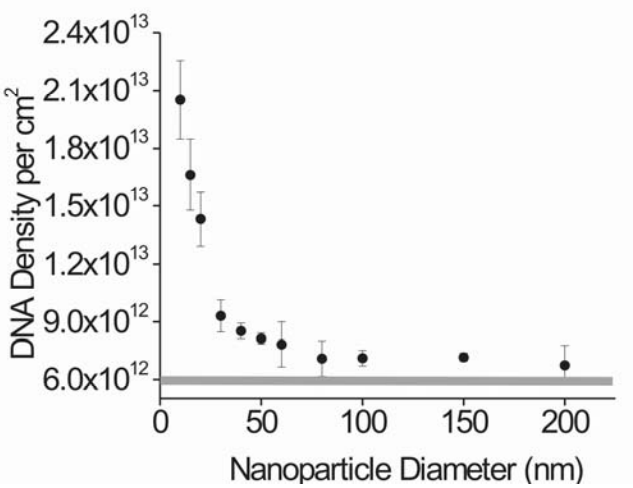

Figure 2.2 Oligonucleotide density determined as a function of AuNP diameter. The gray line represents oligonucleotide loading on a planar gold surface.

The average deflection angle between oligonucleotides attached to the AuNP is directly related to the radius of curvature of the nanoparticle and illustrates the spatial arrangement of the strands as well as how this arrangement is dependent upon the AuNP radius, Scheme 2.1. To calculate the deflection angle between two oligonucleotides on the nanoparticle surface, the above assumptions were used, along with two additional ones. For these calculations, we assume that the oligonucleotides adopt a rod like orientation. To test the validity of this assumption, dynamic light scattering measurements were used to determine the approximate length of the oligonucleotides attached to the AuNPs (Figure 2.3). On average, the oligonucleotides were estimated to be 9 nm in length, similar to the expected value if modeled as rod-like, extended structures (rod-like ssDNA, approximately 10 bases/3 nm, is expected to be shorter than fully outstretched 13.4 nm long single stranded DNA due to coiling).[13, 14] Additionally, we modeled the oligonucleotide-footprint as a circular area,

(Scheme 2.2B) which was used to calculate the deflection angle between oligonucleotides using, eq. 2 and 3:

$$R = \sqrt[2]{\frac{K}{\pi}} \quad (2)$$

$$Deflection\ (\text{deg}) = \left[\frac{2R}{r}\right] \times \frac{180}{\pi} \quad (3)$$

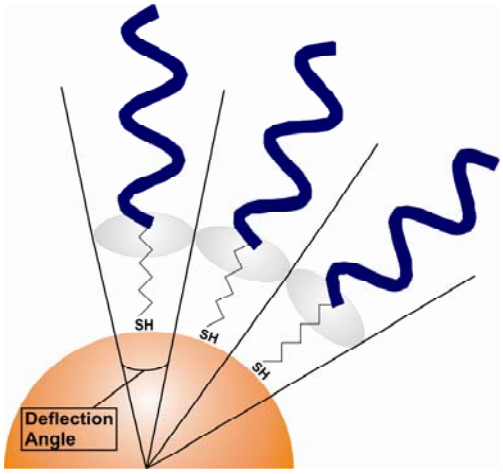

Scheme 2.1 Drawing illustrating how the radius of curvature of the AuNP affects the interaction between neighboring oligonucleotide strands. This interaction is represented by the deflection angle between the oligonucleotides.

where R represents the radius of the footprint approximation on the nanoparticle surface, K is the footprint of the oligonucleotide on the AuNP surface, and r is the average radius of the nanoparticle. Deflection angles were determined for all particle sizes studied and planar gold (Table 2.1, column 5 and Figure 2.5).

2.3.4 Deriving an Equation for Predicting the Loading of Oligonucleotides on Gold Nanorods

Quantitatively predicting surface coverage for a rod is more difficult than a sphere. A rod is a cylindrical body with two flat ends.[15] One must take this geometry into account with weighted contributions from the curved and planar portions of the structure. The surface area of a rod can be calculated using eq 4:

$$S.A.(rod) = 2\pi r^2 + 2\pi rl \quad (4)$$

where r is the radius of the rod and l is the length of the rod. To approximate the number of oligonucleotides on the rod the two end segments (represented by $2\pi r^2$) were assumed to be flat planar surfaces where oligonucleotides have an average footprint of 17.55 nm^2. While they are

not perfectly flat (RMS roughness ~ 15 nm), AFM studies show that these are best modeled as flat rather than curved surfaces.[15] Second, we did not include contributions from adsorption of oligonucleotides on the edges of the cylinder ends. Third, we approximated the footprints of the oligonucleotides on the outer wall of the cylinder (not the ends) as an ellipse. To do this, we used the radius of the nanorod to assign a spacing parameter for oligonucleotides attached to the curved surface of the rod in bands (Scheme 2.3). The data presented in Table 2.1 were used to relate the radius of a nanoparticle to the average footprint diameter in the Y direction. This derivation yielded the relationship shown in eq. 5.

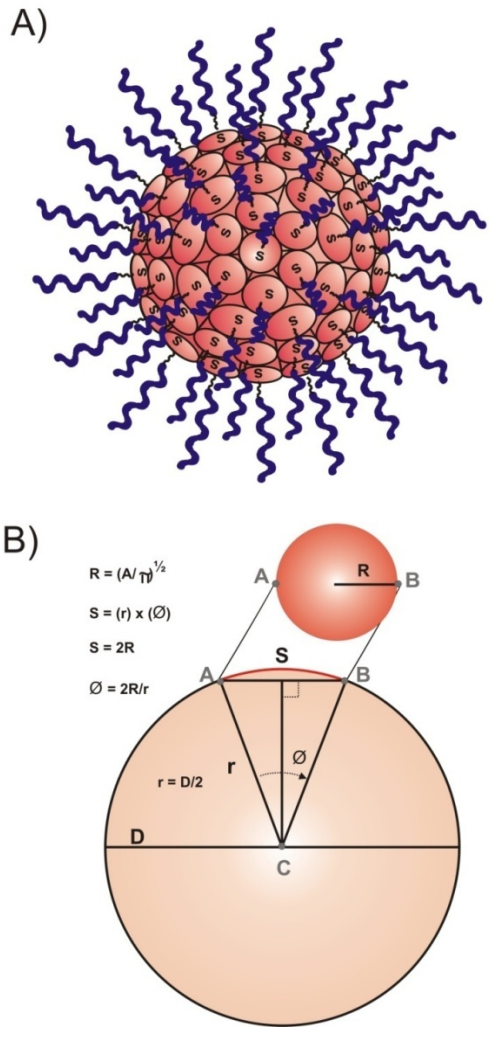

Scheme 2.2 Model of the oligo-modified AuNP Surface. A) Model used to calculate the oligonucleotide footprint. B) Illustration of how the footprint from A) is used to approximate the deflection angle.

$$(5) \qquad Length\ of\ Ellipse\ (nm) = 2\sqrt{\frac{3.3618\ln r + 0.1616}{\pi}}^{2}$$

To estimate the spacing down the long axis of the rod, we assumed that, the oligonucleotides experienced a situation similar to a flat surface, where the spacing was 4.72 nm per oligonucleotide. The total surface area of the entire rod was then divided into oligonucleotide footprint domains to approximate the number of oligonucleotides that can pack on a nanorod of a given length and radius, Eq 6:

$$(6) \qquad \frac{Oligonucleotides}{rod} = \frac{2\pi r^2}{17.55} + \frac{2\pi r}{2\sqrt{\frac{3.3618\ln r + 0.1616}{\pi}}} * \frac{l}{4.72}$$

Where *r* is the radius of the rod and *l* represents the length of the rod (Scheme 2.3).

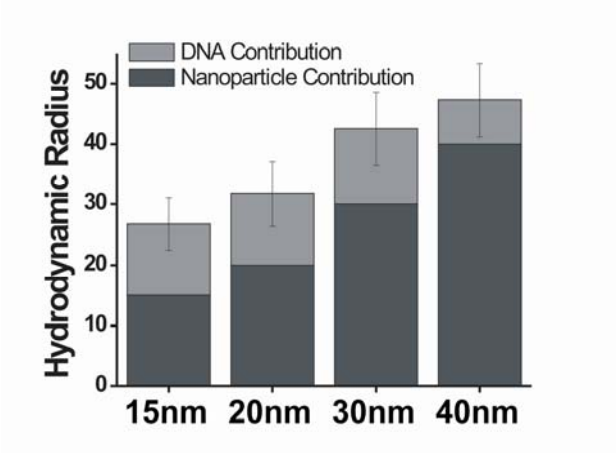

Figure 2.3 Diameter determined by dynamic light scattering measurements. The values presented above are the average of 3 separate measurements

While oligo-AuNPs with average gold core diameters varying from 2 to 250 nm have been prepared and studied previously,[10, 16] the majority of studies have focused on the 13-15 nm range, typically functionalized with oligonucleotides containing 25-35 bases.[17-25] Therefore, for this study we chose 15 nm diameter particles, modified with a 25 base sequence as a representative example (5' – HS - AAA AAA AAA AAA TAT TGA TAA GGA T- FITC - 3'). If one considers that a 15 nm gold particle has a radius of 7.5 nm and compares that to the persistence length of a 25 bp oligonucleotide at approximately 8.5 nm (where 10 base pairs are approximately equivalent to 3 nm),[13] an interesting observation is made: the dimensions of the two are essentially the same. This prompted us to consider the spatial relationship of the gold nanoparticle and the oligonucleotides attached to its surface from a geometric perspective. If one approximates a 15 nm AuNP as a sphere and envisions oligonucleotides attached to the particle surface at one end through a chemical linker (Au-S), one

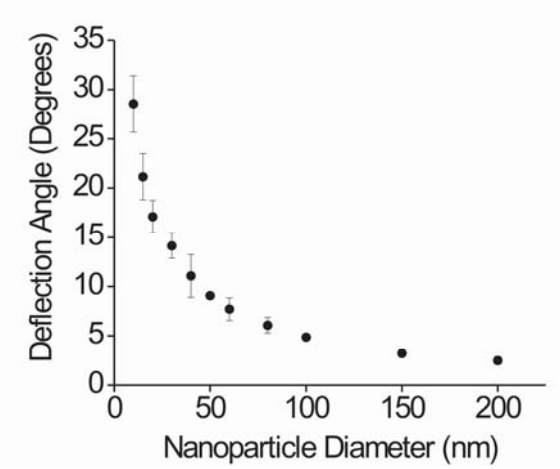

Figure 2.4 Oligonucleotide deflection angle as a function of AuNP diameter.

can make a few key observations (Scheme 2.1). First, the distance between the oligonucleotide strands is closest at the particle surface and grows larger as

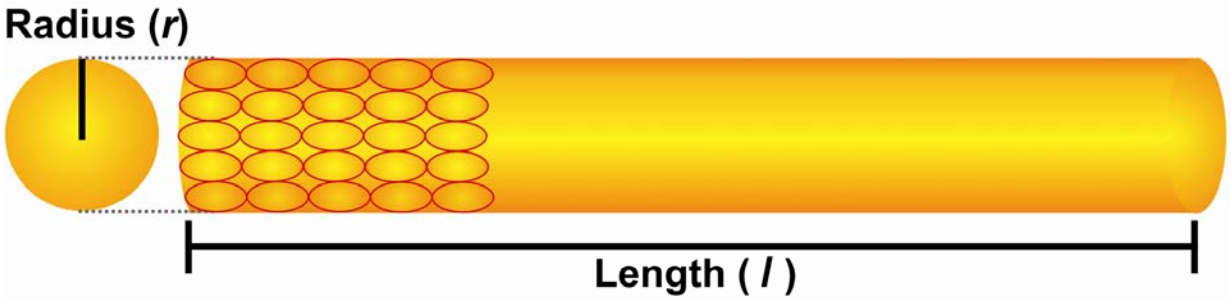

Scheme 2.3 Model of oligonucleotide packing on a gold nanorod surface.

the chain extends from the surface (Scheme 2.1). Second, as particle radius increases, one must move further from the particle surface to maintain comparable inter-oligonucleotide distances. Third, as particle size increases, eventually the oligonucleotides attached to it begin to more closely resemble the spacing of oligonucleotides attached to a flat surface. Thus far, the magnitude of these effects has never been studied, and the particle size that begins to mimic the properties of a flat surface has not been identified.

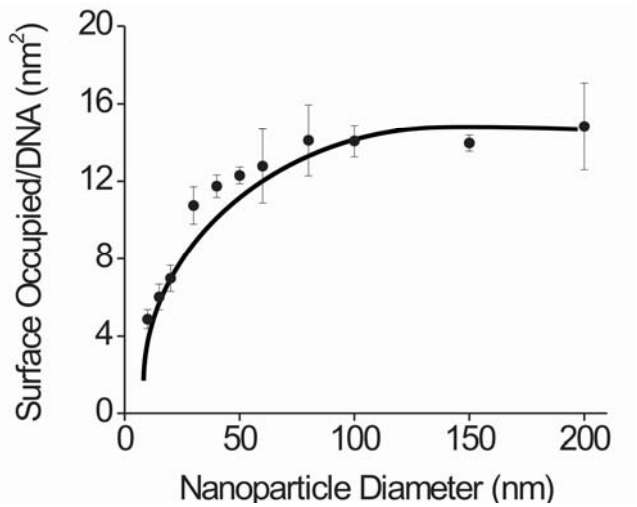

Figure 2.5 Surface Occupied per Oligonucleotide vs. Nanoparticle Diameter

2.4 DISCUSSION

A goal of this work is to determine how changes in the surface curvature of gold nanoparticles affect the organization of thiol-terminated oligonucleotides attached at their

surfaces. Initially, we hypothesized that thiol-terminated oligonucleotides attached to relatively small AuNPs (less than 20 nm diameter) would have significantly more distance between the neighboring strands moving radially out from the surface than their larger particle counterparts, resulting from their highly curved surfaces. This should produce decreased steric interactions between oligonucleotides attached to small AuNPs, thus allowing for more oligonucleotides to attach to the highly curved surface than to the larger flatter surfaces, when equal areas are compared (Figure 2.2). Indeed, our data confirm that the loading of oligonucleotides on Au NPs, smaller than 20 nm, show a dramatic increase in oligonucleotide surface coverage when compared to their larger counterparts. However, when the diameter exceeds 60 nm the oligonucleotide surface coverage approaches the values obtained for a flat gold surface (Figure 2.2, Table 2.1).

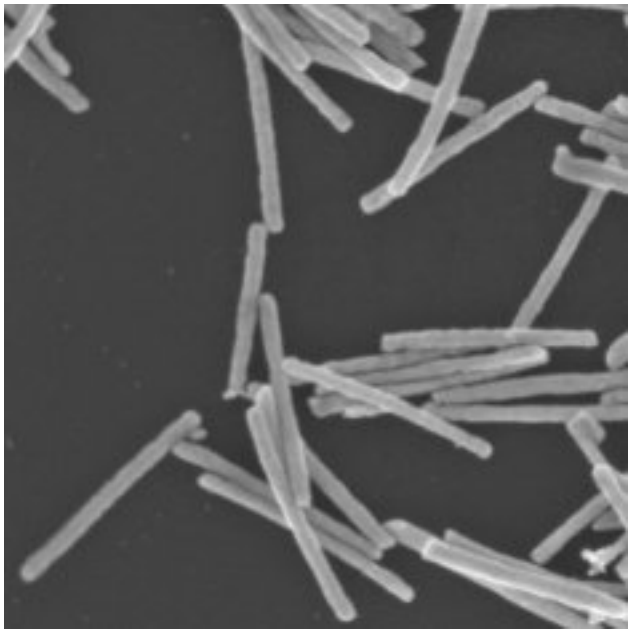

Figure 2.6 SEM of representative gold nanorods; average diameter = 35 ± 5.3 nm and average length = 475 ± 33 nm. The image displayed above shows a 1.5 x 1.5 μm area.

Another way to look at this relationship is to directly compare the estimated deflection angles between the strands as calculated above (Scheme 2.1). This comparison shows that the deflection between the strands is greatest on the smallest particles and exponentially decays to almost no deflection for the largest particles (Figure 2.4). Oligonucleotides on planar gold surfaces exhibit more regular packing and a salt concentration-dependent tilt angle, but do not exhibit a relative deflection angle.[26]

One of the goals this work was to derive a mathematical relationship, which can be used to predict the loading of similar oligonucleotides on anisotropic gold nanostructures. Therefore, we needed to determine the effective footprint of an oligonucleotide (surface area occupied), as a function of particle curvature. Our results show that as nanoparticle diameter decreases and curvature increases, effective footprint decreases (Figure 2.5). This relationship is the foundation of our rod loading derivation (Scheme 2.3). The loading experiments show that one can quantitatively predict saturated oligonucleotide surface coverages for gold nanorods (Figure 2.6). Indeed, the experimentally determined value of 3330 ± 114 corresponds remarkably well with the predicted value of 3,244 oligonucleotides per rod.

2.5 Conclusion

This work provides a way of understanding and predicting oligonucleotide surface coverage on nanoparticles as a function of curvature, shape, and available surface area. Indeed, the data provided are the first quantitative measures of the relationship between particle curvature and oligonucleotide loading. The results show that as particle diameter increases to 60 nm it begins to mimic the properties of a planar surface, and above 100 nm, it behaves virtually identically to a planar surface in terms of oligonucleotide loading. Additionally, we show that the loading of oligonucleotides on gold nanorods can also be accurately predicted using this curvature relationship. Importantly, the geometric models worked out in this manuscript, in principle, could be adapted for many particle shapes simply by using the different geometric equations for surface area.

CHAPTER THREE

Curvature-Induced Base Pair "Slipping" Effects in DNA-Nanoparticle Hybridization

Portions of this chapter appear in [**Hill, H.D.,** Hurst, S.J., Mirkin, C.A., "Curvature-Induced Base Pair Slipping Effects in DNA-Nanoparticle Hybridization" *Nano Lett*. **(2008)** accepted]

Chapter 3: Curvature-Induced Base Pair Slipping Effects in DNA-Nanoparticle Hybridization

3.1 Introduction

Over the past decade, polyvalent oligonucleotide-gold nanoparticle conjugates (DNA-AuNPs) have become the focus of intense research.[1-3] These structures exhibit properties that are often different from the properties of the nanoparticle and free-oligonucleotides from which they are derived,[4,5] and from their monovalent analogues.[6] They have been utilized in the development of novel materials assembly schemes,[7-12] useful and, in certain cases, commercially viable detection systems,[13-28] and intra-cellular gene regulation agents.[29-31] Despite their extensive utility, however, there remain several fundamental questions pertaining to DNA hybridization with these polyvalent structures.

When two types of DNA-AuNPs, functionalized with complementary oligonucleotide sequences, are introduced in one solution, under the appropriate conditions, they will assemble into large polymeric amorphous or crystalline aggregates (Scheme 3.1A).[1,7,8,32-34] This assembly is accompanied by a concomitant dampening and red-shifting of their surface plasmon resonance (SPR) band and a color change from red to blue. This process is reversible, and when heated, the DNA linkages holding the particles together dehybridize (melting of the DNA-AuNPs) in a highly cooperative manner resulting in a recovery of their original spectroscopic signatures and intense red color. These structures typically melt at temperatures higher than one would predict based upon the melting properties of the particle-free DNA.[1,35,36]

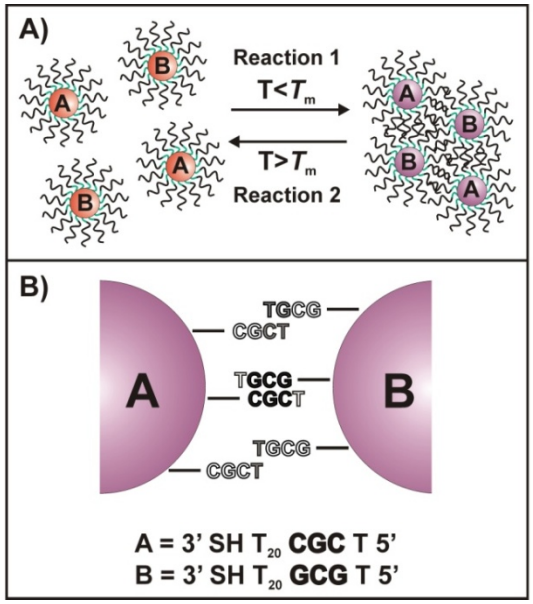

Scheme 3.1. A) General scheme for the hybridization and melting of particles which are functionalized with complementary oligonucleotide sequences termed A and B. B) General scheme (in a 'two-particle' model) showing the potential interactions (normal and "slipping") accessible for DNA-AuNPs functionalized with TCGC– (particle A) and TGCG– (particle B). The interactions possible for oligonucleotides on the particle surface depend on their ability to engage in hybridization with complementary strands on an adjacent particle and are impacted by the radius of curvature of the particles. Black lettering indicates bases involved in normal Watson-Crick interactions, gray lettering indicates bases involved in non-Watson-Crick "slipping" interactions, and white lettering indicates bases that are not involved in hybridization.

This unique behavior has been explained, in part, by the multivalent character of the particles and their ability to engage in multiple hybridization events, which lead to enhanced stability.[36] However, the exact nature of the DNA base interactions contained within these structures has not been completely resolved. Herein, we describe experiments that suggest that these curved particles can engage in two types of hybridization, one that involves complementary strands and normal base pairing interactions and a second "slipping" interaction, which can stabilize the aggregate structures through non-Watson Crick type base pairing interactions (Scheme 3.1B). A "slipping" interaction in this case is defined as a secondary base pairing motif (not necessarily Watson Crick and partial complementarity) that contains fewer total base interactions than the primary and stronger interaction (normal Watson-Crick and full complementarity) of the system, while still imparting a measure of stability onto the nanoparticle aggregate systems.

3.2 Experimental

3.2.1 Materials

Gold nanoparticles (60 nm in diameter, Ted Pella, Redding, CA) and triangular gold nanoprisms (~ 140 nm edge length)[37] were functionalized with a series of 24-mer propyl thiol-modified oligonucleotides according to standard literature protocols with minor modifications.[38-40] The gold nanoparticles and nanoprisms were salt stabilized to 1.0 and 0.15 M NaCl, respectively. The sequences used in this study were composed of: 1) a 3′ propyl thiol moiety, 2) a poly-T spacer, 3) a C and/or G -rich recognition element designed to access a particular set of "slipping" interactions, and 4) a single T capping base on the 5′ end designed to prevent undesired aggregation resulting from G-quartet formation (Table 3.1).[41-43] Extremely short (1-3 base) recognition elements were used in order to limit and easily focus on the possible "slipping" interactions for each system. A poly-T spacer was used since this base has the

Name	Oligonucleotide Sequence
Control	5′ – TTT TTT TTT TTT TTT TTT TTT TTT – $(CH_2)_3$ – SH-3′
TGC-	5′ – TGC TTT TTT TTT TTT TTT TTT TTT – $(CH_2)_3$ – SH-3′
TCG-	5′ – TCG TTT TTT TTT TTT TTT TTT TTT – $(CH_2)_3$ – SH-3′
TCGC-	5′ – TCG CTT TTT TTT TTT TTT TTT TTT – $(CH_2)_3$ – SH-3′
TGCG-	5′ – TGC GTT TTT TTT TTT TTT TTT TTT – $(CH_2)_3$ – SH-3′

Table 3.1 DNA sequences used in experiments

weakest interaction with itself;[44,45] DNA-AuNPs functionalized with the control sequence (Table 3.1) exhibit no hybridization or melting behavior under any of the conditions studied (Figure 3.1).

3.2.2 Instrumentation

The concentrations of both gold nanoparticles and oligonucleotides were determined on a NanoDrop® ND-1000 UV-vis spectrophotometer or a Cary 5000 UV-vis spectrophotometer. Melting experiments were performed using a Cary 100 UV-vis spectrophotometer with temperature control and a 6 x 6 cell changer. All sonication was performed using a Branson 2510 sonicator.

3.2.3 Preparation of Oligonucleotide-Modified Gold Nanoparticles

Oligonucleotide functionalized gold nanoparticles were prepared by literature methods. Briefly, approximately 10 OD of lyophilized oligonucleotides were suspended in 100 millimolar (mM) dithiothreitol (Pierce Biotechnology, Inc. (Rockford, IL)) in 170 mM $NaPO_4$ buffer (pH 8.0) for one hour to reduce their disulfide protecting groups, yielding monothiol DNA. The oligonucleotides were purified from the dithiothreitol solution using NAP-5 columns. Oligonucleotide concentrations were measured on the NanoDrop® and added to the AuNPs at a concentration of 3 nM per milliliter (mL) of AuNPs. The oligonucleotide-AuNP mixture sat at room temperature overnight prior to salt stabilization. For salt stabilization, the concentrations of phosphate buffer and sodium dodecyl sulfate (SDS) were brought to 0.01 M and 0.01 (wt/vol) % respectively. The concentration of NaCl was increased to 0.05 M using 2 M NaCl, 0.01 M PBS while maintaining an SDS concentration of 0.01 %, and the mixture was

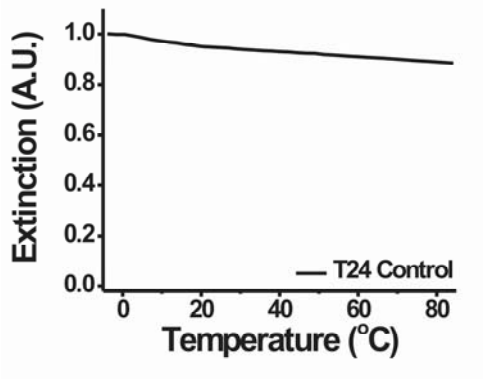

Figure 3.1 Poly T_{24} Control. 60nm Au NPs functionalized with dT_{24} polynucleotides show no hybridization or melting behavior in 1.0 M NaCl 10 mM Phosphate.

sonicated for ~ 10 sec. This process was repeated one more time to bring the NaCl concentration to 0.1 M. Then, the NaCl concentration was raised in 0.1 M increments until a final concentration of 1.0 M NaCl was reached. The salting process was followed by another overnight incubation at room temperature. To remove excess oligonucleotides, the gold nanoparticles were centrifuged, and the supernatant was removed, leaving a pellet of gold nanoparticles at the bottom of an Eppendorf® tube. The particles then were resuspended in 0.01 % Triton® X-100. This washing process was repeated for a total of four supernatant removals. The nanoparticles were stored as a colloidal suspension in 0.01 % Triton® X-100 at 4 ^{o}C until further use.

3.2.4 Hybridization and Melting of Oligonucleotide-Modified Gold Nanoparticles

Complementary DNA-AuNPs (A and B, Scheme 1A) were hybridized overnight at 4 °C. The melting transitions of the aggregates were recorded as the temperature of the solution was ramped from 4 to 95 ^{o}C (at 1 ^{o}C/min) with magnetic stirring. The temperature where the melting transition takes place (T_m) and the breadth of the transition (full width at half maximum, FWHM) provide information about the nature of the DNA interactions linking the DNA-AuNPs;[46] stronger interactions typically lead to systems of aggregates with higher melting temperatures.[47]

3.3 Results

In our initial experiments, we investigated the hybridization/melting behavior of DNA-AuNPs functionalized with sequences containing 2 base pair recognition elements (i.e., A = B = TCG– and A = B = TGC–, Scheme 3.1A, Table 3.1). We chose these particular DNA-AuNP systems because each has the ability to access a combination of “slipping” interactions of different strengths (Figures 3.2B and 3.2C). For example, in a ‘two-particle’ version of the

A)

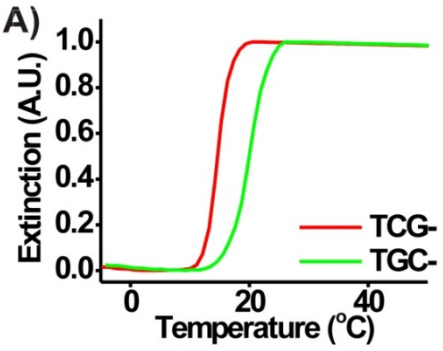

B)

TCG-	
Structure	**Interactions**
–TGCT TCGT–	2 G-C, 2 T-T
–TGCT TCGT–	2 G-T, 1 C-C
–TGCT TCGT–	2 C-T
–TGCT TCGT–	1 T-T

C)

TGC-	
Structure	**Interactions**
–TCGT TGCT–	2 G-C, 2 T-T
–TCGT TGCT–	2 C-T, 1 G-G
–TCGT TGCT–	2 G-T
–TCGT TGCT–	1 T-T

Figure 3.2 A) Melting transitions (monitored at 520 nm) for aggregates of DNA-AuNPs functionalized with 2 base pair sequences (TCG– or TGC–). B) "slipping" interactions possible in a 'two-particle' model for DNA-AuNPs functionalized with TCG–. C) The "slipping" interactions possible in a 'two particle' model for DNA-AuNPs functionalized with TGC–. (Black lettering indicates bases involved in Watson-Crick interactions, gray lettering indicates bases involved in non-Watson-Crick "slipping" interactions, and white lettering indicates bases that are not involved in hybridization.)

variable strength "slipping" model introduced above, we assume that the most favorable interaction, a complementary 2 base pair GC core, forms for both systems. If "slipping" is considered, both of these systems also can participate in G-T, C-T, and T-T interactions, while C-C and G-G interactions are limited to the TGC– and TCG– systems, respectively (Figure 3.2B and 3.2C). Among these non-Watson-Crick interactions, those involving a G base generally are stronger than the analogous interaction involving a C base, and both of these types of interactions are stronger than the interaction of T with itself (i.e., G-G > C-C > G-T > C-T > T-T).[48,49] According to this analysis, we hypothesized that DNA-AuNPs functionalized with TGC– are capable of forming stronger overall hybridization interactions (normal plus "slipping") in a nanoparticle aggregate than those functionalized with TCG–. We further hypothesized that, if "slipping" interactions contribute significantly to aggregate stability, an

increased melting temperature should be observed for aggregates of DNA-AuNPs functionalized with TGC– as compared with aggregates formed from particles functionalized with TCG–. Indeed, we observe that the melting temperature of DNA-linked aggregates comprised of DNA-Au NPs functionalized with TGC– is 5.1 ^{o}C higher than those comprised of DNA-AuNPs functionalized with TCG– in 1.0 M NaCl, 10 mM sodium phosphate buffer, 0.01 % SDS, pH 7.2 (i.e., T_m (TGC–) = 19.9 ^{o}C; T_m (TCG–) = 14.8 ^{o}C, Table 3.2, Figure 3.2A).

We also investigated the hybridization/melting behavior of systems of DNA-Au NPs functionalized with sequences containing a 3 base pair recognition element (i.e., A = B = TCGC– and A = B = TGCG–, Scheme 3.1A, Table 3.1). In these systems, we hypothesized, again using a 'two-particle' model and information about the relative strengths of DNA base pairing interactions,[48,49] that DNA-AuNPs functionalized with TGCG–

A)

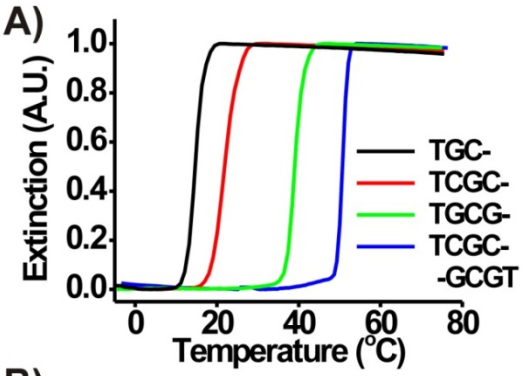

B)

TCGC-	
Structure	**Interactions**
–TCGCT TCGCT–	2 G-C, 2 C-T
–TCGCT TCGCT–	2 G-T, 1 C-C
–TCGGT TGGCT–	2 C-T
–TCGCT TCGCT–	1 T-T

C)

TGCG-	
Structure	**Interactions**
–TGCGT TGCGT–	2 G-C, 2 G-T
–TGCGT TGCGT–	2 C-T, 1 G-G
–TGCGT TGCGT–	2 G-T
–TGCGT TGCGT–	1 T-T

Figure 3.3. A) Melting transitions (monitored at 520 nm) for aggregates of DNA-Au NPs functionalized with sequences containing 2 and 3 base pair recognition elements. B) The "slipping" interactions possible for a 'two-particle' model for DNA-AuNPs functionalized with TCGC–. C) The "slipping" interactions possible in a 'two-particle' model for DNA-AuNPs functionalized with TGCG–.(Black lettering indicates bases involved in Watson-Crick interactions, gray lettering indicates bases involved in non-Watson-Crick "slipping" interactions, and white lettering indicates bases that are not involved in hybridization.)

are capable of forming stronger overall interactions in an aggregate than those functionalized with TCGC– (Figure 2B and 2C). This enhanced stability again is evidenced by an increased melting temperature; we observe that the melting temperature of aggregates comprised of DNA-Au NPs functionalized with TGCG– is 17.5 ^{o}C higher than those comprised of DNA-AuNPs functionalized with TCGC– in 1.0 M NaCl, 10 mM sodium phosphate buffer, 0.01 % SDS, pH 7.2 (i.e., T_m (TGCG–) = 39.5 ^{o}C; T_m (TCGC–) = 22.0 ^{o}C, Table 3.2, Figure 3.2A). In this case, it is possible for each system to form a 2 base pair duplex core, and this likely occurs since the T_m for each of these systems is higher than the T_m for the 2 base pair systems (Table 3.2, Figure 3.2A). In addition, the melting temperatures of both of these aggregate systems are lower than the fully complementary system with 3 base pairings in the recognition element (A = TCGC– and B = TGCG–, Table 3.2, Figure 3.2A). Ultimately, the differences in melting temperature that are observed for both the 2 and 3 base pair systems indicate that the "slipping" interactions of oligonucleotides attached to AuNPs lead to a significant increase in aggregate stability.

3.4 Discussion

To further evaluate if the radius of curvature of the gold nanoparticles is responsible for the "slipping" interactions of the DNA bases we studied the hybridization and melting behavior of DNA functionalized triangular gold nanoprisms (DNA-Au prisms)[37,39] in 0.15 M NaCl, 10 mM sodium phosphate buffer, 0.01 % SDS, pH 7.2. We reasoned that the atomically flat surfaces of triangular gold nanoprisms would *not* foster DNA base "slipping" interactions (**Figure 3.3A**) and therefore differences in melting temperature would *not* be observed for, for example, aggregates of gold nanoprisms functionalized with TGC– and aggregates of those functionalized with TCG–. Aggregates of gold nanoprisms functionalized with TCG– or TGC– in fact had

nearly identical melting profiles and melting temperatures (T_m^{prism} (TCG–) = 81.4 °C or T_m^{prism} (TGC–) = 81.5 °C (Figure 3.3B). This experiment indicates that the difference in T_m seen for aggregates of AuNPs functionalized with TCG– or TGC– (Figure 3.3A) is indeed due to the radius of curvature of the gold nanoparticle and the "slipping" interactions that occur as a result.

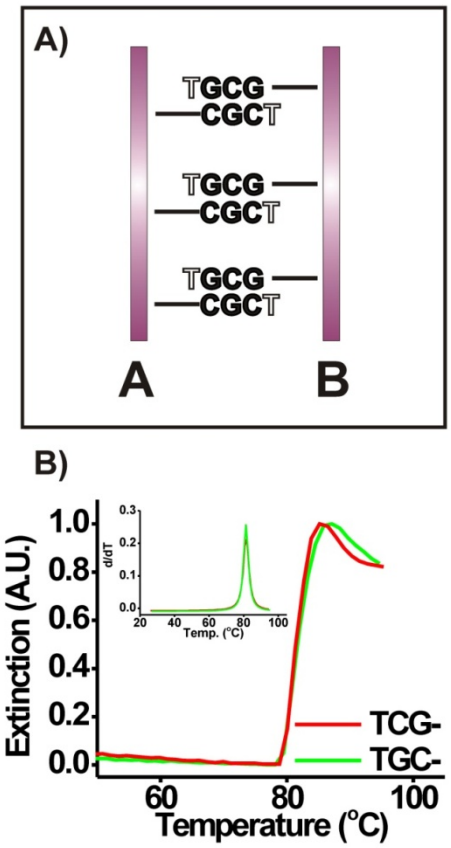

Figure 3.4. A) Diagram (for a 'two-particle' model) showing that "slipping" interactions are not as likely with DNA functionalized-Au prisms (particle A is functionalized with TCGC–, while particle B is functionalized with TGCG–, prisms presented edge on). In contrast, note that, for the same DNA sequences immobilized on AuNPs, "slipping" interactions occur (**Scheme 1B**). Black lettering indicates bases involved in normal Watson-Crick interactions and white lettering indicates bases that are not involved in hybridization. **B)** Melting transitions (monitored at 260 nm) for aggregates of DNA-Au triangular prisms functionalized with sequences containing 2 base pair recognition elements (TCG– or TGC–). Similar melting behavior also was observed at 900 nm.

To gain further insight into the role of base pair "slipping" in nanoparticle aggregation, the thermodynamic parameters (ΔH_{tot}, ΔG, ΔS, and K_{eq}) were explored. It is possible to calculate the total enthalpy (ΔH_{tot}) for an aggregate system by fitting the experimentally obtained melting profiles using the following equation:[46]

$$f = \frac{1}{1 + \exp\left(\left(\frac{\Delta H_{tot}}{R}\right)\left(\frac{1}{T} - \frac{1}{T_m}\right)\right)}$$

Where f is the fraction of the total aggregate in the dispersed state, R is the ideal gas constant in kcal/mol, T is the temperature in Kelvin (K) and T_m is the melting temperature of the nanoparticle

aggregate. Since the equilibrium binding constant (K_{eq}) equals:

$$K_{eq} = \exp\left(\left(\frac{\Delta H_{tot}}{R}\right)\left(\frac{1}{T} - \frac{1}{T_m}\right)\right)$$

the values of ΔH_{tot} (fitted) and the T_m (measured) can be used to calculate K_{eq} for a given temperature *T*. After determining the equilibrium binding constants for the given systems, we were able to calculate the change in Gibbs free energy (ΔG) of the system during the melting process:

$$\Delta G = -RT ln\, K_{eq}$$

Finally, the entropy (ΔS) of melting for the aggregated systems also can be determined at a given temperature, *T*. Selected results from these thermodynamic calculations are shown in Table 3.2 and a complete compilation of all the results is shown in Table 3.2 for all of the sequences tested.

Interesting insight into the system can be gained by analyzing these thermodynamic values (Table 3.2). First, the equilibrium binding constants (K_{eq}) obtained from the calculations (at 4 °C and 25 °C) accurately reflect the physical state (assembled or not) of the nanoparticles tested at these two temperatures (when $T = T_m$, $K_{eq} = 1$; assembled, $K_{eq} > 1$ or dispersed, $K_{eq} < 1$, Table 3.2). These equilibrium binding constants highlight the importance of the contributions from the base pair "slipping" interactions. In the most striking example, we find that the difference in K_{eq} between systems of particles functionalized with TCGC– and those functionalized with TGCG– (which have the same type of normal hybridization interactions but different "slipping" interactions) is ~ 1 x 10^{11} calculated at 4 °C (Table 3.2, Scheme 3.1A).

Further, one can see that, at room temperature, particles functionalized with TCGC– are not expected to form an assembled structure ($K_{eq} < 1$) while those functionalized with TGCG– will readily assemble ($K_{eq} > 1$). In conclusion, we have presented experiments that suggest that DNA strands chemically immobilized on gold nanoparticle surfaces can engage in two types of hybridization, one that involves complementary strands and normal base pairing interactions and a second one assigned as a "slipping" interaction, which can stabilize the aggregate structures through non-Watson Crick type base pairing or less complementary interactions than the primary interaction. The curvature of the particles is a major factor that contributes to these slipping interactions. Indeed, they are not observed with flat gold nanoprism conjugates of the same sequence. Further, when comparing the

Name	T_m (°C)	FWHM (°C)	ΔH_{tot} (kcal/ mol)	ΔS (4°C) (cal/ mol)	ΔS (25°C) (cal/ mol)	ΔG (4°C) (kcal/mol)	ΔG (25°C) (kcal/ mol)	K_{eq} (4°C)	K_{eq} (25°C)
TCG-	**14.8** ± 0.9	**3.2** ± 0.4	**-166.3** ± 8.4	**-538.0** ± 0.03	**-622.5** ± 0.03	**-6.3** ± 0.5	**5.9** ± 0.5	**8.6 x 10^{4}**	**5.0 x 10^{-5}**
TGC-	**19.9** ± 0.4	**5.1** ± 0.4	**-121.4** ± 13.3	**-400.1** ± 0.05	**-461.8** ± 0.05	**-6.6** ± 0.7	**2.1** ± 0.2	**1.5 x 10^{5}**	**2.7 x 10^{-2}**
TCGC-	**22.0** ± 0.7	**5.1** ± 0.3	**-118.6** ± 13.5	**-393.8** ± 0.05	**-454.1** ± 0.05	**-7.2** ± 0.9	**1.2** ± 0.1	**5.0 x 10^{5}**	**1.3 x 10^{-1}**
TGCG-	**39.5** ± 0.6	**3.4** ± 0.3	**-179.3** ± 12.3	**-629.3** ± 0.04	**-720.5** ± 0.04	**-20.4** ± 1.4	**-8.3** ± 0.6	**1.1 x 10^{16}**	**1.2 x 10^{6}**
TCGC--GCGT	**50.7** ± 0.4	**2.5** ± 0.7	**-320.7** ± 118.6	**-1161.2** ± 0.4	**-1324.2** ± 0.4	**-46.7** ±17.1	**-25.4** ± 9.4	**3.1 x 10^{36}**	**4.7 x 10^{18}**

Table 3.2. Thermodynamic values for Reaction 1 (Scheme 3.1A).

melting temperatures of aggregates of AuNPs to that of aggregates of nanoprisms functionalized with the same DNA sequences, we observe that the melting temperatures are much higher in the case of the nanoprism systems (even at a much lower salt concentration, Figure 3.3A, Figure 3.4B). The melting temperature is higher in the nanoprism system in part because the nanoprisms can only engage in the fully complementary base pairing interactions (no "slipping," Scheme 3.2B, Figure 3.4A) and have greater surface contact. Finally, we conclude that a hierarchy of binding strengths for a given set of complementary sequences or sequence functionalized structures can be defined where the overall stability of duplex strands (higher T_ms and effective association constants) goes as: free duplex DNA < free DNA and complementary DNA attached to a flat substrate (i.e. DNA monolayer) < curved or highly faceted polyvalent NPs linked by complementary duplex DNA < polyvalent NPs with large flat terraces linked by complementary duplex DNA (i.e., nanoprisms).

3.5 Conclusion

Presented in this chapter, are experiments that suggest that these curved particles can engage in two types of hybridization, one that involves complementary strands and normal base pairing interactions and second a "slipping interaction", which can stabilize the aggregate structures through non-Watson Crick type base pairing interactions. We compared various types of DNA-AuNPs that can slip to form different interactions showing that they do indeed have different thermodynamic parameters. Ultimately, we show that slipping interactions impart different measures of stability upon their respective nanoparticle aggregate systems.

CHAPTER FOUR

Duplex DNA as a Controllable Spacer for Nanoparticle Crystallization

Chapter 4: Duplex DNA as a Controllable Spacer for Nanoparticle Crystallization

4.1 Introduction

When the concept of programmable materials synthesis from oligonucleotide nanoparticle conjugates was first introduced, a goal was to be able to use DNA to direct the three-dimensional assembly of nanoparticles into discrete preconceived structures.[1] Early demonstrations focused primarily on the formation of amorphous polymers, where rough placement and periodicity of the particles was controllable.[1, 24] Later advances showed that crystallization might be possible and suggested that it might be viable to form different crystal structures from one type of nanoparticle building block but different sequences of DNA.[25, 26] Recently, both our group and the Gang group independently discovered different but related routes for using DNA linkers to effect the crystallization of polyvalent oligonucleotide gold nanoparticle conjugates (DNA-AuNPs).[27, 28] Both groups have shown that with different types of linkers, one can form either face-centered cubic (FCC) or body-centered cubic (BCC) unit cells with unit cell edge lengths as long as 39 nanometers (nm) and as little as 3% inorganic matter by volume. [27-29] In addition to controlling the type of crystal structure, one should, in principle, be able to systematically adjust the lattice constants of these structures by varying the length of oligonucleotide interconnects. Such adjustments would allow for a versatile method of modulating this novel crystalline material with highly tailorable architectural parameters using a single type of DNA-AuNP and the appropriate oligonucleotide linkers (Scheme 4.1C**)**. In this work, we explore that possibility and the consequences of changing oligonucleotide linker length on both the unit cell lattice parameters and the overall crystallinity of the resulting structures.

4.2 Materials

DNA functionalized gold nanoparticles (DNA-AuNPs) were prepared according to literature procedures using AuNPs obtained from BBInternational with an average diameter of 10.3 ± 1 nm. All oligonucleotides (Scheme 1) were synthesized on an Expidite DNA synthesizer and purified by HPLC. Briefly, hexyl-thiol terminated oligonucleotides (5′-HS-A_{10}-AAGACGAATATTTAACAA-3′) were added to the AuNPs at a ratio of 4 nmol per 1 mL of AuNPs. The A_{10} section allows for DNA strand flexibility, while the thiol is used to attach the DNA to the AuNP surface. These DNA-AuNP solutions were then slowly salted to final concentrations of 0.5M NaCl, 10mM sodium phosphate and 0.01% wt/vol SDS and subsequently washed five times (centrifugation at 15k RPM for 40 min, followed by removal of supernatant and resuspension in Nanopure 18.2 MΩ H_2O) to eliminate all unbound DNA from the DNA-AuNPs. UV-Vis absorption spectra for particles and DNA strands were measured on a Cary 100 and converted to concentration using Beer's Law and known extinction coefficients.

Each linker strand contained a 3′ terminus complimentary to the Au-bound DNA strands (5′-TTGTTAAATATTCGTCTT- 3′) and a self-complimentary 5′ GCGC terminus. The 5′ and 3′ ends of the oligonucleotide were connected by a sequence of repeated thymine bases flanked on either end by an adenine "wobble" base to allow DNA strand flexibility. The thymine sections were 13, 26, 39 and 52 bases in length—a fifth linker was synthesized without any additional thymines and with only one wobble base (X-Linker). 13, 26, 39 and 52 base poly-A sequences were synthesized to hybridize with these poly-T sequences to give the system rigidity. The duplex spacers containing the poly-A sequences and poly-T linkers were hybridized by heating them to 55 °C and slowly cooling to room temperature in 0.5 M NaCl, 10 mM H_xPO_4 0.01%

wt/vol SDS. These linker sequences were then added to the solutions of DNA-AuNPs in a 40 to 1 ratio, transferred to quartz capillaries and heated to 45 °C. The temperature was lowered at a rate of 0.1°C/minute until the sample reached 35°C, at which time it was imaged with small-angle x-ray scattering (SAXS).

The SAXS experiments were performed at the Dupont-Northwestern-Dow Collaborative Access Team (DND-CAT) Sector 5 at Argonne National Laboratory. Aqueous samples were placed in 2 mm quartz capillaries and inserted into the beamline equipped with a temperature controlling system; the temperature was controlled within 0.1 °C resolution. Two sets of slits were used to define and collimate a 0.3×0.3 mm^2 x-ray beam (wavelength = 1.03 Å) and a pinhole was used to remove parasitic scattering. Scattered radiation was detected with a CCD camera. The 2D scattering data were azimuthally averaged, and the resulting 1D profiles of scattered intensity as a function of scattering angle, 2θ, were transformed into profiles of scattered intensity as a function of scattering vector, $q(= 4\pi \sin\theta / \lambda)$, using silver behenate as a standard. Dark current subtraction and absorption corrections were applied to normalize the data. Although the scattering from the buffer and capillary are weak compared to the scattering from the gold nanoparticles, buffer data was still used to reduce the data to scattering patterns representative of the particles alone.

4.3 Results and Discussion

The inorganic building block for all experiments presented herein is a 10 nm AuNP functionalized with ~ 58 ± 5 hexyl-thiol terminated 28-mer oligonucleotides (See Supporting Information for detailed methods). To form the crystal structures, linker strands were designed,

Scheme 4.1. Materials Sequence and Design. A) Illustration of the three-dimensional arrangement of particles forming a face-centered cubic lattice showing the effect of increasing linker length on lattice parameters, B) sequences of oligonucleotides used to form the various N = X linkers ranging from 13 duplex spacers up to 52, C) sequences of oligonucleotides used to form the X-linker system.

each with a 3′ end sequence complementary to the Au-bound DNA, a poly(dT) sequence of varying length flanked on both ends by an adenine flexor (to allow DNA strand flexibility) and a self-complementary 5′ GCGC end. The poly(dT) sequences were 13, 26, 39 and 52 bases in length (Scheme 4.1A). To make the particle interconnects more rigid, these poly(dT) sequences were hybridized to complementary poly(dA) sequences of equivalent lengths. A fifth linker was synthesized without a poly(dT) sequence and only one flexor (X-Linker, Scheme 4.1B). Each duplex linker sequence was then added to a different solution of DNA-AuNPs in a 40 to 1 ratio, transferred to a quartz capillary, and heated to 45 °C. The temperature was lowered at a rate of 0.1 °C/min until the samples reached 35 °C, at which time they were characterized by small-angle x-ray scattering (SAXS, Figure 4.1A**)**. Previous work has shown that lowering the temperature of the solution containing the aggregates to approximately 5 °C below the melting transition (T_m) of the DNA interconnects and annealing at this temperature typically yields the most ordered FCC structures.[27]

The 1-dimensional SAXS data (azimuthally averaged intensity versus scattering vector q, Figure 4.1B) allows one to easily observe the effect of increasing linker length on these crystalline structures. For all experiments, $q = (4\pi \sin\theta)/\lambda$ (in 1/Å), where θ and λ are the scattering angle and wavelength of the x-ray used, respectively. The strong intensity of the first peak (moving out radially from the center) followed by a smaller shoulder and two peaks of similar intensity with their positions relative to that of the first peak (q^*) such that $q/q^* = 1, \sqrt{4/3}, \sqrt{8/3}, \sqrt{11/3}$ etc. (Figure 4.4) is indicative of a face-centered cubic arrangement. The 2-dimensional images for all N = X linker length FCC structures can be found in Figure 4.2A-F. As the length of DNA strands separating the particles gets larger, the scattering peaks shift to smaller q values (Figure 4.1B) as expected, since q is inversely proportional to the interparticle spacing (d-spacing) and values of q are as 1/Å.

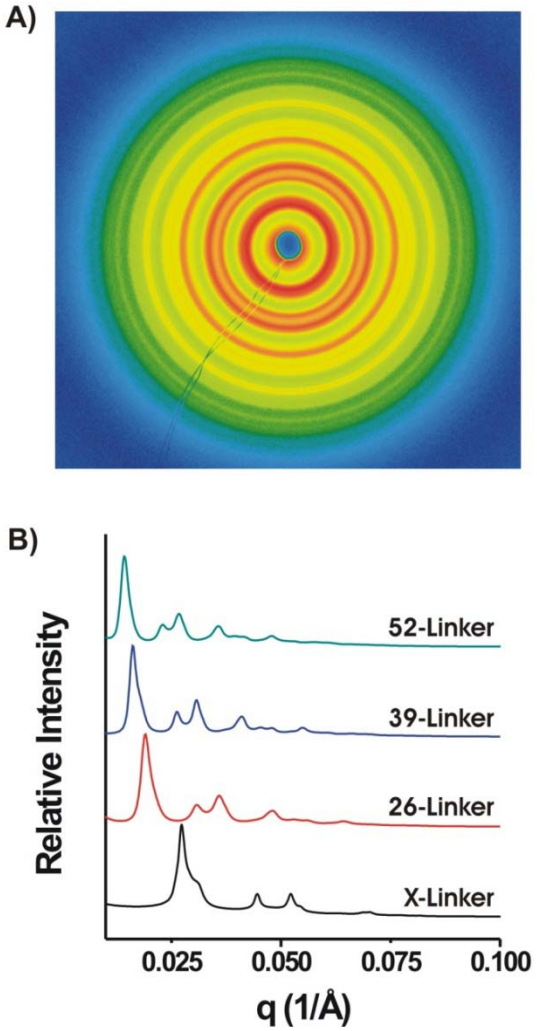

Figure 4.1 2-Dimensional and 1-Dimensional SAXS Data. A) 2-D data collected for the N = 39 linker system displayed in false **color, B) 1**-D line profiles of the 2-D data taken for the X-linker, N = 26, 39 and 52 systems demonstrating that the q* peak shifts to smaller values of q with increasing linker length. The 1-dimensional data for the N = 13 bp linker was not included in Figure 4.1B, as this structure could not be annealed at 35 °C due to the low melting temperature of the A13/T13 duplex region. When N = 13 aggregates were formed at room temperature and subsequently imaged, they did show an FCC structure, but not of the quality of the structures formed with the other linkers (Figure 4.2, 4.3)

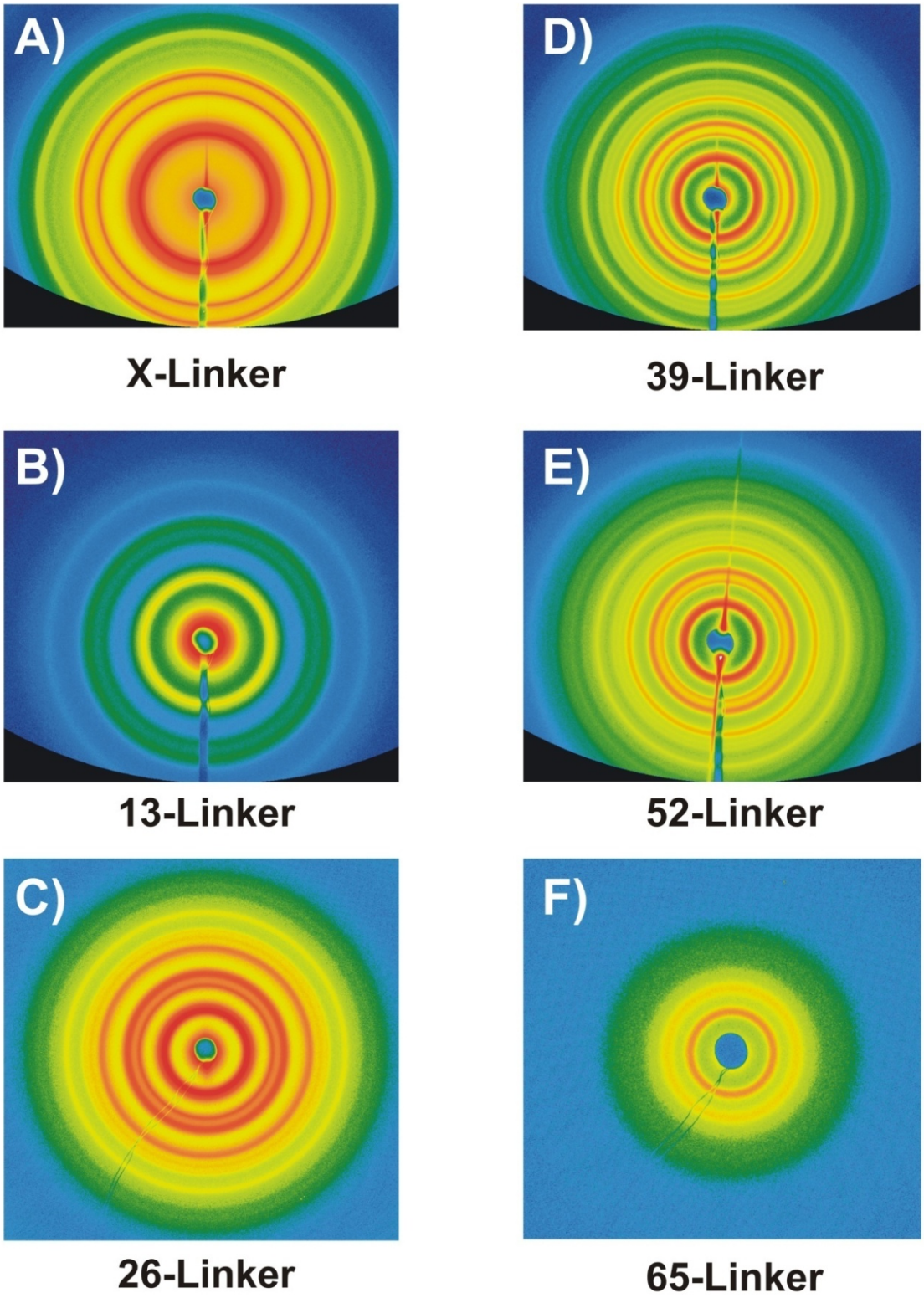

Figure 4.2 2-Dimensional SAXS Images for All Linkers. A) X-Linker, B) 13-Linker, C) 26-Linker, D) 39-Linker, E) 52-Linker, F) 65-Linker.

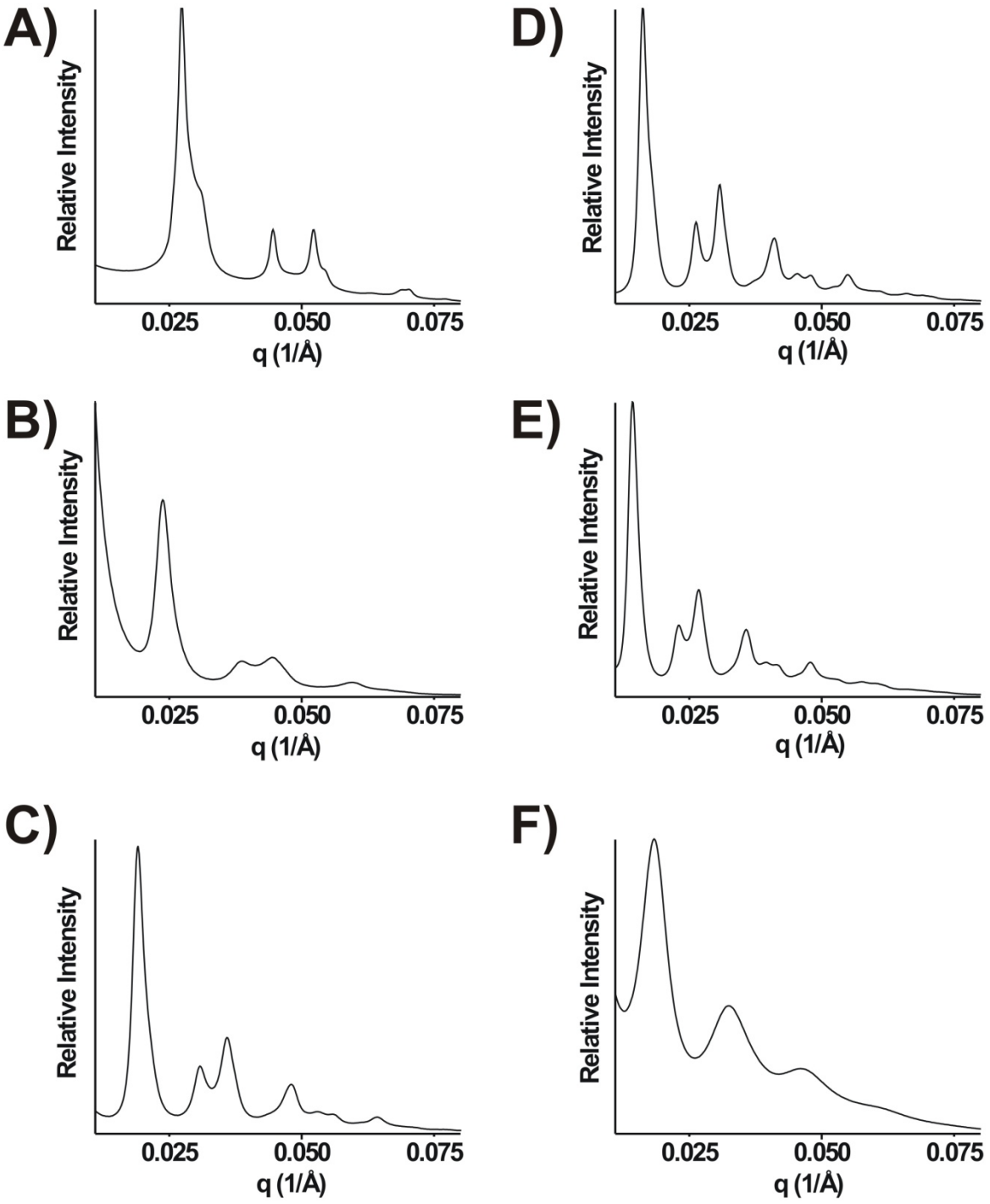

Figure 4.3 1-Dimensional SAXS Images for All Linkers. A) X-Linker, B) 13-Linker, C) 26-Linker, D) 39-Linker, E) 52-Linker, F) 65-Linker.

In analyzing the SAXS data, the position of the first order peak of the FCC unit cell (q*) equals $2\pi/d_{111}$, where d_{111} is the d-spacing of the 111 plane of the FCC crystal. The X-Linker (Figure 4.1B, black trace) shows the closest interparticle spacing and also the clearest delineation of the second peak (shoulder of the larger first peak). As the particle spacing increases, this shoulder can no longer be distinguished from the dominant first peak, (Figure 4.1B, red, blue, and green traces). However, increasing interparticle distance results in higher order scattering peaks observable at larger q values (Figure 4.1B, red, blue and green traces, Figure 4.2 and 4.3). These peaks are predicted by modeling[27] (Figure 4.4) but until now have never been observed for oligonucleotide gold nanoparticle crystals.

It is important to note that the existence of higher order peaks at longer linker lengths does not necessarily indicate larger or better quality FCC crystal structures. The appearance of these peaks is a result of the smaller q* values seen with increased interparticle distances. Intensities of peaks at higher q values are weaker because the detector does not efficiently measure scattering at q values larger than 0.06 $Å^{-1}$ for the 10.3 nm gold particles used in this work. For the range of linker lengths studied, this decrease in intensity results

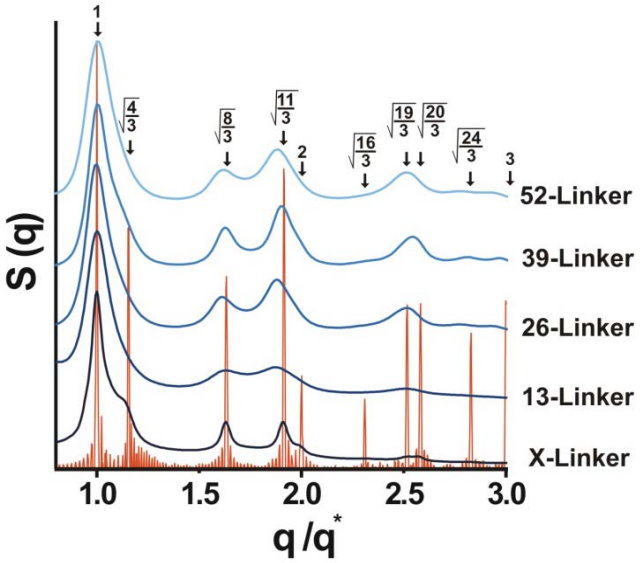

Figure 4.4 Correlating Linker Length with Crystal Quality**.** The orange trace represents the modeled SAXS scattering for a perfectly ordered FCC crystal. The blue traces are the experimental data for the various length linkers and the values above the arrows are the theoretical q/q^* peak locations. The strong correlation between simulated and experimental spectra confirms the presence of highly ordered FCC crystal structures.

in the obscuring of 5th order and higher (X-Linker) and 9th order and higher (52-Linker) peaks (Figure 4.4 and Figure 4.3 1A-1F). Therefore, crystal quality cannot be determined by the number of peaks, but rather by the peak widths, where narrow peaks indicate greater constraint of AuNP position. The data clearly show that shorter linker lengths produce more ordered crystals (Figure 4.4 and Table 4.1).

To determine the extent to which DNA linker strands control the interparticle spacing of the crystals, we plotted the total number of DNA bases between particles versus gold nanoparticle nearest neighbor spacing as measured by SAXS. The nearest neighbor spacing can be calculated with eq. 1:

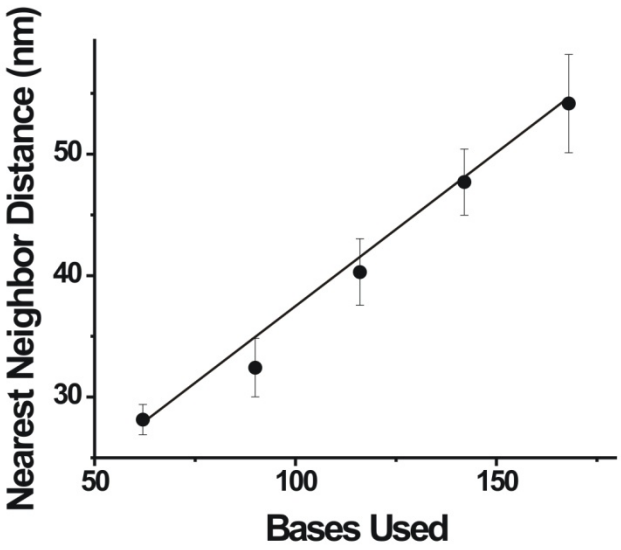

Figure 4.5 Interparticle Spacing as a Function of Total DNA Length. A plot of the gold nearest neighbor distances as a function of the total number of bases used to separate them.

$$D\,(\text{Å}) = \sqrt{6}\pi / q^{*} \qquad (1)$$

where D is the nearest neighbor spacing in Å. When these nearest neighbor spacings are plotted versus number of bases for the linkers, a linear trend is observed with an R^2 value of 0.987. The data follow eq. 2:

$$D\,(nm) = 0.255(nm)x + 11.1(nm) \qquad (2)$$

where D is the gold nanoparticle nearest neighbor distance in nm and x is the total number of bases between the gold nanoparticles. The Y-intercept of 11.1 nm can be attributed to the combined gold nanoparticle radii (~10.3 nm) and the two hexyl-thiol tethering moieties (~0.8 nm). The linearity of this equation allows one to easily design

oligonucleotide linker sequences to form crystals with desired nanoparticle spacings (Figure 4.5). From these measured interparticle distances, it is possible to express a structure's density as a percentage of space filled by the inorganic gold component using eq. 3:

$$\%\ Filled = \frac{4(\frac{4}{3}\pi r^3)}{a^3} * 100 \qquad (3)$$

where r is the radius of the gold nanoparticles in nm and a corresponds to the unit cell edge length in nm, calculated as $\sqrt{2}$ times D (the nearest neighbor distance). From our calculations, crystals with as little as 0.52% inorganic-filled space (in the case of the N = 52 linker) have been formed (Table 4.1). Moreover, we determined the size of the crystalline domains using the Debye-Sherrer formula (eq. 4):

$$t = 0.9\lambda / B\cos\theta \qquad (\mathbf{4})$$

where t is the diameter of the crystal in Å, λ is the wavelength of scattered light in Å, θ is the diffraction angle associated with the q* peak and B is the angular full width at half maximum of

Name	Nearest Neighbor Distance	Unit Cell Edge Length	Volume % Au	Aggregate Diameter	$\Delta q/q^*(\times 10^2)$
X-Linker	28.1 nm	39.8 nm	3.74%	957 nm	1.24
13-Linker	32.4 nm	45.9 nm	2.44%	586 nm	2.41
26-Linker	40.3 nm	57.0 nm	1.27%	769 nm	2.74
39-Linker	47.7 nm	67.5 nm	0.77%	1270 nm	2.72
52-Linker	54.2 nm	76.6 nm	0.52%	1100 nm	4.04

Table 4.1 Trends in FCC Crystal Parameters. Calculations illustrating the effect of DNA linker length on AuNP nearest neighbor distances, unit cell edge length, the percent of the unit cell filled by inorganic matter, aggregate diameter and overall crystal order expressed as a function of the full width at half maximum of the q* peak ($\Delta q/q^*$).

q*. From this analysis, the average diameters of the crystalline domains were determined to be approximately 957, 586, 769, 1270 and 1100 nm for the X, 13, 26, 39 and 52-linker systems, respectively (Table 4.1). An attempt was made to extend the series to an N = 65 linker; however, the aggregate structures did not have a clearly defined FCC unit cell (Figure 4.2F and 4.3F). Interestingly, although previous data from others have indicated that longer linker lengths lead to higher order crystals,[28] our data exhibit the opposite trend. The shorter lengths of duplex DNA provide the gold nanoparticles with less flexible interconnects (demonstrated by narrower peaks in the 1D spectra), as duplex DNA is known to be rigid up to approximately 50 nm.[30] Thus as the linker lengths grow, the nanoparticles become less spatially constrained relative to a perfect FCC lattice, leading to a broadening of the peaks observed for longer linkers as indicated by the $\Delta q/q^*$ values, (Table 4.1 and Figure 4.4).

4.4 Conclusion

In conclusion, through these experiments, we have shown that the use of duplex DNA as a programmable linker allows one to direct the interparticle spacing of bio-inorganic nanomaterials with a high degree of order. In addition to allowing one to program crystal structures with specific gold-gold particle distances and a desired percentage of inorganic-filled space, it should be possible to modify eq. 2 for particles of different sizes by adjusting the Y-intercept value to account for an increase or decrease in the radii of nanoparticle building blocks. Finally, the rules established herein for predicting lattice parameters and controlling general materials architecture should be extendable to assemblies composed of other DNA-modified inorganic, organic, and biological synthons.

CHAPTER FIVE

The Development of the Single Chain Bio-Barcode Assay

Chapter 5: The Development of the Single Chain Bio-Barcode Assay

5. 1 Introduction

The ability to detect biomarkers comprised of nucleic acids, proteins or small molecules at extremely low numbers is critical to the practice of diagnostic medicine, the identification of biological weapons, and fundamental life sciences research. These biological markers can indicate the onset of a neurodegenerative disease, an infection by a deadly microbe, or the environmental presence of a toxin. In medicine, high sensitivity detection is essential for early diagnosis, tracking therapeutic efficacy, and following disease recurrence.

The bio-barcode assay is a promising amplification and detection system that utilizes short oligonucleotides as target identification strands and surrogate amplification units in both protein and nucleic acid detection, [1, 2] (Scheme 5.1). The typical assay involves two types of

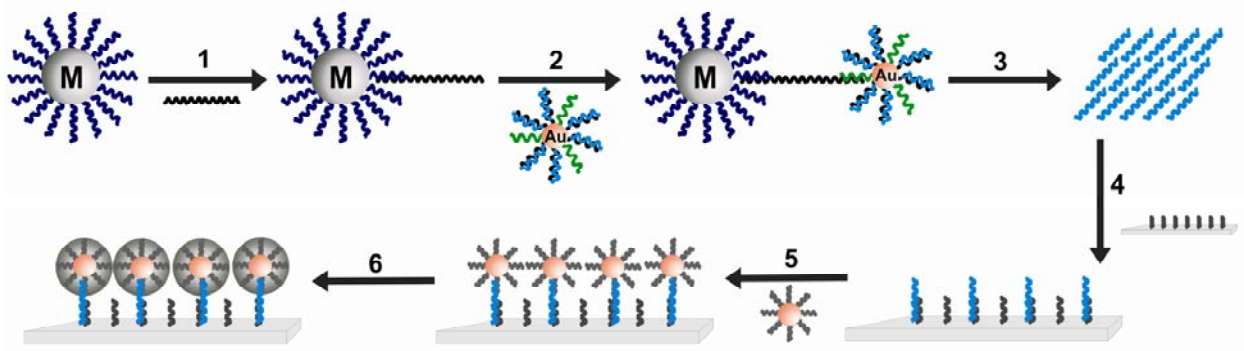

Scheme 5.1 Original Bio-Barcode Assay**.** Gold nanoparticle probe (red) requires three different oligonucleotide strands to accomplish target recognition and amplification.

particles. One particle is magnetic and has recognition elements for the target of interest covalently attached to its surface (Scheme 5.1, Step 1, M : magnetic). The second is a particle (e.g. a gold nanoparticle or a polymer microparticle) that has a recognition agent, which can sandwich the target with the magnetic particle (Scheme 5.1, Step 2). The second particle also

carries oligonucleotides covalently attached to its surface that support complementary oligonucleotides through Watson-Crick base pairing.[3] The hybridized oligonucleotides are the barcode strands. When the sandwich structures are formed, a magnetic field is used to localize and collect them (Scheme 5.1, Step 3). Excess sample is removed and then water or buffer at an elevated temperature is used to release and collect the barcode strands. The strands can be identified on a microarray via scanometric detection[4] with nanoparticle probes (Scheme 5.1, Step 4, 5 and 6), or *in situ* if the barcodes carry with them fluorescent markers.[5] The assay has exhibited low attomolar (aM) sensitivity for a variety of protein targets[1] and high zeptomolar (zM) sensitivity for nucleic acid targets[2] when paired with scanometric readout.

There are several notable features of the bio-barcode assay. With the impressive sensitivity demonstrated thus far, it has the potential to be an alternative to the polymerase chain reaction (PCR) for certain applications, especially those involving *in vitro* bio- and medical diagnostics.[6] Since the barcode oligonucleotides are used as surrogates in both protein and nucleic acid detection, it is a system capable of detecting both classes of targets on the same platform through multiplexing. With regard to proteins, it allows analysis of samples with target concentrations that are four to six orders of magnitude lower than what can be accessed with conventional Enzyme-Linked Immunosorbant Assays, (ELISAs).[1]

Although the barcode assay provides several significant new analytical capabilities, it is not yet in its optimal form. The current design, which typically employs gold nanoparticles (Au-NPs) as the barcode carrier, has several disadvantages. First, in the case of nucleic acid targets, *three* different oligonucleotides are required, which is synthetically demanding and costly. Second, it is difficult to achieve consistent and 100% barcode DNA loading on the support

strands attached to the Au-NP surface, through hybridization.[5] This inefficiency reduces the signal amplification possible and increases variability, limiting the quantitative capabilities of the assay. Third, changes in assay-specific buffer systems (e.g. salt concentrations, surfactants, buffering salts) can lead to changes in the hybridization efficiency of the barcode sequences to the Au-NP linked complements. Fourth, designing recognition sequences, barcode sequences, and barcode-support sequences that do not exhibit cross-reactivity, especially in the case of multiplexed analyte detection, becomes more difficult as the number of targets increases. As a means of addressing these drawbacks, we have designed a new bio-barcode assay that uses a single strand oligonucleotide barcode, which incorporates the recognition element and is terminated with an alkylthiol to generate Au-NP probes. This assay relies on a ligand-exchange process involving dithiothreitol DTT, Scheme 5.2), a common disulfide reducing agent[7] to liberate the covalently attached barcode sequences from the Au-NP probes for assay readout. DTT has been demonstrated to efficiently remove thiolated oligonucleotides from gold surfaces.[5, 8, 9] The major advantage of this novel DTT-induced barcode release system is that fewer oligonucleotides are required (*from 3 to 1*, Scheme 5.3), to prepare the Au-NP probes which makes this method less synthetically

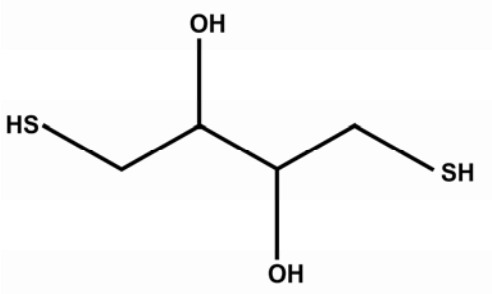

Scheme 5.2 Dithiothreitol Structure

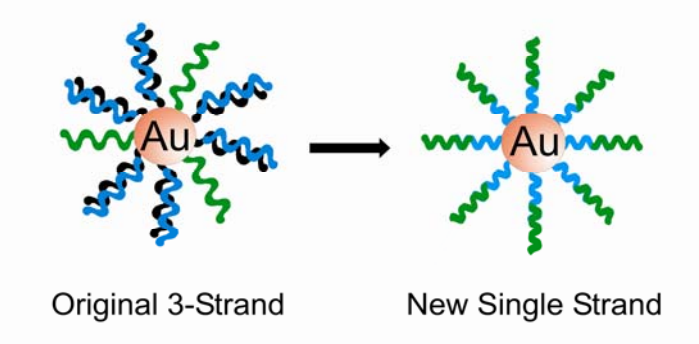

Scheme 5.3 Conversion of Au NP Probe from a 3-strand system to a one strand system.

challenging and particle probe preparation much simpler to perform. The utility of this new bio-barcode assay (Scheme 5.4) is demonstrated by detecting a mock mRNA target (3' poly-A single-stranded DNA) using both scanometric and fluorescent readouts. Furthermore, the ligand exchange method for releasing the barcodes increases the assay's reliability, while maintaining its high sensitivity. Finally, the DTT-based assay provides quantitative information over the low attomolar to mid-femtomolar (fM) target concentration range when coupled with the scanometric assay readout method.

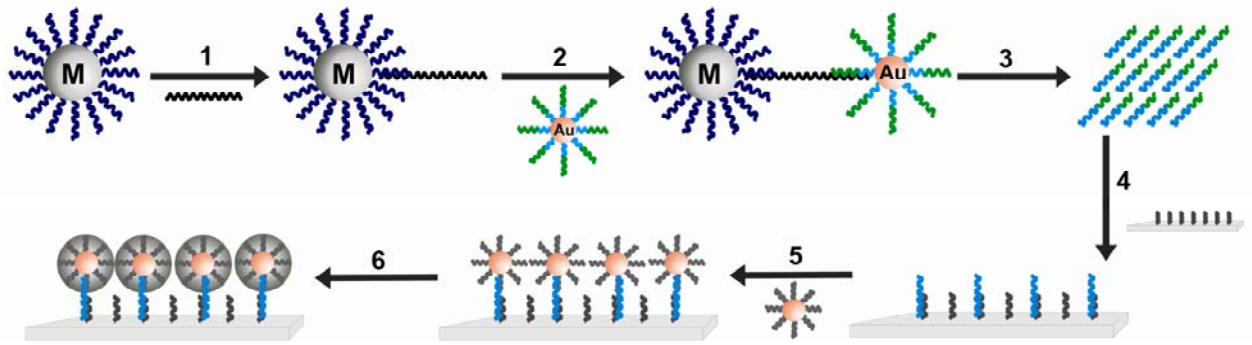

Scheme 5.4 Single Chain Bio-Barcode Assay. Magnetic microparticles (Mag) hybridize to specific targets. Gold nanoparticles (Au) surface-functionalized with target-specific probe strands, and thiolated barcode capture strands with hybridized barcodes, are then added which bind to a non-overlapping target region. After magnetic separation, the barcodes are liberated from the surface of the Au-NP by using DTT. Subsequently the barcodes are detected on the surface of a glass microscope slide using the scanometric method.

5.2 Materials

The oligonucleotides used in this work were synthesized, purified and characterized by Integrated DNA Technologies. The Codelink® microarray slides were purchased from G.E. Healthcare. The oligo-dT_{25} magnetic microparticles were purchased from Dynal Biotech/Invitrogen. All molecular biology grade reagents were purchased from Sigma-Aldrich and used as received. Hybridization gaskets and silver enhancement solutions were purchased from Nanosphere Inc. NANOpure® water (18MΩ, Barnstead Int.) was used for all experiments.

5.3 Experimental

5.3.1 Preparation of Citrate Stabilized Gold Nanoparticles

The preparation of gold colloids takes approximately three hours to complete and in synthetically simple. The process begins by thoroughly cleaning all glassware in aqua regia (3 HCl : 1 HNO_3), rinsing it water and over drying. Then a standard reflux apparatus is assembled and 500 mL of 1 mM Hydrogentetrochloroaurate (III) trihydrate in NANOpure water is brought to a vigorous reflux. To reduce the Au^{3+}, 50 mLs of 38.8 mM sodium citrate tribasic dehydrate in water is added rapidly while stirring. The solution will turn from pale yellow, to clear, to black, to violet to deep red in the course of a minute. Reflux for an additional 15 minutes, before cooling the gold nanoparticles to room temperature and filtering them to remove any large debris. Transmission Electron Microscopy and UV-vis spectroscopy are the best ways to characterize the gold nanoparticle size and dispersity.

5.3.2 Preparation of Gold Nanoparticle Probes

Au-NP probes were prepared according to literature procedures.[2, 3, 13] Briefly, 1 OD of freshly reduced thiolated DNA was added to 1 mL of gold nanoparticles (13 nm or 30 nm, 30 nm: Ted Pella, Inc.) and shaken gently overnight. The system was buffered to a phosphate concentration of 10mM (pH 7.0) including 0.1 percent sodium dodecyl sulfate (SDS). Over the course of three days, the sodium chloride concentration was brought to 0.15 M in a stepwise manner. Particles were then spun (13,000 RPM) and rinsed four times (10 mM sodium phosphate, 0.15M NaCl, 0.01% SDS, pH 7.4) to remove any unbound DNA.

5.3.3 Preparation of Oligonucleotide Arrays

N-hydroxysuccinimide (NHS) activated Codelink glass microarray slides (Amersham, G.E. Healthcare) were used to support spots of amine-terminated oligonucleotides complementary to the particle-bound barcode sequences (5' – GTT TGC CAG GTC TTC CCG –

(PEG Spacer 18)$_2$ – NH_2 – 3', Integrated DNA Technologies, Inc.) according to the manufacturer's protocol. The oligonucleotides were printed in triplicate using a GME 418 robotic pin-and-ring microarrayer (Affymetrix) or were obtained from Nanosphere, Inc (Northbrook, IL). Negative control sequences, non-complementary to the barcode DNA were printed on the array directly adjacent to the barcode-specific oligonucleotides (5' – NH_2 – (Peg Spacer 18)$_2$ – ATC CAG AAG AAC CAA TAA GAA GAT GAG GCA TAG – 3', Integrated DNA Technologies, Inc.).

5.3.4 Detection Protocol

In a typical experiment, 20 μL of pre-rinsed poly-dT(25) magnetic beads [10, 11] (5 mg/mL, Dynal Invitrogen Corp.) were added to a DNase/RNase free 1.5 mL non-stick microcentrifuge tube (Ambion, Inc.). Lysis Binding Buffer (30 μL, Dynal Invitrogen Corp.) and the mock mRNA target (10 μL) (5' - GTT TGC CAG GTC TTC CCG – PEG Spacer 18 – AAA AAA AAA AAA AAA AAA AAA AAA A - 3', Integrated DNA Technologies, Inc.) were added to the test solution. Serial dilutions of the target sequence were detected in parallel during a typical experiment. Negative control samples containing a non-complementary DNA sequence (86 fM, 5' - ACA CAA CTG TGT TCA CTA GCG TTG AAC GTG GAT GAA GTT G - 3', Integrated DNA Technologies, Inc.) were also conducted with each experiment. Hybridization between the 3'-poly-A portion of the target and the oligo(dT)$_{25}$ magnetic beads proceeded for one hour at 37 °C under gentle agitation. Magnetic beads were separated from the solution using a magnetic field and rinsed once with 75 μL Au-NP buffer (0.15 M NaCl, 0.01 M sodium phosphate, 0.1% SDS, pH 7.4). Magnetic particles were re-suspended in 40 μL of Au-NP buffer and 10 μL of target specific Au-NP probes (1 nM final concentration for 13 nm particles, 100 pM concentration for 30 nm particles). Au-NP probes were allowed to hybridize with the

complementary sequence bound to the magnetic particles for one hour at 37 °C while shaking gently. Using the magnetic separator, the reaction mixture was washed five times using 75 µL of the Au-NP buffer. Following the final wash, the mixture was re-suspended in 50 µL of freshly prepared Au-NP buffer containing 0.1 M DTT to release the thiolated oligonucleotide barcodes from the surface of the Au-NPs. Ligand-exchange was allowed to proceed for 45 minutes at 37 °C while shaking (in the case of fluorescence detection, the mixture was held for 15 minutes at 37 °C, and then 30 minutes at room temperature as the Alexa-488 dye is unstable at elevated temperature for a prolonged period of time). Magnetic particles were removed from the mixture using the magnetic separator. The supernatant containing free barcodes was placed in a clean microcentrifuge tube and centrifuged (13,000 RPM) for 30 minutes to remove any potential residual Au-NPs. The supernatant was then interrogated for the presence and quantity of bio-barcodes using either fluorescence or the chip-based scanometric assay.

5.3.5 Fluorescent Detection of Alexa-488 Labeled Barcode DNA

In the case of fluorescent detection of barcode DNA from assays using 13 nm and 30 nm Au-NP probes, the fluorescence intensity of the supernatant (100 µL sample: 50 µL from assay, 50 µL Au-NP buffer to bring to minimum volume) from each assay was measured using a fluorometer in a 96-well format (Molecular Devices, Gemini EM, bottom read mode). Target samples in a dilution series (amplified via the barcode approach), negative control samples, and a dilution series of free Alexa-488 labeled barcodes as a calibration standard were run on the same plate (Costar, 96 well, black/clear bottom). In addition, the number of barcodes on the surface of the Au-NPs (13 nm and 30 nm) was determined by exposing aliquots of Au-NP probes (13nm: 1 nM, 30 nm: 100 pM) to DTT at concentrations known to liberate the barcode oligonucleotides (0.1 M for 45 min). The fluorescence intensity of the solutions were measured at 517 nm using a

fluorescent plate reader and used to calculate the average number of barcodes per particle, based on a literature procedure for determining the surface coverage of oligonucleotides on gold nanoparticle probes.[5]

5.3.6 Scanometric Detection of Universal Barcode DNA

For scanometric barcode detection, DTT liberated barcodes (15 μL, 5' – CGG GAA GAC CTG GCA AAC –PEG Spacer 18 – AGC TAC GAA TAA – $(CH_2)_3$ – SH – 3', Integrated DNA Technologies, Inc.) in Au-NP buffer plus 0.1 M DTT were added to the microarray slide under hybridization wells (Nanosphere, Inc.). Barcode hybridization proceeded for one and a half hours at 37 °C in a humidity chamber. After hybridization, the slides were washed using Au-NP buffer (3 times at room temperature), and a solution of universal Au-NP probes (13nm, 5' – HS – $(CH_2)_6$ – AAA AAA AAA ATT ATT CGT AGC T – 3', Integrated DNA Technologies, Inc.) was added to the array using the hybridization wells (15 μL, 50 pM final universal probe concentration in Au-NP buffer). The universal probe was allowed to hybridize for 45 minutes at 37 °C. The slide was washed copiously, twice with 0.5 M $NaNO_3$ containing 0.02% Tween 20 and 0.01% SDS, and then with three washings in 0.5 M $NaNO_3$ (all at room temperature) to remove chloride ions and non-specifically bound universal Au-NP probes. Afterwards, the arrays were dried using a bench top spinner, silver enhancement solution (Nanosphere, Inc.) was added for Au-NP signal amplification (1 mL total volume/array, 5.5-minute development time). The reaction was terminated by washing the slides with NANOpure water (18 MΩ, Barnstead International) and spin-drying. Light scattering images from the silver enhanced assay regions of the substrate were recorded using the high-resolution Verigene ID system (Nanosphere, Inc.) or a conventional flatbed scanner. Quantification of spot intensity was performed using GenePix Pro 6 software (Molecular Devices).

5.4 Results and Discussion

5.4.1 Results of Fluorophore Labeled Barcode Assay

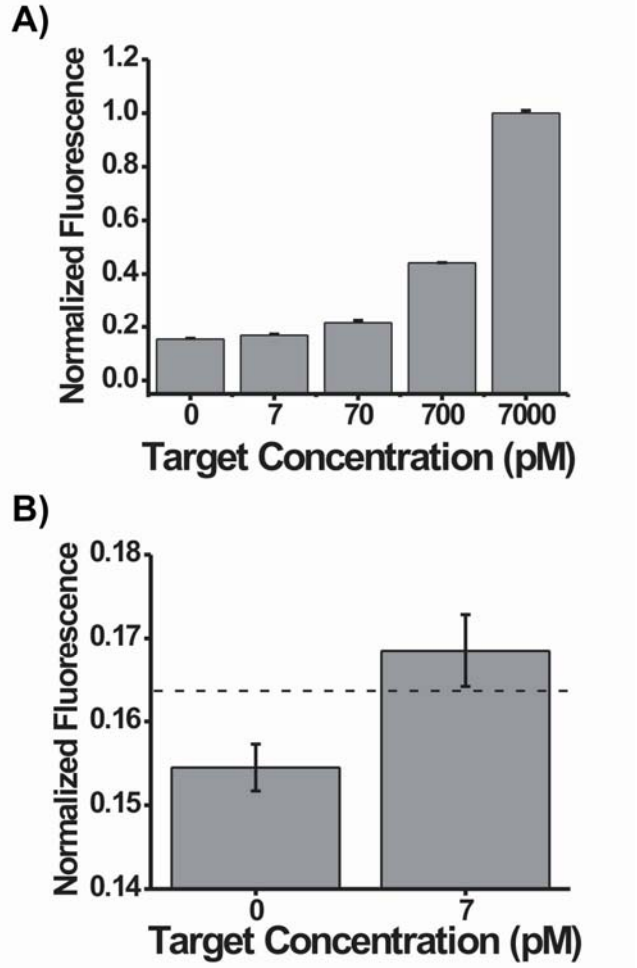

Figure 5.1 Fluorescence Bio-Barcode Assay Readout Using 30nm Au NP Probes. **A)** Shows the complete series of target concentrations tested. **B)** Shows the lowest concentration (7 pM) compared to the blank. The dashed line represents three times the standard deviation of the blank.

Through the use of fluorophore-labeled oligonucleotide barcodes, target concentrations in the low picomolar range could be detected using a fluorescent plate reader and the DTT-based bio-barcode assay. Due to the difference in number of barcodes carried by the 13 nm Au-NP probes and the 30 nm Au-NP probes, the detection limit of the 30 nm Au-NP probes (Figure 5.1, 7 pM) was slightly lower than what could reliably be achieved with the 13 nm Au-NP probes (Figure 5.2 B, 14 pM). To determine the lower limit of free barcode concentration that could be detected by fluorescence, the emission of the Alexa-488 modified barcode sequence (5' – CGG GAA GAC CTG GCA AAC – PEG Spacer 18 – TTT TT – Internal Alexa 488 – $(CH_2)_3$ – SH – 3', Integrated DNA Technologies, Inc.) at 517 nm, as a function of concentration, was measured using a typical calibration curve approach. The lowest detectable concentration was determined to be approximately 700 pM with a linear increase in fluorescence as a function of concentration (data not shown). Since 13 nm and 30 nm

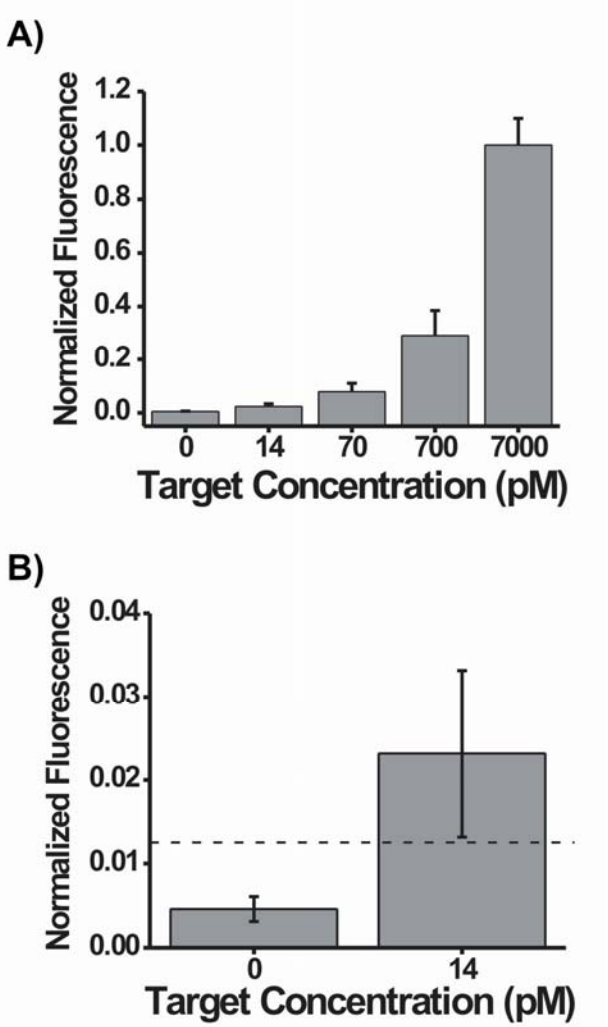

Figure 5.2 Fluorescence Bio-Barcode Assay Readout Using 13nm Au NP Probes. A**)** Shows the complete series of target concentrations tested. B) Shows the lowest concentration (14 pM) compared to the blank. The dashed line represents seven standard deviations above the blank.

Au-NP probes have on average 100 and 300 barcodes immobilized on their surfaces, respectively,[5] theoretically one could use the fluorescence-based bio-barode approach to detect targets in a sample that are as dilute as 7 pM for 13 nm Au-NP probes and 3 pM for 30 nm Au-NP probes. Due to a slight background associated with the negative controls (which were run with a highly mismatched target where no binding was expected), statistically significant detection limits are slightly higher than the theoretical lower limits. The measured signal at 7 pM target concentration shows no overlap with the negative control in the assays utilizing the 30 nm Au-NP probes. In fact, there are seven standard deviations (measured from control signal) that separate the first standard deviations for the two signals. For the assays with the 13 nm Au-NP probes, there was clear differentiation between the signal for the target at 14 pM and the negative control. In this case, the two signals were separated by six standard deviations as measured from the negative control. Of note is that while fluorescent barcode readout requires a fluorometer for assay analysis and sacrifices some sensitivity as

compared to the scanometric approach, it can be completed about three hours faster than the scanometric assay, which requires approximately six hours to complete.

5.4.2 Scanometric Detection of Barcode DNA

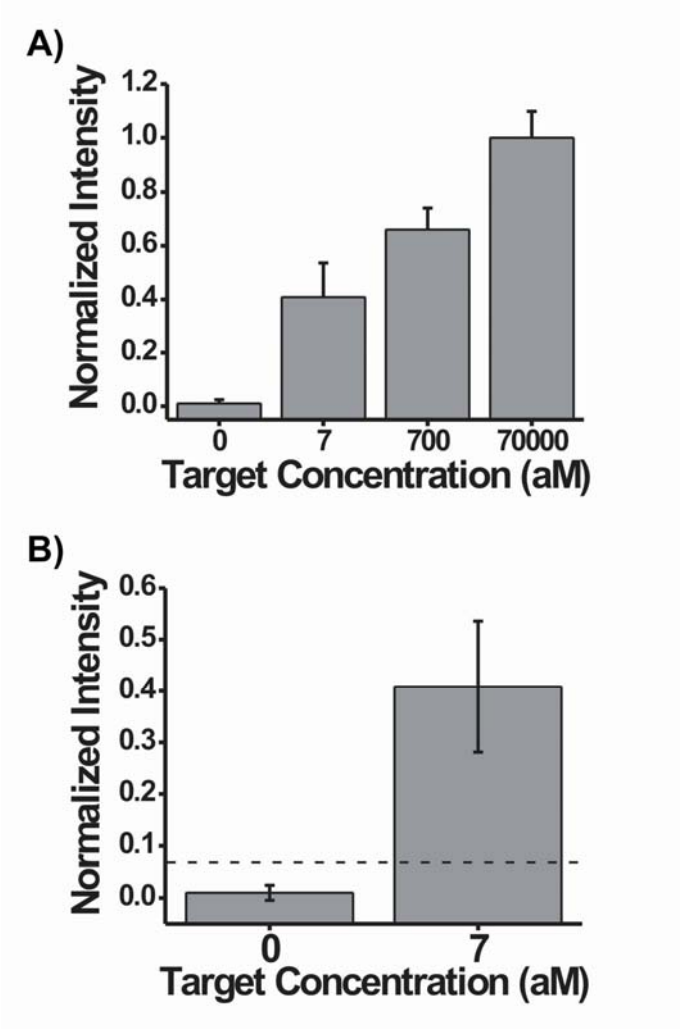

Figure 5.3 13nm Scanometric Readout of the Bio-Barcode Assay**.** A) Data showing the entire concentration range tested. B) A zoom in of the control and 7 aM data points, showing that the 7 aM signal is above the threshold of the control.

With either 13 nm or 30 nm Au-NP probes, the DTT-based bio-barcode assay is capable of detecting target concentrations down to 7 aM when coupled with the scanometric readout method (Figures 5.3 and 5.4). However, even without the barcode amplification, the scanometric method is capable of detecting free oligonucleotide targets with a sensitivity of 100 aM - 1 fM. The scanometric method itself is therefore approximately four orders of magnitude more sensitive than fluorescence in the configurations used for this work.[12, 13] Thus, using the DTT release approach, one would expect that 13 nm particles, each supporting ~100 barcodes[15], should result in a target detection limit between 1 - 10 aM. In order to test this hypothesis, we studied the assay over the 7 aM to 70 fM target concentration range. Indeed, as observed in Figure 5.3, the sensitivity of the DTT-based bio-barcode assay in conjunction with

the scanometric readout was 7 aM for the mock mRNA target. There was no observable hybridization between the released barcode sequences or the universal probe and non-complementary negative control sequences printed on the array, nor was there appreciable signal for the negative control samples involving the highly mismatched target (Figure 5.3). In fact, at 7 aM, the positive target signal and background signal as measured from the negative control are separated by approximately 20 standard deviations. Thirty nanometer Au-NP probes, each with ~300 barcodes, should perform comparable to, if not better than, 13 nm Au-NP probes because there should be a factor of three increase in amplification. Indeed, 30 nm particles exhibited a similar sensitivity over a comparable concentration range (Figure 5.4). The 30 nm Au-NP signal at 7 aM has larger error bars than the 13 nm data, because only three replicates were represented. In general, we found the 13 nm Au-NPs to be more stable than the 30 nm Au-NPs, and since the smaller particle probes offered adequate sensitivity, we did not further refine the assay based upon the 30 nm probes. In both cases, the error bars are disproportionately large at the lowest target concentration levels, which can be attributed to

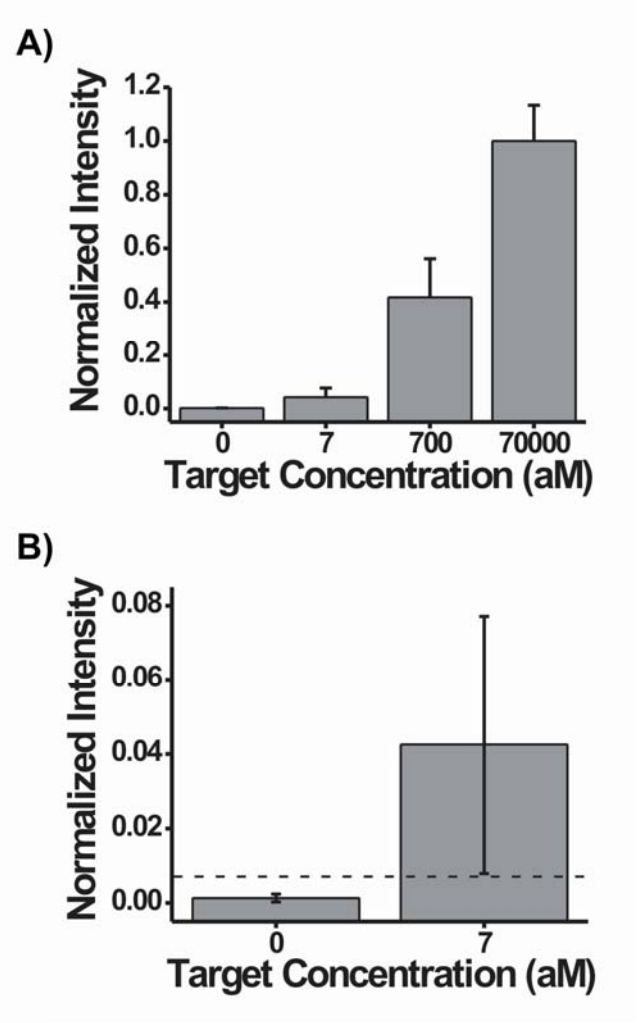

Figure 5.4 30nm Scanometric Readout of the Bio-Barcode Assay. A**)** Data showing the entire concentration range tested. B) A zoom in of the control and 7 aM data points, showing that the 7 aM signal is above the threshold of the control.

human error that can be expected in an assay with a number of manual steps. As the concentration of target decreases, such fluctuations have a larger impact on the detection error. These variances are important in that they can limit the assay sensitivity. Future automation of the assay should lead to an even greater degree of reproducibility, especially at the lowest concentrations. It was determined that the dynamic range of the DTT-based bio-barcode assay was in the 7 aM - 7 fM target concentration range. Between 7 fM and 70 fM and at higher target concentrations, the spot intensities become saturated. Over the full range of target concentrations studied, the free barcode DNA concentration would be expected to be between approximately 700 aM and 7 pM, assuming 100% target capture efficiency. The scanometric assay is known to work over this concentration range, and such capabilities have been demonstrated by our group and others.[4, 13, 14] Additionally, although more time consuming (approximately 6 hours), the bio-barcode assay coupled with the scanometric readout is at least five orders of magnitude more sensitive than fluorometric detection of oligonucleotides.

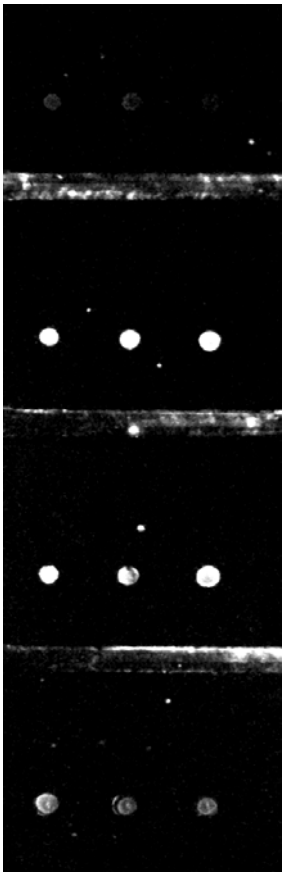

Figure 5.5 A Chip showing Concentration range with 13nm AuNPs. **Top**-Control, Next three from top to bottom 700, 70 and 7 aM

Finally, in the original bio-barcode assay, chip-to-chip comparison and quantification is cumbersome and can suffer from fluctuations in assay conditions, leading to nonlinear dose responses, (Representative Chip, Figure 5.5). Absolute limits of detection can be easily identified, but only semi-quantitative data can be extracted over a large concentration range. However, with the development of this DTT-based bio-barcode assay, chip-to-chip comparisons and signal quantification are now possible. In addition, the Au-

NP probes are more stable and reliable because the barcode strands are covalently attached to the gold particle surface as opposed to being hybridized to support strands. This new system allows for the comparison and quantification of data obtained on multiple days, with different batches of probes and buffers; thus greatly expanding the quantitative capabilities of the bio-barcode assay.

5.5 Conclusion

The bio-barcode assay is a powerful way of detecting nucleic acid sequences without the use of PCR for target amplification. Herein, we have reported the use of dithiothreitol (DTT) as a ligand-exchange method for liberating barcode sequences from Au-NP probes. The assay can be read using either fluorescence or scanometric method, with the latter providing a significant sensitivity advantage. Although fluorescence readout is not competitive with the scanometric method from a sensitivity standpoint, it can be completed faster and provides a basis for comparison that demonstrates the functional aspects of the assay in a more conventional format, and allowed us to determine the efficiency of the barcode removal process via DTT exchange. Using the scanometric readout method, we were able to demonstrate the high sensitivity of the DTT-based bio-barcode assay (7 aM), while maintaining the potential for assay multiplexing. In terms of copy number, the scanometric assay coupled with the DTT-based bio-barcode approach allows one to detect approximately 40 target strands in a 10 μL sample. Most notably, the new approach transforms the bio-barcode assay from a semi-quantitative to highly quantitative approach with a dynamic range that spans at least four orders of magnitude.

CHAPTER SIX

Non-Enzymatic Detection of Bacterial Genomic DNA using the Bio-Barcode Assay

Chapter 6: Non-Enzymatic Detection of Bacterial Genomic DNA using the Bio-Barcode Assay

6.1 Introduction

Polymerase chain reaction (PCR)-based amplification techniques[1-3] have become standard methodologies for the detection of nucleic acids.[4, 5] With the advent of quantitative real time PCR and variants of it such as reverse transcription PCR, one can now detect nucleic acid targets in a highly quantitative manner and assess important processes like gene expression.[6-10] Though there are many benefits to PCR such as sensitivity, production of a usable product fragment, and the ability to sequence that fragment, there are times when these features of PCR are not necessary and the cumbersome nature of PCR is a disadvantage. For example, in the case of point-of-care biological detection applications, where speed is critical and the enzymatic constraints and cost of PCR are limiting,[11] an enzyme-free approach could be a major advantage.

The recently developed bio-barcode assay for the detection of protein and nucleic acid targets is potentially capable of filling this void. This assay has several forms, [12-16] and has shown promise in the high sensitivity detection of protein and oligonucleotide targets. In addition, it has the ability to simultaneously detect many different targets in one sample.[17-19] Recently it has been adapted to a microfluidic chip-based format, an important step towards automation.[20] With respect to nucleic acids, thus far, all proof-of-concept work has involved short nucleic acids in very clean environments (buffer). The complexities of the target and sample media are often limiting factors for any nucleic acid assay, especially ones that rely on enzymes for amplification. This made us wonder if the bio-barcode assay could overcome such limitations. Herein, we describe the development of a new version of the bio-barcode assay that utilizes blocking strands to inhibit target rehybridization and allows one to detect double stranded genomic DNA at a

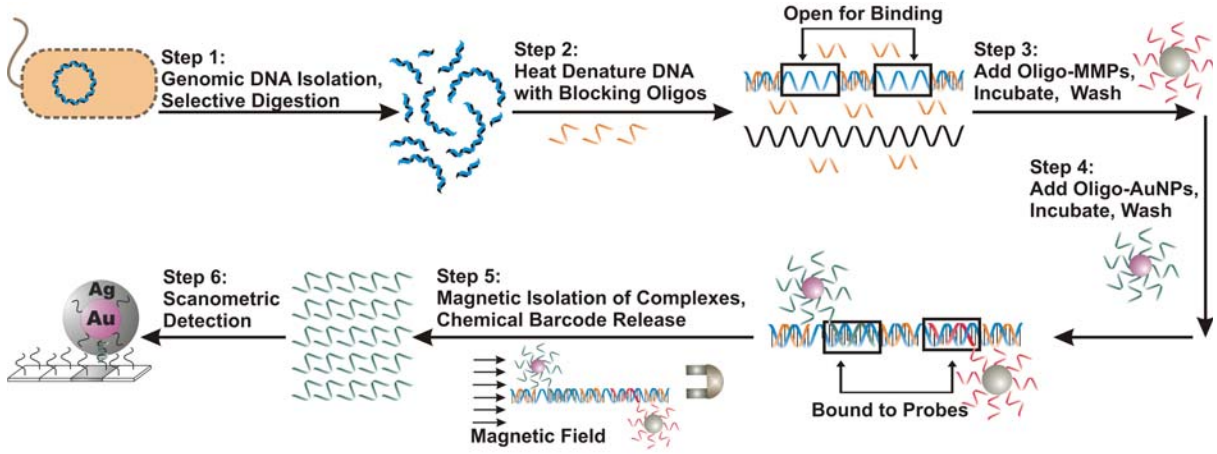

Scheme 6.1 Genomic Bio-Barcode Assay**.** The first step is to isolate the genomic DNA from the bacterial cells and cut it with a restriction enzyme. This cut prevents the DNA from super coiling during heating and gives smaller target pieces. The next step is to introduce blocking oligonucleotides designed to flank the probe binding sites and prevent strand rehybridization after thermal denaturation. The blocking oligonucleotides are used in excess to out compete the native strand during hybridization. The target region is now "propped" open and accessible for probe binding. Magnetic microparticles (oligo-MMPs) are used to capture the targets from the sample and then washed. An excess of oligonucleotide modified gold nanoparticle probes (oligo-AuNPs) is added to the assay solutions which results in the sandwiching of the target with the oligo-MMP. Unbound oligo-AuNPs are removed by washing. The barcodes are chemically released for scanometric detection and quantification.

limit-of-detection (LOD) of 2.5 fM ($7.5x10^4$ copies/50μL). Proof-of-concept studies in the context of *Bacillus subtilis* DNA detection are reported, (Scheme 6.1).

Gold nanoparticles heavily functionalized with oligonucleotides (oligo-AuNPs), are the cornerstone of the bio-barcode assay.[21] These oligo-AuNPs have a variety of attributes with respect to probe design. They are easily functionalized,[21] highly tailorable,[22, 23] remarkably stable,[24] catalytic,[25] and cooperative binders (they exhibit unusually sharp melting transitions when hybridized to complementary DNA).[26] These sharp melting transitions can confer a considerable selectivity advantage to the oligo-AuNPs over their PCR primer counterparts.[27] Oligo-AuNPs serving as amplification agents in the bio-barcode assay, through the chemical release of their oligonucleotide "barcodes," have several potential advantages over Taq-Polymerase or other DNA replication enzymes. For example, the oligo-AuNP probes are stable

for extended periods (greater than 6 months) at ambient temperature,[21] and are resistant to degredation,[28] while polymerases, like most enzymes, need to be stored at 4 °C or below. Oligo-AuNPs also function in a host of complex conditions such as sodium chloride concentrations up to 1 M,[29] different buffers such as Tris (2-Amino-2-(hydroxymethyl)-1,3-propanediol), Phosphate (Na_2HPO_4, NaH_2PO_4), Borate ($Na_2B_4O_7$), MOPS (3-(*N*-Morpholino)-propanesulfonic acid) and in the presence of metal ions or small molecules without adverse effects on their activity.[30-37]

The bio-barcode assay combines target specific oligo-AuNPs with a second homogenous capture agent (a magnetic microparticle functionalized with a different target specific oligonucleotide, oligo-MMP). The oligo-MMP is used to capture and isolate the target of interest from the sample solution, prior to the addition of the oligo-AuNPs. The MMP-target-AuNP complex allows for rapid isolation and subsequent washing prior to oligonucleotide barcode release. The barcodes can be easily detected via the Scanometric method, which exhibits an LOD for short purified oligonucleotides of 100 aM.[25, 38]

6.2 Experimental

6.2.1 Culture Media and Bacterial Strains

Routine growth and maintenance of *Bacillus subtilis 168* (American Type Culture Collection # 23857) was done in Luria-Bertani (LB) media (Fisher Scientific) and on solidified plates using LB agar (Fisher Scientific). All cultures were maintained at 30 °C on plates or in liquid form with shaking at 160 rpm and 30 °C. All growth media were sterilized by autoclave treatment prior to use.

6.2.2 Genomic DNA Isolation

B. subtilis cells were grown in 50 mL of liquid media in 125 mL flasks overnight and harvested after 10 hours of growth. The cells were split into two 25 mL aliquots and spun down at 8,000 rpm for 10 minutes. The supernatant was then removed, and the aliquots were resuspended in 5 mL of 50 mM Tris, 50 mM EDTA at pH 8.0 and frozen for no less than 1 hour at -20 °C. Frozen cells in a 50 mL conical tube were placed on ice, and 500 μL of 10 mg/mL lysozyme (Fisher Scientific) dissolved in 250 mM Tris, pH 8.2 were added to the tube. The cells-lysozyme mixture was allowed to slowly warm to room temperature over a two-hour period. Next, 1 mL of a 1 mg/mL solution of Proteinase K (Fisher Scientific) in 50 mM Tris, 0.4 M ETDA, 0.5 M SDS, pH 7.5 was incubated with the cells at 50 °C for 1 hour. Afterward, RNase A (1 μL, Ambion Inc./Applied Biosystems) was added to degrade all RNA contamination. Following RNA degradation, the genomic DNA was removed from the other cellular debris by phenol-chloroform extraction and ethanol precipitation. The integrity and size of the genomic

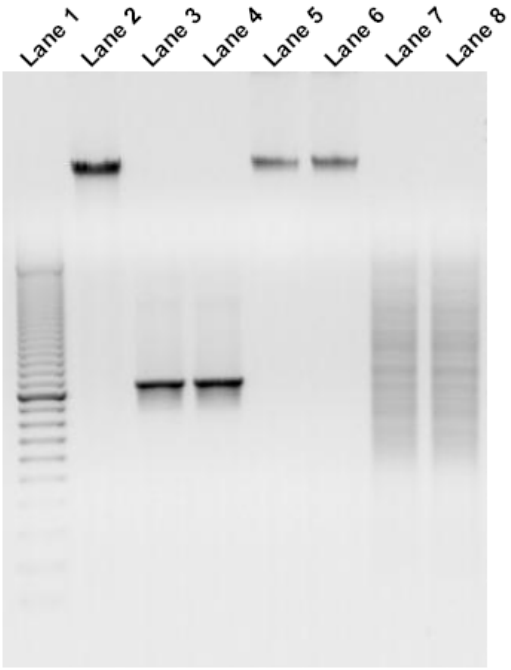

Figure 6.1 Nucleic Acid Testing**.**
Lane 1 – 100 bp PCR Ladder (BioRad)
Lane 2 – B.S. Genomic DNA (ATCC)
Lane 3 – PCR confirmation (ATCC)
Lane 4 – PCR confirmation (Mirkin)
Lane 5 – Genomic DNA (Mirkin)
Lane 6 – Genomic DNA (Mirkin)
Lane 7 – Digested DNA (HpyCH4V)
Lane 8 – Digested DNA (HpyCH4V)
Conditions:
1% Agarose, 1xTBE, 120V, 60 min.

DNA was confirmed by gel electrophoresis using a 1% agarose gel with ethidium bromide (Bio-Rad, ReadyAgarose™ Gels) with 1 x TBE (Tris, Boric Acid, EDTA) buffer at 120 volts for 1 hour. (Figure 6.1, lane 5/6) The size of the genomic DNA isolated was compared with commercially available DNA isolated by ATCC for *B. subtilis 168* (Figure 6.1, Lane 2).

6.2.3 Probe Design

Probes were designed from the alpha subunit of the tryptophan synthase gene (bp 2371552-2370749) from *Bacillus subtilis 168*. All probes were tested against the NCBI BLAST search engine, with the magnetic and gold probe sequences being unique to *B. subtilis*. Two of the three blocking sequences (center and 5') had a homology to one other organism, while the 3' blocker was specific only for *B. subtilis.* Probes were designed to fall within a region of the genome that could be cut easily with the restriction enzyme HpyCH4V (New England Biolabs). This was done to allow for de-circularization of the genomic DNA and prevention of super coiling during the heat denaturation step of the assay. Probe specificity was confirmed by routine Southern Blot analysis (data not shown). Oligonucleotide sequences are given in Table 6.1.

Table 6.1. Oligonucleotide Sequences

Name	Sequence
Forward Primer	5'-AGA CTC TAA TGC AGT CAC CAA CGC-3'
Reverse Primer	5'-TGC TCC CAA TAT AAC GTA TGC TGC-3'
Magnetic Probe	5'-HS- $(CH_2)_6$ -iSp18-CCG CAA TGA GTT CAA TTC ATC CGT GTA CCC-3'
Gold Probe	5'-AAG CCA TGA GGT GAC GTA TAT TTC TTT AGT-iSp9-AGC TAC GAA TAA-$(CH_2)_3$-SH-3'
Scanometric	5'-HS- $(CH_2)_6$ - AAA AAA AAA ATT ATT CGT AGC T–3'
Chip Capture	5'-ACT AAA GAA ATA TAC GTC ACC TCA TGG CTT-$(iSp18)_2$-NH_2-3'
Center Blocking	5'-TTG AAC AAG CCG AGG GGT TCG TCT ACT GTG TAT CT-3'
5' Blocking	5'-ATT GAC GGT CTG CTT GTT CCG GAT CTG CCA TTA GA-3'
3' Blocking	5'-TGT TCC GGT TGC TGT AGG GTT CGG TAT ATC AAA CC-3'
Melting Au NP	5'-HS-$(CH_2)_6$-A_{10}-AC TAA AGA AAT ATA CGT CAC CTC ATG GCT T-3'
Melting MMP	5'-HS-$(CH_2)_6$-A_{10}- GG GTA CAC GGA TGA ATT GAA CTC ATT GCG G-3'
AuNP Target (*trp1*)	5'-FITC-AA GCC ATG AGG TGA CGT ATA TTT CTT TAG T-3'
MMP Target (*trp 3*)	5'-FITC-CC GCA ATG AGT TCA ATT CAT CCG TGT ACC C-3'

iSpX = Polyethylene Glycol (X units of ethylene oxide)

6.2.4 Oligonucleotides

All specialty oligonucleotides were purchased from Integrated DNA Technologies (Coralville, IA) and were purified by HPLC. Standard desalting was used to purify PCR primers and blocking strands. Prior to use, the oligonucleotides were stored at - 80 °C in a dried state. Working solutions of the oligonucleotides were stored at - 20 °C.

6.2.5 Quantitative PCR

The copy number of genomic DNA per mL (isolated from *B. subtilis* cells) was determined using quantitative real-time PCR (qPCR). A LightCycler 2.0 instrument and LightCycler Software Version 4.0 (Roche Applied Sciences) were used to run the qPCR reactions and quantify the data respectively. Primers were designed to amplify a 1066 base pair fragment of the genomic DNA from *B. subtilis* (Table 6.1). A LightCycler FastStart DNA Master SYBR Green kit (Roche Applied Sciences) was used to generate the PCR reactions. Each PCR reaction was carried out in a 20 μL capillary (Roche Scientific) by placing the capillary tube in a cooling rack (4° C), combining and mixing the reagents in an eppendorf tube at 4°C, spinning the reactants into the capillary tubes, and thermally cycling. Since the real-time reporter used (SYBR Green) is an intercalating fluorophore where total fluorescence depends on product length, a standard curve for the qPCR had be constructed beforehand. To do this, end-point PCR was run using Qiagen's Taq PCR Master Mix following the manufacturer's protocol. During each amplification, primer concentrations of 0.5 μM were used with approximately 0.1 μg of template. The reactions were done in 100 μL PCR tubes in strips of 8 (Fisher Scientific) on a GeneAmp® PCR System (Applied BioSystems). The thermal profile consisted of an initial 8-minute denaturation step at 95 °C, followed by 45 cycles of denaturation at 95 °C for 55 seconds,

annealing at 52 °C for 45 seconds, and extension at 72 °C for 120 seconds. Following the 45 cycles, the product sequence was completed with an extension step at 72 °C for an additional 10 minutes. The PCR product size was confirmed by gel electrophoresis using a 1% agarose gel with ethidium bromide (Bio-Rad, ReadyAgarose™ Gels) with 1 x TBE (Tris, Boric Acid, EDTA) buffer at 120 volts for 1 hour (Figure S1, Lane 3/4). The remaining PCR product, not run on the gel, was purified using a MinElute PCR purification kit (Qiagen Inc.) following the manufacturer's instructions. The PCR product was quantified using UV-visible spectroscopy, and then was used to generate a standard curve for qPCR. (Figure 6.2)

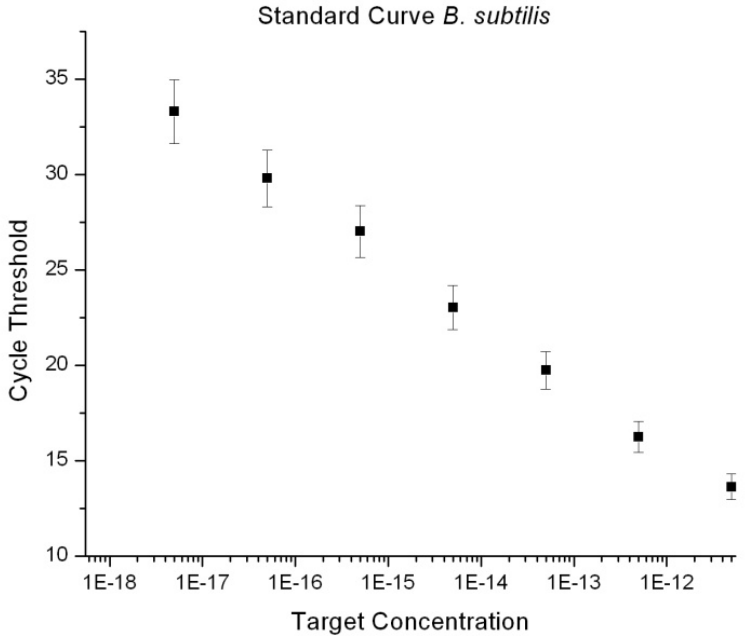

Figure 6.2 Standard curve for Real-Time PCR

6.2.6 Magnetic Particle Functionalization with DNA

Oligonucleotide-functionalized magnetic microparticles (Oligo-MMPs) were prepared according to literature procedures.[17, 39] Briefly, 2.8 μm amine-functionalized magnetic microparticles (Dynal Corp/Invitrogen) were coupled to thiolated oligonucleotide strands using

the hetero-bi-functional crosslinker sulfo-SMPB (Pierce Biotechnology). Unreacted amine sites were passivated with sulfo-NHS acetate (Pierce Biotechnology). Oligo-MMPs were stored at 4 °C in 10 mM phosphate buffered saline (0.15M NaCl, PBS) with 0.001% sodium azide as a preservative. Oligo-MMPs were washed three times with PBS prior to use in the assay.

6.2.7 Gold Nanoparticle Functionalization with DNA

Oligo-AuNP probes were prepared according to literature procedures.[39] Briefly, 4 nanomoles of freshly reduced thiolated DNA was added to 1 mL of 13 ± 2 nm gold nanoparticles and shaken gently overnight. The system was buffered to a phosphate concentration of 10 mM (pH 7.0) including 0.01 percent sodium dodecyl sulfate (SDS). Over the course of one day, the sodium chloride concentration was brought to 0.15 M in a stepwise manner. Particles were then spun (13,000 rpm) and rinsed four times (10 mM phosphate, 0.15 M NaCl, 0.01% SDS, pH 7.4) to remove any unbound DNA. Probes were stored in excess DNA until needed, at which time they were purified as described above.

6.2.8 Melting Analysis

In order to determine the maximum assay stringency, or the upper temperature limit to heat denature and eliminate non-specific hybridization events in solution, we determined the melting temperatures (T_m) for each of the probes (oligo-AuNP and oligo-MMP probe sequences) with their respective targets in a 1:1 ratio (**S**cheme 6.2). In a typical melting experiment, AuNPs were functionalized with a 5'-thiol-modified probe sequence (Table 6.1) and allowed to hybridize to one equivalent of a 5' Fluorescein (FITC)-modified complementary DNA sequence specific to the targeted regions within the tryptophan synthase gene (*trp 1*; AuNP target, *trp 3*; MMP target).

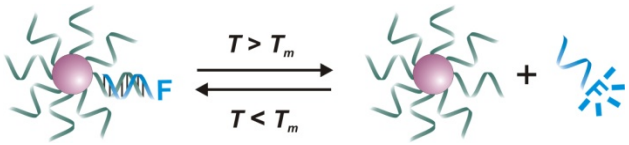

Scheme 6.2 Melting Analysis Set-Up

All experiments were allowed to equilibrate for over 24 h in 10 mM phosphate buffer, 0.15 M NaCl, 0.1% SDS, pH 7.4 (assay buffer) to ensure that equilibrium has been reached. Binding of the nanoparticle probes to a complementary target sequence modified with a molecular fluorophore resulted in quenching and decreased fluorescence intensity. Subsequent heating resulted in dissociation of the probe/target complex and a recovery of fluorescence intensity, providing a way to spectroscopically monitor the melting transition (**Figure 6.3**). Fluorescence measurements were performed on a Molecular Devices Gemini EM Microplate spectrofluorometer with temperature control. Comparison of the *trp 1* (Au NP) probe-target (T_m = 64.1 ± 0.5 °C) and *trp 3* (MMP) probe-target (T_m = 70.1 ± 1.1 °C) complexes after dissociation

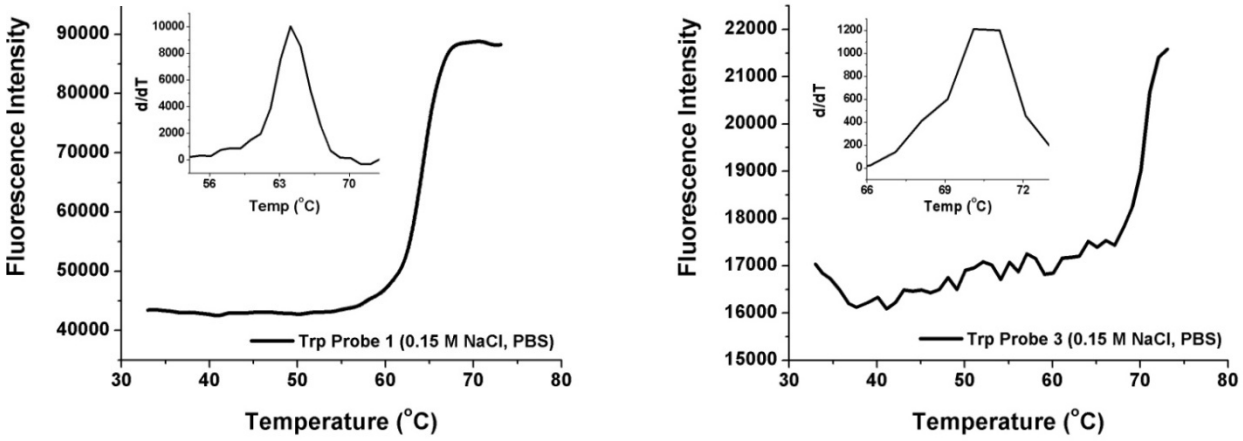

Figure 6.3 Probe Melting Analysis. A) Melting curve for the duplex formed between an oligo-AuNP probe and its fluorophore labeled complement (sequences given in Table 6.1) B) Melting curve for the duplex formed between the oligo-MMP probe and its fluorophore labeled complement (sequences given in Table 6.1). The fluorescence of the complementary strands is quenched when they are bound to the AuNP and is recovered when the duplexes melt with the fluorophore strand being released into solution.

revealed a difference of 6 ^{o}C in the T_m. The lowest T_m value was used to determine the thermal stringency for the assay. A temperature 14 °C below that lowest melting temperature (40 °C) was chosen to ensure that no probe-target complexes would dehybridize under stringent conditions.

6.2.9 Preparation of Oligonucleotide Arrays

N-hydroxy succinimide (NHS) activated Codelink glass microscope slides (Amersham Biosciences) were used to support microarrays of amine-terminated oligonucleotides complementary to the Au particle-bound barcode sequences and were prepared according to the manufacturer's protocol. The "capture" oligonucleotides were printed in triplicate using a GME 418 robotic pin-and-ring microarrayer (Affymetrix). The chips were allowed to couple overnight at 70% humidity, and were then passivated in 0.2 % SDS at 50 °C for 30 minutes to hydrolyze all unreacted NHS groups.

6.2.10 Genomic DNA Bio-Barcode Assay

Bacillus subtilis cells were isolated from culture by centrifugation, and the genomic DNA was isolated as described above using lysozyme and proteinase K. The genomic DNA was then cut using the restriction endonuclease HpyCH4V (New England Biolabs). A restriction digestion step was needed to prevent DNA super-coiling during the heating and subsequent detection. A dilution series of genomic DNA was made for testing with the bio-barcode assay. Additionally, an aliquot of the genomic DNA was quantified using qPCR as described above. Assays were assembled in nuclease free eppendorf tubes (Ambion Inc) containing 5 μL of genomic DNA sample, 1 μL of each blocking oligonucleotide (200 μM) and 32 μL of assay buffer. The assays were mixed thoroughly and placed at 95 °C for 10 minutes to denature the genomic DNA fragments. After 10 minutes, the temperature was lowered to 72 °C, and 10 μL of

oligo-MMPs (20 mg/mL) were added to each tube. The reactions were mixed well, and placed at 40 °C for 2 hours while mixing in an end over end manner to ensure that the oligo-MMPs did not settle. The oligo-MMPs with the target bound were then washed 3 times with 100 µL of assay buffer to remove all unbound nucleic acids and remaining components from the restriction digest. This step is especially important as DTT, which is used in the restriction buffer, can react with the oligo-AuNP probes in the next step. To the washed oligo-MMPs-target complexes 40 µL of assay buffer and 10 µL of 500 pM freshly cleaned oligo-AuNPs were added. The reactions were vortexed, and placed at 40 °C with end-over-end mixing for one hour. The reactions were then washed five times using 1000 µL of assay buffer to remove all unbound oligo-AuNPs. The supernatant was removed after the 5th wash and the complexes were resuspended in 50 µL of 0.5 M DTT in assay buffer. The tubes were then placed at 50 °C for 15 minutes, followed by 45 minutes 25 °C to liberate the thiolated oligonucleotide barcodes from the surface of the gold nanoparticle through ligand exchange.[14] Following barcode release, the oligo-MMPs were isolated using a magnet and the remaining supernatant was transferred to a new nuclease free eppendorf tube. Next, 15 µL of sample was pipetted into a slide chamber well (Nanosphere Inc) assembled on a chip prepared as described above. The barcode samples on the chip were heated to 60 °C and then allowed to hybridize to their complement for 1 hour at 37 °C while shaking at 120 rpm. The chips were then washed three times in assay buffer and reassembled with clean slide chambers. To each well 15 µL of universal probe solution (500 pM universal AuNP, 10% formamide in assay buffer) was added. The probes were allowed to hybridize for 45 minutes at 37 °C while shaking at 120 rpm. The gaskets were then removed and the slides were washed twice in 0.5 M $NaNO_3$, 0.2 % Tween 20, 0.1 % SDS, washed three times in 0.5 M $NaNO_3$ and

finally quickly dipped in cold (4 °C) 0.1 M $NaNO_3$. The slides were spun dry, and equal parts silver stain solution A and B (Nanosphere Inc.) were placed on top of the slide so that the entire surface was covered. The silver enhancement was carried out for 3 minutes before being terminated by washing with Nanopure® water (18 MΩ, Barnstead). The slide was dried and imaged using a high resolution Verigene ID (Nanosphere Inc.), and the spot intensity was analyzed using GenePix Software (Molecular Devices). A representative image of the data obtained from an assay (as displayed in false color using GenePix Software) can be seen in Figure 6.3A.

6.3 Results and Discussion

A typical assay was performed by digesting circular genomic DNA isolated from *Bacillus subtilis* cells with 1 unit of HpyCH4V to yield smaller linear DNA fragments, Scheme 1. In eppendorf tubes, 5 μL of target DNA at various concentrations, 1 μL of each blocking oligonucleotide (200 μM) and 32 μL of buffer, were mixed, and the target strands were denatured at 95 °C for 10 minutes. Following denaturation, the samples were cooled to 72 °C, and 10 μL of oligo-MMPs (20mg/mL) were added to the reaction vessel and placed on a rotating shaker at 40 °C for 2 hours to facilitate target capture. Following target capture, the samples were thoroughly washed to remove all contaminants, and the oligo-AuNP probes (500pM) were added to the assay. After hybridization for an hour at 40 °C, the sandwich complexes were washed extensively, and the barcodes were chemically (dithiothreitol, DTT) released for scanometric detection.[25] The slides after silver amplification were imaged with a Verigene ID system (Nanosphere Inc.), which records the scattered light from the silver amplified spots and provides quantitative information regarding the concentration of barcode oligonucleotides.

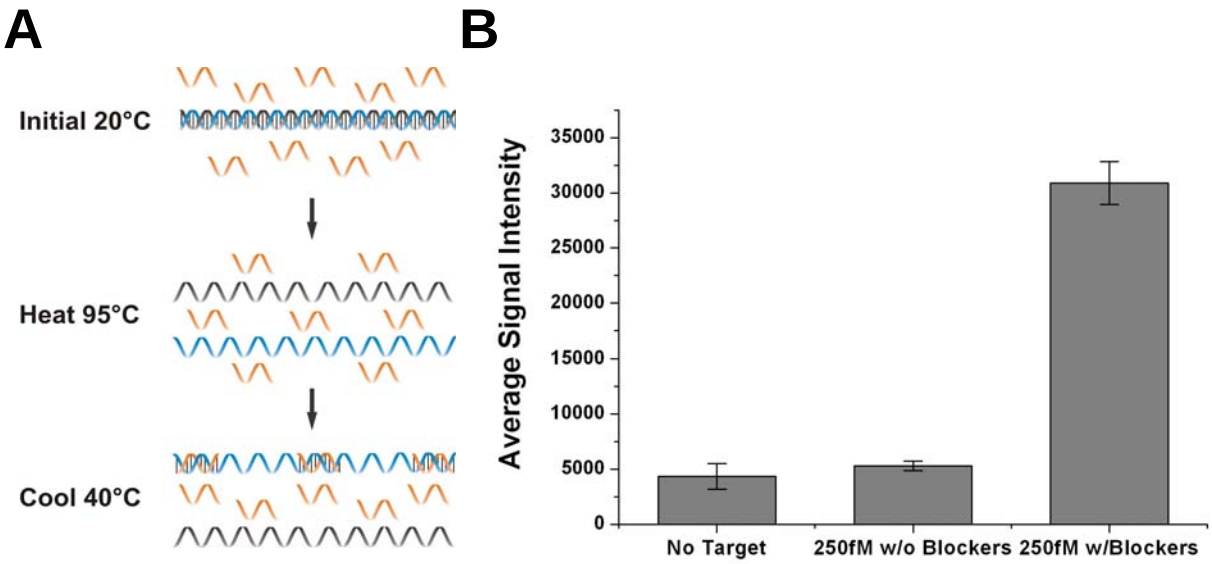

Figure 6.4 Blocking Oligonucleotide Functionality**.** A) Scheme showing how the blocking oligonucleotides are designed to prevent genomic DNA strand rehybridization. B) This graph shows the importance of the blocking oligonucleotides to the function of the bio-barcode assay. It is clearly seen that without blockers the signal obtained in the assay is the same as that with no target, while in the presence of blockers a large signal is obtained indicating that the genomic DNA is available for hybridization to probes.

To detect genomic DNA using the bio-barcode assay, separation of the duplex targets into their single strand forms is critical for probe binding. However, the conditions required to thermally denature DNA are very harsh (95 °C), and the oligo-MMPs (iron oxide nanoparticles embedded in a polymer scaffold) deteriorate under such conditions. Chemical denaturants are not an option, as they prevent the oligo-MMPs from hybridizing to the target as well. To overcome the challenge of denaturing DNA duplexes and keeping them apart long enough to allow the oligo-MMPs to hybridize required the implementation of blocking oligonucleotides, a modification of a strategy that has been used in scanning probe detection techniques.[40] These blocking oligonucleotides (blockers) consisted of three different 35 base pair sequences, designed to flank the particle probe binding sites. In the assay, the blockers were used in great excess (~1:10^6, target: blocker) to prevent strand rehybridization (Figure 6.4A).[40] When the duplex DNA is

heated to 95 °C with an excess of blockers, the duplex thermally denatures, and as the solution cools, the kinetics of blocker binding should be faster than that of native strand re-hybridization.[41] This should result in open regions of the duplex. To test this hypothesis we ran the bio-barcode assay under various conditions to determine the effectiveness of the blockers (Figure 6.4B). The left most sample labeled "no target" was run with digested λ-phage DNA as a negative control and 4 μM of each of the three blocking oligonucleotides. The sample in the center was run with 250 fM target only, and the third sample (far right) was run with 250 fM target and 4 μM of each of the three blockers. The impact of the blockers is significant. The signals obtained for the λ-phage DNA and the target without blocking strands fall within each other's standard deviations, while the target sample that contained the blockers shows a six-fold increase in signal. These experiments demonstrated that the blocking oligonucleotides are critical to the success of the bio-barcode assay's ability to detect genomic DNA.

In order to evaluate the sensitivity and dynamic range of the assay in the presence of blockers, a digestion mixture was diluted into a series of solutions. The bio-barcode assay is capable of detecting bacterial genomic DNA down to the low femtomolar concentration range, with a limit of detection of 2.5 fM (final concentration in the assay, 7.5×10^4 copies under the stated conditions, Figure 6.5). The row of spots labeled 250 fM clearly exhibits the most intense red color, indicating the strongest signal (Figure 6.5A). The spots at 25 fM target concentration show an orange/yellow color indicating a moderate to high signal intensity. The 2.5 fM spots show a yellow/green intensity, which is distinct from the blue color seen at the 0 fM (no target) row at the top of the slide. Additionally, the quantified data (5 independent experiments) presented in Figure 3.5B show that the signal at 2.5 fM is greater than three standard deviations

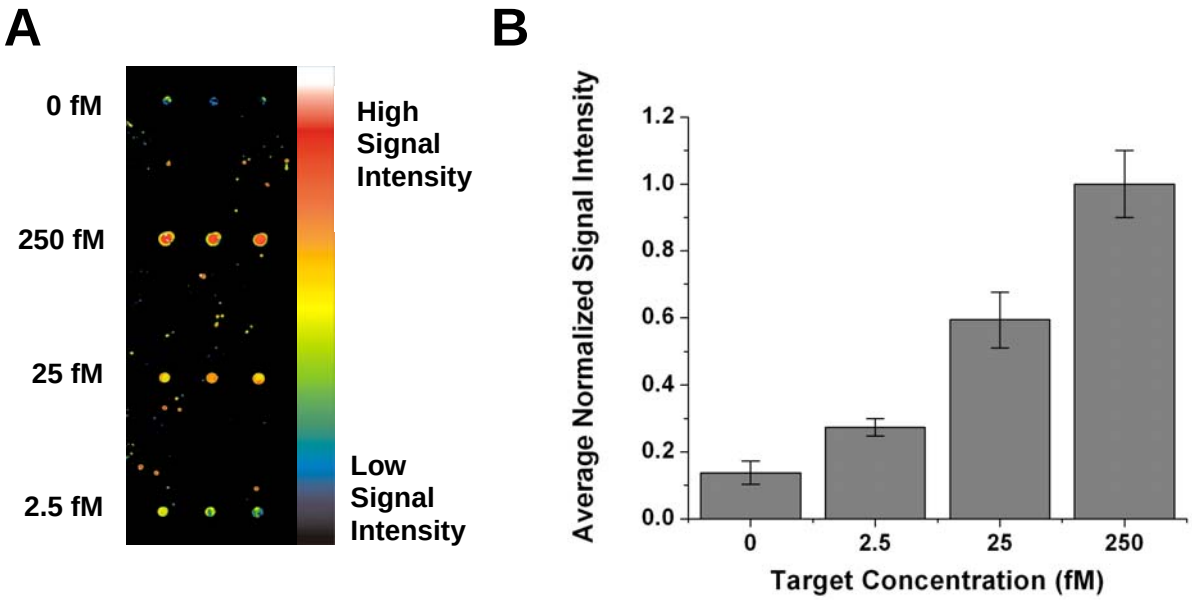

Figure 6.5 Genomic DNA Detection Results. A) This image is a representative slide from a single assay; showing that 2.5 fM is distinguishable from the 0 fM (no target) sample. The grey scale image from the Verigene ID is converted to color using GenePix 6.0 software (Molecular Devices**).** B) The data shown above is an average of 5 independent runs of the genomic DNA bio-barcode assay.

above the control signal. The normalized assay is log linear through the femtomolar concentration range, and becomes non-linear above 1 pM due to saturation of the scattering signal as read by the Verigene ID. This saturation issue can be easily solved by diluting the barcodes prior to their detection by the scanometric method, thereby allowing one to span the femtomolar and higher concentration range with this method.[25]

6.4 Conclusion

We have demonstrated the ability of the bio-barcode assay to detect bacterial genomic DNA with an LOD of 2.5 fM. The integration of blocking oligonucleotides proved to be a critical addition to the assay, which ultimately allowed for the detection of genomic duplex DNA isolated from *B. subtilis* cells. This work paves the way for the transition of the bio-barcode assay from a laboratory technique to one that can be deployed in the field for the rapid and

accurate detection of biological terrorism agents. *Bacillus subtilis* was chosen as a model system since it is a close family member of the lethal bacterium *Bacillus anthracis*, which in its spore form is the biological weapon Anthrax.[42] In the future, the bio-barcode assay may be coupled with automated field-deployable sample collection technologies to potentially produce a system for continuous biological surveillance.

REFERENCES AND NOTES

CHAPTER ONE

(1) Daniel, M.C.; Astruc, D. *Chem. Rev.* **2004**, 104, 293-364.

(2) H. Tait (ed.), "Five thousand years of glass", London: The British Museum Press, **1991**.

(3) Helcher, H.H. *Aurum Potabile oder Gold Tinstur*; J. Herbord Klossen: Breslau and Leipzig, **1718**.

(4) Antonii, F. *Panacea Aurea-Auro Patabile*; Bibliopolio Frobeniano: Hamburg **1618**.

(5) Kunckles, J. *Nuetliche Observationes oder Anmerkungen von Auro und Argento Potabili;* Schutzens: Hamburg, **1676**.

(6) Faraday, M. *Philos. Trans.,* **1857,** *147,* 141-181.

(7) Graham, T. *Philos. Trans. R. Soc.,* **1861,** *151,* 183-190.

(8) Turkevitch, J.; Stevenson, P.C.; Hiller, J., *Discuss. Faraday Soc.,* **1951,** *11,* 55-75.

(9) Bredig; *Z. Angew. Chem.,* **1898,** *11,* 951.

(10) Davies; *J. Physic. Chem.,* **1929,** *33,* 276.

(11) Weisner; *Inorganic Colloid Chemistry*, **1933,** *1*, 40.

(12) Garbowski; *Ber.,* **1903,** *36*, 1215.

(13) Ostwald; *Kleiner Praktikum der Kolloidchemie,* **1920,** 2nd Ed.

(14) Thiessen; *Z. Inorg. Chem.* **1929,** *180,* 57.

(15) Donau; *Monatsh*, **1905,** *25,* 525.

(16) Hauser and Lynn, *Experiments in Colloid Chemistry*, Mc Graw Hill, **1940**, 18.

(17) Frens, G.; *Nature Phys. Sci.* **1973,** *241,* 20-22.

(18) Mie, G,; *Ann. Phys.,* **1908,** *25,* 377-445.

(19) C. A. Mirkin, R. L. Letsinger, R. C. Mucic, J. J. Storhoff,; *Nature, **1996**, 382,* 607-609.

(20) Rosi, N.L,; Mirkin, C.A., *Chem. Rev.* **2005,** *105,* 1547-1562.

(21) Penn, S.G.; Lin, H.; Natan, M.J.; *Curr. Opin. Chem. Bio.*, **2003,** *7,* 609-615.

(22) Csáki, A.; Möller, R.; Fritzsche, W.; *Expert Rev. Mol. Diag.* **2002,** *2,* 89-94.

(23) Goodman, C.M.; Rotello, V.M.; *Mini-Reviews in Org. Chem.,* **2004,** *1,* 103-114.

(24) Buckle, P. E.; Davies, R. J.; *Biosenor. Bioelec.* **1993**, *8*, 355-363.

(25) Rosi, N.L.; Giljohann, D.A,; Thaxton, C.S.; Lytton-Jean, A.K.R.; Han, M.S.; Mirkin, C.A.; *Science,* **2006,** 312, 1027-1030.

(26) Kirchner, C.; Liedel, T.; *el al. Nano Lett.*, **2005,** *5* , 331 -338.

(27) Male, K. B.; Lachance, B.; *et al. Anal. Chem.,* **2008,** 80, *14*, 5487–5493.

(28) Lyon, L. A.; Musick, M. D.; Natan, M. J.; *Anal. Chem.,* **1998**, *70*, 5177-5183.

(29) Nice, E. C.; Catimel, B.; *Bioessays,* **1999**, *21*, 339-352.

(30) Silin, V.; Plant, A.; *Trends in Biotech.* **1997**, *15*, 353-359.

(31) Taton, T.A.; Mirkin, C. A.; Letsinger, R. L.; *Science,* **2000**, *289*, 1757-1760.

(32) Lytton-Jean, A. K. R.; Mirkin, C. A.; *J. Am. Chem. Soc.* **2005**, *127*, 12754-12755.

(33) Xu, J.; Craig, S. L.; *J. Am. Chem. Soc.,* **2005**, *127*, 13227-13231.

(34) Elghanian, R.; Storhoff, J. J.; Mucic, R.C.; Letsinger, R.L.; Mirkin, C.A.; *Science* **1997**, *277*, 1078-1081.

(35) Storhoff, J. J.; Lazarides, A. A,; Mucic, R. C.; Mirkin, C. A.; Letsinger, R. L; Schatz, G. C.; *J. Am. Chem. Soc.,* **2000**, *122*, 4640-4650.

(36) Park, S-J.; Lazarides, A. A.; Mirkin, C. A.; Letsinger, R. L. *Angew. Chem., Int. Ed.* **2001**, *40*, 2909-2912.

(37) Park, S. J.; Lazarides, A. A.; Storhoff, J. J.; Pesce, L.; Mirkin, C. A. *J. Phy. Chem. B* **2004**, *108*, 12375-12380.

(38) Park, S. Y.; Lytton-Jean, A. K. R.; Lee, B.; Weigand, S.; Schatz, G. C.; Mirkin, C. A. *Nature* **2008**, *451*, 553-556.

(39) Nykypanchuk, D.; Maye, M. M.; van der Lelie, D.; Gang, O. *Nature* **2008**, *451*, 549-552.

(40) R. C.; Wu, G. S.; Li, Z.; Mirkin, C. A.; Schatz, G. C.; *J. Am. Chem. Soc.,* **2003**, *125*, 1643-1654.

(41) Storhoff, J. J.; Elghanian, R.; Mucic, R. C.; Mirkin, C. A.; Letsinger, R. L; *J. Am. Chem. Soc.,* **1998**, *120*, 1959-1964.

(42) Li, H. X.; Rothberg, L.; *Proc. Nat. Acad. Sci.* **2004**, *101*, 14036-14039.

(43) Li, H. X.; Rothberg, L.; *J. Am. Chem. Soc.,* **2004**, *126*, 10958-10961.

(44) Liu, J. W.; Lu, Y.; *J. Am. Chem. Soc.,* **2003**, *125*, 6642-6643.

(45) Liu, J. W.; Lu, Y.; *Anal. Chem.,* **2004**, *76*, 1627-1632.

(46) Huang, C. C.; Huang, Y. F.; Cao, Z. H.; Tan, W. H.; Chang, H.T.; *Anal. Chem.,* **2005**, *77*, 5735-5741.

(47) Storhoff, J. J.; Lucas, A. D.; Garimella, V.; Bao, Y. P.; Muller, U. R.; *Nat. Biotech.* **2004**, *22*, 883-887.

(48) Han, M. S.; Lytton-Jean, A. K. R.; Oh, B. K.; Heo, J.; Mirkin, C.A.; *Angew. Chem. Int. Ed.,* **2006**, *45*, 1807-1810.

(49) Schena, M.; Shalon, D.; Davis, R. W.; Brown, P. O.; *Science,* **1995**, *270*, 467-470.

(50) He, L.; Musick, M. D.; Nicewarner, S. R.; Salinas, F. G.; Benkovic, S. J.; Natan, M. J.; *J. Am. Chem. Soc.,* **2000**, *122*, 9071-9077.

(51) Yguerabide, J.; Yguerabide, E. E.; *J. Cell. Biochem.,* **2001**, 84, *S31,* 71-81.

(52) Yguerabide, J.; Yguerabide, E. E.; *Anal. Biochem.,* **1998**, *262*, 137-156.

(53) Taton, T. A.: Lu, G.; Mirkin, C. A.; *J. Am. Chem. Soc.,* **2001**, *123*, 5164-5165.

(54) Park, S. J.; Taton, T. A.; Mirkin, C. A.; *Science* **2002**, *295*, 1503-1506.

(55) Cao, Y. W. C.; Jin, R. C.; Mirkin, C. A.; *Science* **2002**, *297*, 1536-1540.

(56) Storhoff, J. J.; *et al. Biosen. Bioelec.,* **2004**, *19*, 875-883.

(57) Bao, Y. P.; *et al. Nuc. Acid. Res.,* **2005**, 33, *2*, e15.

(58) Patolsky, F.; Lichtenstein, A.; Willner, I.; *J. Am. Chem. Soc.,* **2000**, *122*, 418-419.

(59) Patolsky, F.; Ranjit, K. T.; Lichtenstein, A.; Willner, I.; *Chem. Comm.,* **2000**, 1025-1026.

CHAPTER TWO

(1) Alivisatos, P.,. *Nat. Biotech.* **2004,** 22, *1*, 47-52.

(2) Daniel, M. C.; Astruc, D., *Chem. Rev*. **2004,** 104, *1*, 293-346.

(3) Niemeyer, C. M., *Angew. Chem. Int. Ed*. **2001,** 40, *22*, 4128-4158.

(4) Rosi, N. L.; Mirkin, C. A., *Chem. Rev.* **2005**, 105, *4*, 1547-1562.

(5) Chang, M. M. C.; Cuda, G.; Bunimovich, Y. L.; Gaspari, M.; Heath, J. R.; Hill, H. D.; Mirkin, C. A.; Nijdam, A. J.; Terracciano, R.; Thundat, T.; Ferrari, M., *Current Opinion Chem. Biol.* **2006**, 10, *1*, 11-19.

(6) Taton, T. A.; Mirkin, C. A.; Letsinger, R. L., *Science* **2000**, 289, *5485*, 1757-1760.

(7) Rosi, N. L.; Giljohann, D. A.; Thaxton, C. S.; Lytton-Jean, A. K. R.; Han, M. S.; Mirkin, C. A., *Science* **2006**, 312, *5776*, 1027-1030.

(8) Giljohann, D. A.; Seferos, D. S.; Patel, P. C.; Millstone, J. E.; Rosi, N. L.; Mirkin, C. A.,. *Nano. Lett.* **2007**, 7, *12*, 3818-3821.

(9) Lytton-Jean, A. K. R.; Mirkin, C. A., *J. Am. Chem. Soc.* **2005**, 127, *37*, 12754-12755.

(10) Hurst, S. J.; Lytton-Jean, A. K. R.; Mirkin, C. A., *Anal. Chem.* **2006**, 78, *24*, 8313-8318.

(11) Luedtke, W. D.; Landman, U., *J. Phys. Chem.* **1996**, 100, *32*, 13323-13329.

(12) Luedtke, W. D.; Landman, U., *J. Phys. Chem. B.* **1998**, 102, *34*, 6566-6572.

(13) Bloomfield, V. A. C., D. M.; Tinoco, J. I., Nucleic Acids: Structures, Properties, and Functions. University Science Books: Sausalito, CA, 2000.

(14) Smith, S. B.; Cui, Y.; Bustamante, C., *Science* **1996**, 271, *5250*, 795-799.

(15) Banholzer, M. J.; Li, S.; Ketter, J. B.; Rozkiewicz, D. I.; Schatz, G. C.; Mirkin, C. A., *J. Phys. Chem C.* **2008**, 112, *40*, 15729-15734.

(16) Lee, J.-S.; Seferos, D. S.; Giljohann, D. A.; Mirkin, C. A., *J. Am. Chem. Soc*. **2008**, 130, *16*, 5430-5431.

(17) Bao, Y. P.; Huber, M.; Wei, T. F.; Marla, S. S.; Storhoff, J. J.; Muller, U. R., *Nuc. Acids. Res.* **2005**, 33, *2,* 883-887.

(18) Dillenback, L. M.; Goodrich, G. P.; Keating, C. D., *Nano. Lett.* **2006**, 6, *1*, 16-23.

(19) Elghanian, R.; Storhoff, J. J.; Mucic, R. C.; Letsinger, R. L.; Mirkin, C. A., *Science* **1997**, 277, *5329*, 1078-1081.

(20) Huang, C. C.; Huang, Y. F.; Cao, Z. H.; Tan, W. H.; Chang, H. T., *Anal. Chem*. **2005**, 77, *17*, 5735-5741.

(21) Witten, K .G., Eckert, T., Richtering, W., Simon, U. *Phys. Chem. Chem. Phys.* **2008**, 10, 1870 - 1875.

(22) Kim, A. J.; Biancaniello, P. L.; Crocker, J. C. *Langmuir* **2006**, 22, *5*, 1991-2001.

(23) Liu, J. W.; Lu, Y., *J. Am. Chem. Soc.* **2003**, 125, *22*, 6642-6643.

(24) Nykypanchuk, D.; Maye, M. M.; van der Lelie, D.; Gang, O., *Nature* **2008**, 451, *(7178,* 549-552.

(25) Park, S. Y.; Lytton-Jean, A. K. R.; Lee, B.; Weigand, S.; Schatz, G. C.; Mirkin, C. A., *Nature* **2008**, 451, *7178*, 553-556.

(26) Sam, M.; Boon, E. M.; Barton, J. K.; Hill, M. G.; Spain, E. M., *Langmuir* **2001**, 17, *19*, 5727-5730.

(27) Beaucage, S. L.; Caruthers, M. H., *Tet. Lett.* **1981**, 22, *20*, 1859-1862.

(28) Martin, C. R., Nanomaterials: A Membrane-Based Synthetic Approach. **1994**; 266, 1961-1966.

(29) Routkevitch, D.; Bigioni, T.; Moskovits, M.; Xu, J. M., *J. Phys. Chem.* **1996**, 100, *33*, 14037-14047.

(30) Love, J. C.; Estroff, L. A.; Kriebel, J. K.; Nuzzo, R. G.; Whitesides, G. M., *Chem. Rev.* **2005**, 105, *4*, 1103-1169.

CHAPTER THREE

(1) Mirkin, C. A.; Letsinger, R. L.; Mucic, R. C.; Storhoff, J. J., *Nature* **1996**, *382*, 607-609.

(2) Niemeyer, C. M., *Angew. Chem. Int. Ed.* **2001**, *40*, 4128-4158.

(3) Storhoff, J. J.; Mirkin, C. A., *Chem. Rev.* **1999**, *99*, 1849-1862.

(4) Daniel, M.-C.; Astruc, D., *Chem. Rev.* **2004**, *104*, 293-346.

(5) Hayat, M. A., *Colloidal Gold: Principles, methods, and applications*. Academic Press: San Diego, 1989.

(6) Alivisatos, A. P.; Johnsson, K. P.; Peng, X.; Wilson, T. E.; Loweth, C. J.; Bruchez, M. P.; Schultz, P. G., *Nature* **1996**, *382*, 609-611.

(7) Park, S. Y.; Lytton-Jean, A. K. R.; Lee, B.; Weigand, S.; Schatz, G. C.; Mirkin, C. A., *Nature* **2008**, *451*, 553-556.

(8) Nykypanchuk, D.; Maye, M. M.; Lelie, D. van der; Gang, O., *Nature* **2008**, *451*, 549-552.

(9) Niemeyer, C. M.; Simon, U., *Eur. J. Inorg. Chem.* **2005**, 3641-3655.

(10) Dillenback, L. M.; Goodrich, G. P.; Keating, C. D., *Nano Lett.* **2006**, *6*, 16-23.

(11) Witten, K. G.; Bretschneider, J. C.; Eckert, T.; Richtering, W.; Simon, U., *Phys. Chem. Chem. Phys.* **2008**, *10*, 1870 - 1875.

(12) Kim, A. J.; Biancaniello, P. L.; Crocker, J. C., *Langmuir* **2006**, *22*, 1991-2001.

(13) Medley, C. D.; Smith, J. E.; Tang, Z.; Wu, Y.; Banrungsap, S.; Tan, W., *Anal. Chem.* **2008**, *80*, 1067-1072.

(14) Nam, J.-M.; Thaxton, C. S.; Mirkin, C. A., *Science* **2003**, *301*, 1884-1886.

(15) Liu, J. W.; Lu, Y., *J. Am. Chem. Soc.* **2003**, *125*, 6642-6643.

(16) Liu, J. W.; Lu, Y., *Anal. Chem.* **2004**, *76*, 1627-1632.

(17) Alivisatos, P., *Nature Biotech.* **2004**, *22*, 47-52.

(18) Huang, C. C.; Huang, Y. F.; Cao, Z. H.; Tan, W. H.; Chang, H. T., *Anal. Chem.* **2005**, *77*, 5735-5741.

(19) Lee, J.-S.; Han, M. S.; Mirkin, C. A., *Angew. Chem. Int. Ed.* **2007**, *46*, 4093-4096.

(20) Han, M. S.; Lytton-Jean, A. K. R.; Oh, B.-K.; Heo, J.; Mirkin, C. A., *Angew. Chem. Int. Ed.* **2006**, *45*, 1807-1810.

(21) Rosi, N. L.; Mirkin, C. A., *Chem. Rev.* **2005**, *105*, 1547-1562.

(22) Storhoff, J. J.; Marla, S. S.; Bao, Y. P.; Hagenow, S.; Mehta, H.; Lucas, A.; Garimella, V.; Patno, T.; Buckingham, W.; Cork, W.; Muller, U. R., *Biosens. Bioelectron.* **2004**, *19*, 875-883.

(23) Storhoff, J. J.; Lucas, A. D.; Garimella, V.; Bao, Y. P.; Muller, U. R., *Nature Biotech.* **2004**, *22*, 883-887.

(24) Taton, T. A.; Mirkin, C. A.; Letsinger, R. L., *Science* **2000**, *289*, 1757-1760.

(25) Katz, E.; Willner, I., *Angew. Chem. Int. Ed.* **2004**, *43*, 6042-6108.

(26) Niemeyer, C. M.; Ceyhan, B.; Hazarika, P., *Angew. Chem. Int. Ed.* **2003**, *42*, 5766-5770.

(27) Maxwell, D. J.; Taylor, J. R.; Nie, S., *J. Am. Chem. Soc.* **2002**, *124*, 9606-9612.

(28) Dai, Q.; Liu, X.; Coutts, J.; Austin, L.; Huo, Q., *J. Am. Chem. Soc.* **2008**, *130*, 8138-8139.

(29) Giljohann, D. A.; Seferos, D. S.; Patel, P. C.; Millstone, J. E.; Rosi, N. L.; Mirkin, C. A., *Nano Lett.* **2007**, *7*, 3818-3821.

(30) Rosi, N. L.; Giljohann, D. A.; Thaxton, C. S.; Lytton-Jean, A. K. R.; Han, M. S.; Mirkin, C. A., *Science* **2006**, *312*, 1027-1030.

(31) Seferos, D. S.; Giljohann, D. A.; Rosi, N. L.; Mirkin, C. A., *ChemBioChem* **2007**, *8*, 1230-1232.

(32) Hill, H. D.; Macfarlane, R. J.; Senesi, A. J.; Lee, B.; Park, S. Y.; Mirkin, C. A., *Nano Lett.* **2008**, *8*, 2341-2344.

(33) Storhoff, J. J.; Lazarides, A. A.; Mucic, R. C.; Mirkin, C. A.; Letsinger, R. L.; Schatz, G. C., *J. Am. Chem. Soc.* **2000**, *122*, 4640-4650.

(34) R. A. Reynolds, III.; Mirkin, C. A.; Letsinger, R. L., *J. Am. Chem. Soc.* **2000**, *122*, 3795-3796.

(35) Elghanian, R.; Storhoff, J. J.; Mucic, R. C.; Letsinger, R. L.; Mirkin, C. A., *Science* **1997**, *277*, 1078-1081.

(36) Hurst, S. J.; Hill, H. D.; Mirkin, C. A., *J. Am. Chem. Soc.* **2008**, *130*, 12192-12200.

(37) Millstone, J. E.; Park, S.; Shuford, K. L.; Qin, L.; Schatz, G. C.; Mirkin, C. A., *J. Am. Chem. Soc.* **2005**, *127*, 5312-5313.

(38) Hurst, S. J.; Lytton-Jean, A. K. R.; Mirkin, C. A., *Anal. Chem.* **2006**, *78*, 8313-8318.

(39) Millstone, J.E.; Georganopoulou, D. G.; Xu, X.; Wei, W.; Li, S.; Mirkin, C. A., *Small* **2008**, in press.

(40) Demers, L. M.; Mirkin, C. A.; Mucic, R. C.; R. A. Reynolds, III.; Letsinger, R. L.; Elghanian, R.; Viswanadham, G., *Anal. Chem.* **2000**, 5535-5541.

(41) Li, Z.; Mirkin, C. A., *J. Am. Chem. Soc.* **2005**, *127*, 1170-1178.

(42) Seela, F.; Jawalekar, A. M.; Anup, M.; Chi, L.; Zhong, D., *Chem. Biodivers.* **2005**, *2*, 84-91.

(43) Wu, Z.-S.; Guo, M.-M.; Shen, G.-L.; Yu, R.-Q., *Anal. Bioanal. Chem.* **2007**, *387*, 2623-2626.

(44) Saenger, W., *Principles of Nucleic Acid Structure*. Springer-Verlag: New York, NY, 1984.

(45) Bloomfield, V. A.; Crothers, D. M.; I. Tinoco, J., *Nucleic Acids: Structures, Properties, and Functions*. University Science Books: Sausalito, CA, 2000.

(46) Jin, R.; Wu, G.; Mirkin, C. A.; Schatz, G. C., *J. Am. Chem. Soc.* **2003**, *125*, 1643-1654.

(47) Lytton-Jean, A. K. R.; Mirkin, C. A., *J. Am. Chem. Soc.* **2005**, *127*, 12754-12755.

(48) Kabeláč, M.; Hobza, P., *Phys. Chem. Chem. Phys.* **2007**, *9*, 903-917.

(49) Pranta, J.; Wierschke, S. G.; Jorgensen, W. L., *J. Am. Chem. Soc.* **1991**, *113*, 2810-2819.

CHAPTER FOUR

(1) Mirkin, C. A.; Letsinger, R. L.; Mucic, R. C.; Storhoff, J. J. *Nature* **1996**, *382*, 607-609.

(2) Alivisatos, A. P.; Johnsson, K. P.; Peng, X. G.; Wilson, T. E.; Loweth, C. J.; Bruchez, M. P.; Schultz, P. G. *Nature* **1996**, *382*, 609-611.

(3) Rosi, N. L.; Giljohann, D. A.; Thaxton, C. S.; Lytton-Jean, A. K. R.; Han, M. S.; Mirkin, C. A. *Science* **2006**, *312*, 1027-1030.

(4) Seferos, D. S.; Giljohann, D. A.; Hill, H. D.; Prigodich, A. E.; Mirkin, C. A. *J. Am. Chem. Soc.* **2007,** *129*, 15477-15479.

(5) Daniel, M. C.; Astruc, D. *Chem. Rev.* **2004**, *104*, 293-346.

(6) Liu, J. W.; Lu, Y. *J. Am. Chem. Soc.* **2003**, *125*, 6642-6643.

(7) Ozin, G. A., Arsenault, A. C. *Nanochemistry: A Chemical Approach to Nanomaterials*; Royal Society of Chemistry: Cambridge, UK, **2005**.

(8) Liu, J. W.; Lu, Y. *Angew. Chem., Int. Ed.* **2006**, *45*, 90-94.

(9) Niemeyer, C. M. *Angew. Chem., Int. Ed.* **2001**, *40*, 4128-4158.

(10) Katz, E.; Willner, I. *Angew. Chem., Int. Ed.* **2004**, *43*, 6042-6108.

(11) Niemeyer, C. M.; Simon, U. *Eur. J. Inorg. Chem.* **2005**, 3641-3655.

(12) Dillenback, L. M.; Goodrich, G. P.; Keating, C. D. *Nano. Lett.* **2006,** *6*, 16-23.

(13) Hurst, S. J.; Lytton-Jean, A. K. R.; Mirkin, C. A. *Anal. Chem.* **2006**, *78*, 8313-8318.

(14) Park, S. Y.; Stroud, D. *Phy. Rev. B* **2003**, *67*, 212202.

(15) Lytton-Jean, A. K. R.; Mirkin, C. A. *J. Am. Chem. Soc.* **2005**, *127*, 12754-12755.

(16) Storhoff, J. J.; Mirkin, C. A. *Chem. Rev.* **1999**, *99*, 1849-1862.

(17) Nykypanchuk, D.; Maye, M. M.; van der Lelie, D.; Gang, O. *Langmuir* **2007**, *23*, 6305-6314.

(18) Taton, T. A.; Mirkin, C. A.; Letsinger, R. L. *Science* **2000**, *289*, 1757-1760.

(19) Baiancaniello, P. L.; Kim, A. J., Crocker, J. C. *Phys. Rev. Lett.* **2005**, *94*, 058302.

(20) Park, S. Y.; Stroud, D. *Phy. Rev. B* **2003**, *68*, 224201.

(21) Park, S. Y.; Lee, J. S.; Georganopoulou, D.; Mirkin, C. A.; Schatz, G. C., *J. Phys.Chem.B* **2006,** *110*, 12673-12681.

(22) Strable, E.; Johnson, J. E.; Finn, M. G. *Nano. Lett.* **2004**; *4*, 1385-1389.

(23) Kim, A. J.; Biancaniello, P. L.; Crocker, J. C., *Chem. Phys. Lett.* **2006**, *22*, 1991-2001.

(24) Storhoff, J. J.; Lazarides, A. A.; Mucic, R. C.; Mirkin, C. A.; Letsinger, R. L.; Schatz, G. C. *J. Am. Chem. Soc.* **2000**, *122*, 4640-4650.

(25) Park, S-J.; Lazarides, A. A.; Mirkin, C. A.; Letsinger, R. L. *Angew. Chem., Int. Ed.* **2001**, *40*, 2909-2912.

(26) Park, S. J.; Lazarides, A. A.; Storhoff, J. J.; Pesce, L.; Mirkin, C. A. *J. Phy. Chem. B* **2004**, *108*, 12375-12380.

(27) Park, S. Y.; Lytton-Jean, A. K. R.; Lee, B.; Weigand, S.; Schatz, G. C.; Mirkin, C. A. *Nature* **2008**, *451*, 553-556.

(28) Nykypanchuk, D.; Maye, M. M.; van der Lelie, D.; Gang, O. *Nature* **2008**, *451*, 549-552.

(29) Xiong, H.; van der Lelie, D.; Gang, O. *J. Am. Chem. Soc.* **2008**; *130*, 2442-2443.

(30) Schellman, J. A.; Harvey. C. H. *Biophys. Chem.* **1995**. *55*, 95–114.

CHAPTER FIVE

(1) Nam, J. M.; Thaxton, C. S.; Mirkin, C. A. *Science*, **2003,** 301, 1884-1886.

(2) Nam, J. M.; Stoeva, S. I.; Mirkin, C. A. *J. Am. Chem. Soc.* , **2004,** 126, 5932-5933.

(3) Mirkin, C. A.; Letsinger, R. L.; Mucic, R. C.; Storhoff, J. J. *Nature*, **1996,** *382*, 607-609.

(4) Taton, T. A.; Mirkin, C. A.; Letsinger, R. L. *Science* **2000,** 289, 1757-1760.

(5) Demers, L. M.; Mirkin, C. A.; Mucic, R. C.; Reynolds, R. A.; Letsinger, R. L.; Elghanian, R.; Viswanadham, G. *Anal. Chem.* **2000,** 72, 5535-5541.

(6) Georganopoulou, D. G.; Chang, L.; *et al. Proc. Natl. Acad. Sci. U.S.A.* **2005,** 102, 2273-2276.

(7) Braakman, I.; Helenius, J.; Helenius, A. *Nature* **1992,** 356, 260-262.

(8) Letsinger, R. L.; Elghanian, R.; Viswanadham, G.; Mirkin, C. A. *Bioconj. Chem.* **2000,** 11, 289-291.

(9) Li, Z.; Jin, R. C.; Mirkin, C. A.; Letsinger, R. L. *Nuc. Acids Res.* **2002,** 30, 1558-1562.

(10) Raineri, I.; Moroni, C.; Senn, H. P. *Nuc. Acids Res.* **1991,** 19, 4010-4010.

(11) Klein, C.A.; Seidl, S.; *et al. Nat. Biotechnol.* **2002,** 20, 387-392.

(12) Karrer, E. E.; Lincoln, J. E.; *et al. Proc. Natl. Acad. Sci.,* **1995,** 92, 3814-3818.

(13) Cao, Y. C.; Jin, R.; Mirkin, C. A. *Science* **2002,** 297, 1536-1540.

(14) Storhoff, J. J.; Marla, S. S.; Garimella, V.; Mirkin, C. A. "Labels and Detection Methods," *Microarray Technology and its Applications* **2004,** 147-174.

(15) DNA sequence loading on the surface of the gold nanoparticles was measured according to reference 5.

CHAPTER SIX

(1) Saiki, R. K.; Scharf, S.; Faloona, F.; Mullis, K. B.; Horn, G. T.; Erlich, H. A.; Arnheim, N. *Science* **1985**, *230*, 1350-1354.

(2) Mullis, K.; Faloona, F.; Scharf, S.; Saiki, R.; Horn, G.; Erlich, H. *Cold Spring Harbor Symposia on Quantitative Biology* **1986**, *51*, 263-273.

(3) Scharf, S. J.; Horn, G. T.; Erlich, H. A. *Science* **1986**, *233*, 1076-1078.

(4) Kary, B. M. *Angew. Chem. Int. Ed.* **1994**, *33*, 1209-1213.

(5) Jochen-Wilhelm, A. P. *ChemBioChem* **2003**, *4*, 1120-1128.

(6) Bowtell, D. S., *DNA Microarrays: A Molecular Cloning Manual*; Cold Spring Harbor Press: Cold Spring Harbor, NY, **2003**.

(7) DeRisi, J. L.; Iyer, V. R.; Brown, P. O. *Science* **1997**, *278*, 680-686.

(8) Gibson, U. E. M.; Heid, C. A.; Williams, P. M. *Gen. Res.* **1996**, *6*, 995-1001.

(9) Heid, C. A.; Stevens, J.; Livak, K. J.; Williams, P. M. *Gen. Res.* **1996**, *6*, 986-994.

(10) Higuchi, R.; Fockler, C.; Dollinger, G.; Watson, R. *Bio-Technology* **1993**, *11*, 1026-1030.

(11) Mirkin, C. A.; Thaxton, C. S.; Rosi, N. L. *Expt. Rev. Mol. Diag.* **2004**, *4*, 749-751.

(12) Nam, J. M.; Park, S. J.; Mirkin, C. A. *J. Am. Chem. Soc.* **2002**, *124*, 3820-3821.

(13) Nam, J. M.; Stoeva, S. I.; Mirkin, C. A. *J. Am. Chem. Soc.* **2004**, *126*, 5932-5933.

(14) Thaxton, C. S.; Hill, H. D.; Georganopoulou, D. G.; Stoeva, S. I.; Mirkin, C. A. *Anal. Chem.* **2005**, *77*, 8174-8178.

(15) Oh, B. K.; Nam, J. M.; Lee, S. W.; Mirkin, C. A. *Small* **2006**, *2*, 103-108.

(16) Bao, Y. P.; Wei, T. F.; Lefebvre, P. A.; An, H.; He, L. X.; Kunkel, G. T.; Muller, U. R. *Anal. Chem.* **2006**, *78*, 2055-2059.

(17) Stoeva, S. I.; Lee, J. S.; Smith, J. E.; Rosen, S. T.; Mirkin, C. A. *J. Am. Chem. Soc.* **2006**, *128*, 8378-8379.

(18) Stoeva, S. I.; Lee, J. S.; Thaxton, C. S.; Mirkin, C. A. *Angew. Chem. Int. Ed.* **2006**, *45*, 3303-3306.

(19) Georganopoulou, D. G.; Chang, L.; Nam, J. M.; Thaxton, C. S.; Mufson, E. J.; Klein, W. L.; Mirkin, C. A. *P. Natl. Acad. Sci. USA* **2005**, *102*, 2273-2276.

(20) Goluch, E. D.; Nam, J. M.; Georganopoulou, D. G.; Chiesl, T. N.; Shaikh, K. A.; Ryu, K. S.; Barron, A. E.; Mirkin, C. A.; Liu, C. *Lab on a Chip* **2006**, *6*, 1293-1299.

(21) Mirkin, C. A.; Letsinger, R. L.; Mucic, R. C.; Storhoff, J. J. *Nature* **1996**, *382*, 607-609.

(22) Li, Z.; Jin, R.; Mirkin, C. A.; Letsinger, R. L. *Nucleic Acids Res.* **2002**, *30*, 1558-1562.

(23) Cao, Y. W. C.; Jin, R.; Mirkin, C. A. *Science* **2002**, *297*, 1536-1540.

(24) Storhoff, J. J.; Lazarides, A. A.; Mucic, R. C.; Mirkin, C. A.; Letsinger, R. L.; Schatz, G. C. *J. Am. Chem. Soc.* **2000**, *122*, 4640-4650.

(25) Taton, T. A.; Mirkin, C. A.; Letsinger, R. L. *Science* **2000**, *289*, 1757-1760.

(26) Jin, R.; Wu, G. S.; Li, Z.; Mirkin, C. A.; Schatz, G. C. *J. Am. Chem. Soc.* **2003**, *125*, 1643-1654.

(27) Lytton-Jean, A. K. R.; Mirkin, C. A. *J. Am. Chem. Soc.* **2005**, *127*, 12754-12755.

(28) Rosi, N. L.; Giljohann, D. A.; Thaxton, C. S.; Lytton-Jean, A. K. R.; Han, M. S.; Mirkin, C. A. *Science* **2006**, 312, 1027 - 1030.

(29) Hurst, S. J.; Lytton-Jean, A. K. R.; Mirkin, C. A. *Anal. Chem.* **2006**, *78*, 8313-8318.

(30) Han, M. S.; Lytton-Jean, A. K. R.; Oh, B. K.; Heo, J.; Mirkin, C. A. *Angew. Chem. Int. Ed.* **2006**, *45*, 1807-1810.

(31) Han, M. S.; Lytton-Jean, A. K. R.; Mirkin, C. A. *J. Am. Chem. Soc.* **2006**, *128*, 4954-4955.

(32) Lee, J-S, Han, M. S. Mirkin, C. A. *Angew. Chem. Int. Ed.* **2007**, *46*, 4093-4096.

(33) Liu, J. W.; Lu, Y. *J. Am. Chem. Soc.* **2003**, *125*, 6642-6643.

(34) Liu, J. W.; Lu, Y. *Anal. Chem.* **2004**, *76*, 1627-1632.

(35) Daniel, M. C.; Astruc, D. *Chem. Rev.* **2004**, *104*, 293-346.

(36) He, L.; Musick, M. D.; Nicewarner, S. R.; Salinas, F. G.; Benkovic, S. J.; Natan, M. J.; Keating, C. D. *J. Am. Chem. Soc.* **2000**, *122*, 9071-9077.

(37) Huang, C. C.; Huang, Y. F.; Cao, Z. H.; Tan, W. H.; Chang, H. T. *Anal. Chem.* **2005**, *77*, 5735-5741.

(38) Storhoff, J. J., Sudhakar S.; Viswanadham, G.; Mirkin, C A. In *Microarray Technology and Its Applications*; Mueller, U. R. N., Dan V., Ed.; Springer GmbH: Berlin, Germany, **2005**, pp 147-179.

(39) Hill, H. D., Mirkin, C. A. *Nat. Protoc.* **2006**, *1*, 324-336.

(40) Minunni, M.; Tombelli, S.; Fonti, J.; Spiriti, M. M.; Mascini, M.; Bogani, P.; Buiatti, M. *J. Am. Chem. Soc.* **2005**, *127*, 7966-7967.

(41) Minunni, M.; Mannelli, I.; Spiriti, M. M.; Tombelli, S.; Mascini, M. *Anal. Chim. Acta* **2004**, *526*, 19-25.

(42) Atlas, R. M. *Ann. Rev. Microbio.* **2002**, *56*, 167-185.

APPENDIX

(1) Nam, J. M.; Thaxton, C. S.; Mirkin, C. A.; *Science,* **2003**, *301*, 1884-1886.

(2) Nam, J. M.; Stoeva, S. I.; Mirkin, C. A.; *J. Am.Chem. Soc.,* **2004,** *126*, 5932-5933.

(3) Mirkin, C. A.; Letsinger, R. L.; Mucic, R. C.; Storhoff, J. J.; *Nature* 1996, *382*, 607-609.

(4) Storhoff, J. J.; Lazarides, A. A.; *et al., J. Am. Chem. Soc.,* **2000**, *122*, 4640-4650.

(5) Storhofff, J. J. ; Elghanian, R. ; Mirkin, C. A. ; Letsinger, R. L. ; *Langmuir,* **2002,** *18*, 6666-6670.

(6) Jin, R. C.; Wu, G. S.; *et al., J. Am. Chem. Soc., 2003,* *125*, 1643-1654.

(7) Lytton-Jean, A. K. R. ; Mirkin, C. A.; *J. Am. Chem. Soc.,* **2005**, *127*, 12754-12755.

(8) Demers, L. M.; Ostblom, M., *et al., J. Am. Chem. Soc.,* **2002,** *124*, 11248-11249.

(9) Thaxton, C. S.; Hill, H. D.; *et al.*, *Anal. Chem.,* **2005,** *77*, 8174-8178.

(10) Demers, L. M.; Mirkin, C. A.; *et al.*, *Anal. Chem.,* **2000**, *72*, 5535-5541.

(11) Taton, T. A.; Mirkin, C. A.; Letsinger, R. L.; *Science,* **2000,** *289*, 1757-1760.

(12) Cao, Y. W. C. ; Jin, R. C.; Mirkin, C. A.; *Science,* **2002,** *297*, 1536-1540.

(13) Oh, B. K.; Nam, J. M.; Lee, S. W.; Mirkin, C. A.; *Small* 2006, *2*, 103-108.

(14) Stoeva, S. I.; Lee, J. -S.; Smith, J. E.; Rosen, S. T.; Woodruff, T. K.; Mirkin, C. A.; *J. Am. Chem. Soc.* 2006, *Submitted*.

(15) Lee, J.-S.; Thaxton, Stoeva, S.I.; C. S.; Mirkin, C.A.; *Angew. Chem. Int. Ed.,* **2006,** *45*, 3303-3306.

(16) Frens, G.; *Nature-Physical Science* **1973,** *241*, 20-22.

APPENDIX

The Bio-Barcode Assay for Proteins and Nucleic Acids: A Detailed Protocol

A.1 Introduction:

The capability to detect various biomarkers comprised of nucleic acids or proteins at exceptionally low numbers is vital to the practice of diagnostic medicine, the identification of biological weapons agents, and basic life sciences research. These biological markers can indicate the onset of a neurodegenerative disease, an infection by a virus, or the environmental presence of a potentially toxic or lethal pathogen. High sensitivity detection is essential for early disease diagnosis, tracking therapeutic efficacy, blood and food supply screening applications, and following disease recurrence.

The bio-barcode assay is a promising new amplification and detection technique that utilizes short oligonucleotides as target identification strands and surrogate amplification units in both protein and nucleic acid detection,[1, 2] (Figure A.1). The technique uses the many advantageous properties of oligonucleotide-functionalized gold nanoparticles including ease of fabrication, tighter oligonucleotide binding capabilities, stability under a variety of conditions, catalytic ability, and optical properties.[3-8] The typical assay involves two types of particles. One particle is a magnetic microparticle and has recognition elements for the target of interest (e.g. antibody, oligonucleotide, aptamer) covalently attached to its surface. The second is usually a gold nanoparticle that has another recognition agent, which can form a sandwich around the target in conjunction with the magnetic particle. This gold nanoparticle also carries hundreds of thiolated single strand oligonucleotides attached to its surface; these are the barcodes. After incubating the two particle types with the target, and the sandwich structures have formed, a magnetic field is used to localize and collect them, while unattached gold nanoparticle probes are washed away. After the excess gold nanoparticles are removed and a dithiothreitol (DTT)

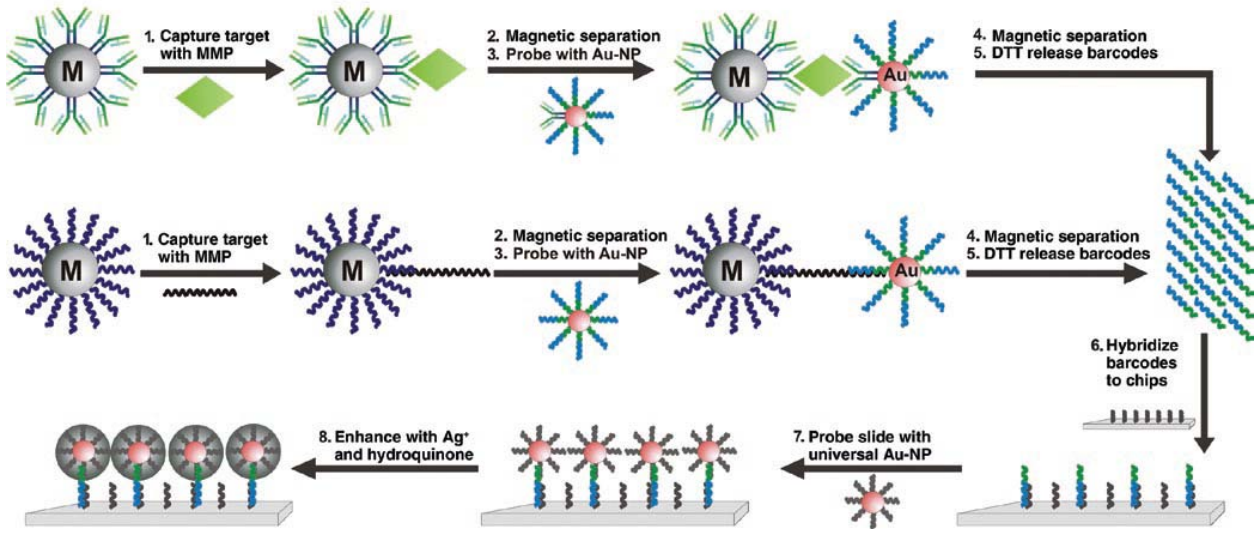

Figure A.1 Bio-Barcode Assay for DNA and Protein Detection. A) Schematic representation of protein detection using the bio-barcode assay. B) Representation of nucleic acid detection using the bio-barcode assay. C) Schematic Representation of the scanometric detection method.

solution at elevated temperature is used to release the barcode strands from the gold nanoparticles through ligand exchange[9,10]. The liberated barcode strands can be identified on a microarray via scanometric detection[11] with more nanoparticle probes, or *in situ* if the barcodes carry with them a detectable marker (e.g. fluorophore, chemiluminescent probe, Raman active dye or redox active moiety)[10, 12]. Under controlled conditions, the assay has exhibited low attomolar (10^{-18}) sensitivity for a variety of protein targets[1] and high zeptomolar (10^{-19}) sensitivity for nucleic acid targets[2] when paired with scanometric readout.

This appendix covers all of the steps needed to perform the bio-barcode assay from start to finish in detail. To generate all the reagents for the bio-barcode assay takes approximately three days to complete. Of that time, approximately 14 hours is active and the remainder is incubations. This version of bio-barcode assay takes around 9 hours to perform for nucleic acid detection, and 10 hours for protein detection. It is not optimized for speed, but rather to ensure proper target capture and oligonucleotide hybridization. Other versions have been implemented

that require as little as 90 minutes[13]. In total, reagent synthesis, probe preparation, and detection takes four days. It should be noted that probes can be stored at 4°C for weeks at a time, and multiple assays can be run with them.

A. 2 Materials and Equipment

A.2.1 Reagents

A.2.1.1 Gold Nanoparticle Synthesis

Sodium citrate tribasic dihydrate >99.0% (Sigma-Aldrich) [$HOC(COONa)(CH_2COONa)_2 \cdot 2H_2O$]

Hydrogen tetrachloroaurate (III) trihydrate >99.9% (Sigma-Aldrich)[$HAuCl_4 \cdot 3H_2O$]

Aqua regia cleaning solution [3 HCl: 1 HNO_3]

CAUTION Corrosive

NANOpure water (Barnstead) or other super water (e.g. MilliQ)

0.45 μm acetate filter (Millipore)

A.2.1.2 Magnetic Particle Functionalization

Sodium phosphate monobasic, molecular biology grade [NaH_2PO_4]

Sodium phosphate dibasic, molecular biology grade [Na_2HPO_4]

Sodium chloride, molecular biology grade [NaCl]

Hydrochloric acid [HCl]

CAUTION Can cause burns.

Sodium hydroxide [NaOH]

CAUTION Can cause burns.

NANOpure water (Barnstead) or other super water (e.g. MilliQ)

A.2.1.2.1 With DNA

Dynabeads® M-270 Amine (Invitrogen)

Synthetic oligonucleotide probe with disulfide linker (HPLC purified)

Anhydrous dimethyl sulfoxide (DMSO) <99.9% [$(CH_3)_2SO$]

Dithiothreitol (DTT), molecular biology grade [$C_4H_{10}O_2S_2$]

Nap-5™ column (GE Healthcare)

50mg Succinimidyl-4-(p-Maleimidophenyl)-Butyrate (SMPB, Pierce) [$C_{18}H_{16}N_2O_6$]

100mg Sulfosuccinimidyl acetate (Sulfo-NHS-acetate, Pierce) [$C_6H_6O_7NSNa$]

A.2.1.2.2 With Antibodies

Dynabeads® M-270 Tosyl (Invitrogen)

Monoclonal antibody

Boric acid, molecular biology grade [H_3BO_3]

Tris(hydroxymethyl)aminomethane (Tris), molecular biology grade [$NH_2C(CH_2OH)_3$

A.2.1.3 Gold Nanoparticle Functionalization with DNA

Sodium phosphate monobasic, molecular biology grade [NaH_2PO_4]

Sodium phosphate dibasic, molecular biology grade [Na_2HPO_4]

Sodium chloride, molecular biology grade [NaCl]

Hydrochloric acid [HCl] Caution can cause burns.

Sodium hydroxide [NaOH] Caution can cause burns.

NANOpure water (Barnstead) or other super water (e.g. MilliQ)

A.2.1.3.1 With DNA

13nm gold colloid (synthesized above)

Synthetic oligonucleotide probe with disulfide linker (HPLC purified)

Nap-5™ column (GE Healthcare)

Dithiothreitol (DTT), molecular biology grade [$C_4H_{10}O_2S_2$]

Sodium dodecyl sulfate (SDS), molecular biology grade [$C_{12}H_{25}OSO_3Na$]

A.2.1.3.2 With DNA and Antibodies

30nm gold nanoparticles (Ted Pella, Inc.)

Polyclonal antibody or second monoclonal antibody

Synthetic oligonucleotide probe with disulfide linker (HPLC purified)

Nap-5™ column (GE Healthcare)

Dithiothreitol (DTT), molecular biology grade [$C_4H_{10}O_2S_2$]

A.2.1.4 Bio-Barcode Assay Components for Protein and Nucleic Acid Detection

Formamide, molecular biology grade (aliquot, store 4°C) [CH_3NO]

tRNA, 10,000units (Sigma)

Dithiothreitol (DTT), molecular biology grade [$C_4H_{10}O_2S_2$]

Sodium phosphate monobasic, molecular biology grade [NaH_2PO_4]

Sodium phosphate dibasic, molecular biology grade [Na_2HPO_4]

Sodium dodecyl sulfate (SDS), molecular biology grade [$C_{12}H_{25}OSO_3Na$]

Tween 20 or Polysorbate 20, molecular biology grade [$C_{58}H_{114}O_{26}$]

Bovine serum albumin (BSA, Ambion)

Hydrochloric acid [HCl] Caution can cause burns.

Sodium hydroxide [NaOH] Caution can cause burns.

NANOpure water (Barnstead) or other super water (e.g. MilliQ)

A.2.1.4.1 Scanometric Detection

Microarray slides spotted with capture oligonucleotide (4/10 well layout)

Silver enhancement solutions A/B (Nanosphere Inc. or Sigma)

Sodium nitrate, molecular biology grade [$NaNO_3$]

Tween 20 or Polysorbate 20, molecular biology grade [$C_{58}H_{114}O_{26}$]

Sodium dodecyl sulfate (SDS), molecular biology grade [$C_{12}H_{25}OSO_3Na$]

Formamide, molecular biology grade (aliquot, store 4°C) [CH_3NO]

NANOpure water (Barnstead) or other super water (e.g. MilliQ)

A.2.1.4.2 Florescence Detection

NANOpure water (Barnstead) or other super water (e.g. MilliQ)

Fluorophore reference standards

Fluorophore labeled gold nanoparticle oligonucleotide barcode

A.2.2 Equipment

A.2.2.1 Gold Nanoparticle Synthesis

Magnetic stir plate

Heating mantle

UV-Visible spectrophotometer and cuvette

Drying oven

500 mL volumetric flask

50 mL volumetric flask

1000 mL 2 neck round bottom flask

Reflux condenser

Rubber septa

Large stir bar

Tygon® tubing

Glass pipettes or plastic spatula

Teflon tape

1000 mL all glass filter holder apparatus

500 mL amber colored glass storage container

Transmission electron microscope (TEM) may also be required

A.2.2.2 Magnetic Particle Functionalization with DNA

UV-Visible spectrophotometer and cuvette

Refrigerator (4°C)

Magnetic separators: 2 mL, 15 mL, and 50 mL

Lyophilizer

pH meter

Orbital, rocking, or rotating shaker

50 mL conical tubes

15 mL conical tubes

1.5 mL microfuge tubes

10 mL syringes

18 gauge needles

Aluminum foil

A.2.2.3 Magnetic Particle Functionalization with Antibodies

UV spectrophotometer and cuvette

Refrigerator (4°C)

Magnetic separator: 2mL

pH meter

Orbital, rocking, or rotating shaker

1.5 mL microfuge tubes

A.2.2.4 Gold Nanoparticle Functionalization with DNA

UV spectrophotometer and cuvette

Orbital or rocking shaker

Bench top vortex

Lyophilizer

pH meter

20 mL clear borosilicate glass vials (conventionally known as EPA vials)

1.5 mL microfuge tubes

Aluminum foil

A.2.2.5 Gold Nanoparticle Functionalization with DNA and Antibodies

UV-Visible spectrophotometer and cuvette

Refrigerator (4°C)

Orbital or rocking shaker

Microcentrifuge

Bench top vortex

Lyophilizer

pH meter

pH paper

20 mL clear borosilicate glass vials (conventionally known as EPA vials)

1.5mL microfuge tubes

A.2.2.6 Bio-Barcode Assay Components for Protein and Nucleic Acid Detection

Eppendorf thermal mixer or temperature controlled orbital shaker

Magnetic separator: 2 mL

Vortex

Microcentrifuge

1.5 mL microfuge tubes

A.2.2.6.1 Scanometric Detection

VerigeneID™ (Nanosphere Inc) or traditional flatbed scanner

Hybridization gaskets 4 well or 10 well layout (Nanosphere Inc)

Slide spinner for drying

50 mL conical tubes

Controlled humidity chamber

A.2.2.6.2 Florescence detection

Fluorescence plate reader or fluorometer

Micorcentrifuge

Fluorescence cuvette or 96 well Costar Black/Clear bottom microtiter plate

A.2.2.7 Quantification Software

GenePix Pro (Molecular Devices), ImageQuant (GE Healthcare) or any other intensity quantification software, though GenePix is preferred.

A.3 Bio-Probe Design and Selection

A.3.1 Oligonucleotide Probe Design

Oligonucleotide probes for nucleic acid detection are generated using the NCBI BLAST nucleotide search function with the DNA sequences for a gene of interest from the organism in question (http://www.ncbi.nlm.nih.gov/BLAST/). Additionally, PCR primer design software can be used to generate probe sequences. Traditionally these sequences are 25-35 base pairs in length. It is important when designing sequences for use as probes that the end sequences of the oligonucleotides without the thiol (which will extend off the particle), not contain multiple C or G residues, as these can cause particle aggregation. Additionally, it is desirable that the melting temperatures of the probes fall within a narrow range. The oligonucleotide probes should be unique to the target showing little or no complementarities with other organism genomes, and both the magnetic and gold probe sequences must be complementary to either the sense or antisense strand of the target. It is important to check the sequences for potential self-complementarities and hairpin formation, which can hinder the bio-barcode assay. The design of barcodes to use in conjunction with protein detection is simpler than the DNA case, and can be any sequence that the operator desires. Typically, the barcode is a 15mer sequence assigned to each specific protein target of interest. These sequences must be checked for self-dimerization and hairpin formation, and should not contain C or G residues at the end.

In addition to the target specific sequence, a universal sequence is included if scanometric assay readout is going to be used. This universal sequence is 5' - AGC TAC GAA TAA -3'. A polyethylene glycol 9mer is used between the universal sequence and the probe sequence, to separate the two. If using the fluorescence method an oligo $(dA)_{10}$ sequence is used to space the recognition element away from the nanoparticle surface. In either case, the universal sequence or

the oligo $(dA)_{10}$ are placed between the thiol linkage and the recognition element/barcode sequence.

For mRNA detection, Dynabeads® oligo $(dT)_{25}$ (Invitrogen) magnetic microparticles can be used for total mRNA isolation in order to perform the bio-barcode assay from cell lysates. The kit can be used until the mRNA has been bound to the magnetic particle, before continuing with the bio-barcode assay as further described.

A.3.2 Antibody Selection:

The selection of antibodies for use in the bio-barcode assay can be the difference between great and poor results. When choosing antibodies, it is imperative that they bind to different epitopes on the antigen; in order to form a sandwich structure. It is suggested that antibodies optimized for ELISA be used as these antibodies are known to react with distinct epitopes. Generally, the monoclonal antibody is conjugated to the magnetic particle and either a monoclonal or a polyclonal antibody is used to generate the gold nanoparticle probe. In certain cases, an antibody does not react well with the gold nanoparticle surface and will cause particle aggregates or an oily film to form. If this is the case, try swapping the antibody from the magnetic particle to the gold particle, and vice versa. New antibodies will have to be chosen if the problem persists.

A.3.3 Scanometric Capture Probe Design

The capture probe spotted on the glass slide surface for the scanometric detection is complementary to the unique 15mer barcode sequence in protein detection, and is complementary to the recognition element in nucleic acid detection. The amine functionality must be attached to this capture oligonucleotide in such a way that when the barcode binds to the

capture strand, the universal probe "sticky end" extends away from the surface into the surrounding solution. In order to position the capture strand away from the glass surface for better binding, two (polyethylene glycol 18) spacers are placed between the amino-functional group and the capture sequence. These oligonucleotides should be ion exchange HPLC purified.

A.3.3.1 Universal Probe

The design work for this probe is complete. The sequence is as follows:

5' - Thiol Modifier - AAA AAA AAA ATT ATT CGT AGC T - 3'

This sequence has been tested using the BLAST nucleotide function and does not show high complementary to any other DNA sequence listed with NCBI. The universal sequence is extremely useful for multiplexed detection of protein or nucleic acid targets within one sample.[14,15]

A.3.4 Probe Functionalization with Bio-Molecules

A.3.4.1 Magnetic Particle Functionalization with DNA

Passivation buffer 1: 150 mM phosphate buffer + 150 mM NaCl (pH=8.0)

10.119 g Na_2HPO_4

0.449 g NaH_2PO_4

4.383 g NaCl

500 mL NANOpure water

Coupling buffer: 100 mM phosphate buffer + 200 mM NaCl (pH=6.9-7.0)

4.392 g Na_2HPO_4

2.291 g NaH_2PO_4

5.884 g NaCl

500 mL NANOpure water

Disulfide Cleavage Buffer: 170 mM phosphate buffer (pH=8.0)

11.468 g Na_2HPO_4

0.509 g NaH_2PO_4

500 mL NANOpure water

Storage Buffer: 10 mM phosphate buffer + 200 mM NaCl (pH=7.4)

.570 g Na_2HPO_4

.118 g NaH_2PO_4

5.844 g NaCl

500 mL NANOpure water

·pH buffers with 5 M NaOH and 5 M HCl prepared in NANOpure water.

CAUTION: can cause burns.

A.3.4.2 Magnetic Particle Functionalization with Antibodies

Borate Buffer: 100 mM borate buffer (pH=9.5)

3.091 g H_3BO_3

500 mL NANOpure water

Washing Buffer: 10 mM phosphate buffer + 150 mM NaCl (pH=7.4)

0.562 g Na_2HPO_4

0.125 g NaH_2PO_4

4.383 g NaCl

500 mL NANOpure water

Passivation Buffer 2: 200 mM Tris (pH=8.5)

1.210 g Tris: $NH_2C(CH_2OH)_3$

50 mL NANOpure water

·pH buffers with 5 M NaOH and 5 M HCl prepared in NANOpure water.

CAUTION can cause burns.

A.3.4.3 Gold Nanoparticle Functionalization with DNA and with DNA and Antibodies

Salting Buffer: 10 mM phosphate buffer + 2 M NaCl (pH 7.0)

0.0562 g Na_2HPO_4

0.0125 g NaH_2PO_4

5.844 g NaCl

50 mL NANOpure water

Phosphate Adjustment Buffer: 100 mM phosphate buffer (pH 7.0)

0.562 g Na_2HPO_4

0.125 g NaH_2PO_4

50 mL NANOpure water

Surfactant Solution: 10 % SDS (W/V)

10 g sodium dodecyl sulfate

90 mL NANOpure water

·pH buffers with 5 M NaOH and 5 M HCl prepared in NANOpure water.

CAUTION can cause burns.

A.3.4.4 Bio-Barcode Assay Components for Protein and Nucleic Acid Detection

The bio-barcode assay can be performed in a host of different media owing to the ability to clean the samples prior to the addition of the Au-NP probes. The magnetic particles allow for the selective isolation the target of interest from a complex mixture of proteins, nucleic acids, lipids, carbohydrates, and other contaminants. To date, protein detection has been conducted in buffers, human cerebral spinal fluid, goat, donkey, and human serum samples. In the case of DNA detection, isolation of the nucleic acid can be achieved from essentially any source. There are many commercially available kits (e.g. Promega, Qiagen, Sigma) for the isolation of total DNA from soil, water, feces, tissue, and blood to name a few. As with any biological detection assay, sample preparation and handling are critical. All samples should be stored at 4°C or below if possible to prevent degradation from nucleases or proteases. (It should be noted that current investigations are on going to optimize the protocols for protein detection in serum and genomic DNA detection).

Assay Buffer: 10 mM phosphate + 150 mM NaCl + 0.1 % SDS (pH=7.4)

0.562 g Na_2HPO_4

0.125 g NaH_2PO_4

4.383 g NaCl

500 mL nanopure water

For protein detection (Option C) , omit SDS and include 0.1 % BSA and 0.025 % Tween 20.

·pH buffers with 5 M NaOH and 5 M HCl prepared in NANOpure water.

CAUTION can cause burns.

A.3.4.5 Scanometric detection:

Slide Washing Buffer A: 0.5 M $NaNO_3$ + 0.01 % SDS + 0.02 % Tween20

21.25 g $NaNO_3$

500 μLs 10% SDS

100 μLs Tween20

500 mL NANOpure water

Slide Washing Buffer B: 0.5 M $NaNO_3$

21.25 g $NaNO_3$

500 mL NANOpure water

Slide Washing Buffer C: 0.1 M $NaNO_3$ (Store at 4°C)

2.125 g $NaNO_3$

500 mL NANOpure water

A.3.5 Equipment Set Up

A.3.5.1 Scanometric Detection

A hybridization chamber in required during the heated steps of the scanometric detection to prevent evaporation from the sample wells. The chamber is easy to make, simply take an empty box used to hold pipette tips, and place 15 mLs of the *Assay Buffer* into the bottom, then set the slides on top of the empty tip rack, and place the lid on top.

A.4 Procedures

A.4.1 13nm Gold Nanoparticle Synthesis

1| Clean all glassware with aqua regia, rinse copiously with nanopure water, and dry in oven at 100°C. Wash stir bar in round bottom flask at this time.

CAUTION Aqua regia and oven can cause burns.

2| Blow out glassware with N_2 or air and assemble reflux apparatus with the 2 neck round bottom flask, reflux condenser, and rubber septa. Use Teflon tape to protect joints, not grease. Be sure to clamp the round bottom and reflux condenser separately.

3| Prepare 500 mLs of 1 mM Hydrogentetrochloroaurate (III) trihydrate with NANOpure water in the 500 mL volumetric flask. (0.1969 g Au + 500 mL H_20) CRITICAL STEP

Do not use a metal spatula; use a glass pipette, or plastic spatula. Metal spatulas will cause the reduction of the gold salt onto their surface.

4| Pour the gold solution into the round bottom flask and bring to vigorous boil while stirring. Make sure that the water is flowing through the reflux condenser at this time.

5| While gold solution heats, prepare 50 mLs of 38.8 mM sodium citrate tribasic dihydrate with NANOpure water in the clean 50 mL volumetric flask. (0.5704 g citrate + 50 mL H_20)

6| Once the gold solution is refluxing vigorously (1 drip per second), remove the rubber septa and quickly add all sodium citrate solution. Reseal. Reflux 15 minutes.

·The solution will turn from yellow to clear, to black, to purple to deep red.

7| After 15 minutes, turn heat off and allow the reaction to cool to room temperature. This generally takes between 2 and 4 hours.

·*Pause Point:* cooling overnight is acceptable, if cooling overnight turn water flow through contender to extremely low or off.

8| Assemble 1000 mL all-glass filter holder apparatus with the 0.45 μm acetate filter.

9| Filter cool gold nanoparticle mixture and transfer gold nanoparticles into the clean amber storage bottle.

10| Measure λ_{max} for the particles. To do this, blank the UV-vis spectrophotometer with NANOpure water. Then dilute 500 µLs of Au-NPs into 1 mL of NANOpure water, and take the absorbance spectrum for this sample.

·Well-formed 13 nm particles should have a λ_{max} of approximately 519 nm, and a peak width of approximately 50 nm. For additional characterization, TEM is recommended.

11| Store 13 nm gold nanoparticles at room temperature.

A.4.2 Magnetic Particle Functionalization with DNA (for Antibodies perform OPTION A)

12| Remove amine functionalized magnetic microparticles (MMPs) from refrigerator approximately 15 minutes prior to use and allow them to warm to room temperature. Resuspend by slow vortex to avoid foaming.

13| Lyophilize 25 nmoles of DNA to be coupled to the MMPs during step 20 incubation time.

14| Take 1 mL of the MMPs and place in a 1.5 mL microfuge tube. Use a magnetic separator to extract MMPs to the side of the microfuge tube in order to remove supernatant. (1 mL = 30 mg MMPs, 1.75 x 10^{-6} mol NH_2/1000 mg MMP, therefore 5.25 x 10^{-6} mol NH_2/30 mg MMP)

15| Wash the MMPs three times with 1.5 mL DMSO using a syringe. Be sure to remove all supernatant, as the next reaction is water sensitive.

16| Turn off overhead lights for steps 17-21. This is done because the cross-linking reagent is not photo-stable.

17| Dissolve 50 mg SMPB in 1 mL DMSO, do this in the SMPB bottle to prevent reagent loss.

18| Add the 1 mL of SMPB/DMSO solution to dry the MMPs and resuspend them. Transfer the MMP-SMPB solution into a 50 mL conical tube.

19| Wash the SMPB bottle twice with 2 mLs DMSO and 1.5 mL microfuge tube 2 times with 1 mL DMSO. Add all DMSO washes to the 50 mL conical tube containing the MMPs.

20| Add an additional 7.8 mL DMSO to the 50 mL conical tube to bring the final SMPB concentration to approximately 9.9 mM (15.8mL total volume).

21| Wrap the conical tube in foil and place on an orbital with the tube lying on its side or rotating shaker for 4-4.5 hours. Tube needs to be on its side for optimal mixing.

CRITICAL STEP Do not exceed 5 hours. Doing so can greatly reduce coupling efficiency during the next step. Perform steps 22-28 during this incubation.

22| Prepare 1 mL of 0.1 M DTT solution in the *Disulfide Cleavage Buffer*.

CRITICAL STEP This solution must be made fresh every time.

23| Add 100 µL DTT solution (step 22) to the 25 nmoles of lyophilized DNA, wrap in foil, and let stand at room temperature for 2-3 hours. Vortex occasionally.

24| 15 minutes prior to the completion of disulfide cleavage, begin flushing Nap-5 column with NANOpure water. At least three column volumes of NANOpure water must flush through before adding DNA.

25| Once all the water has run through the column, add the 100 µLs of DNA/DTT to the column.

26| Allow the 100 µLs to flow into the column before adding 400 µLs of NANOpure water. Allow this volume to flow through the column uncollected.

27| Then add 950 µLs NANOpure water to the column and collect the flow through 3-4 drops at a time in 1.5mL microfuge tubes.

28| Use a UV-spectrophotometer and the absorbance at 260 nm to determine the DNA location and concentration using Beers Law. Generate at least 325 µLs of a10 µM solution using the coupling buffer, it may be necessary to combine multiple tubes of DNA.

$$A=\varepsilon C l$$

ε= molar absorbtivity C= concentration l= cell path length

30| Wash the MMPs three times with 15 mL DMSO; change tubes between second and third wash. Cover particles with foil while separating.

31| Wash the MMPs twice with *coupling buffer*; change tube after second wash. Cover particles with foil while separating.

32| Resuspend MMPs in 1 mL *coupling buffer*, take all MMPs, and place in 1.5 mL microfuge tube. Use magnet to remove supernatant.

33| Add 300 µLs of the 10 µM DNA solution from step 28 to the MMPs, close and wrap in foil. Save the remaining DNA to take a pre-coupling concentration. Shake overnight at room temperature.

PAUSE POINT: This step goes overnight

34| Remove supernatant and save for post-coupling efficiency calculation.

35| Transfer MMPs in 1 mL *coupling buffer* into a 15 mL conical tube. Wash three times with 10 mL *coupling buffer*. Change tube between second and third wash.

36| Wash the MMPs twice with *passivation buffer 1*, changing to a 50 mL conical tube between wash one and two.

37| Dissolve 100 mg sulfo-NHS-acetate in 35 mLs of the *passivation buffer 1*. Add this solution to the dry MMPs.

38| Wrap in foil and shake on side or end over end for one hour at room temperature.

39| Wash the MMPs three times with 20 mL *passivation buffer 1*, changing tubes between wash two and three.

40| Wash twice with 20 mL *storage buffer*, final resuspension in 3 mL *storage buffer* to give a final concentration of 10 mg/mL.

41| Store MMPs at 4°C. Do not freeze.

42| Calculate the coupling efficiency by measuring change in DNA concentration before and after the reaction. Use Beer's Law (Step 28) and the equation below:

Coupling efficiency % = {[(M before)-(M after)]/(M before)} x 100

M= molarity

A.4.3 Gold Nanoparticle Functionalization with DNA (for DNA and antibodies perform Option B)

43| Lyophilize 5 nmoles thiolated oligonucleotide probe.

44| Prepare 1 mL of 0.1 M DTT solution in the *Disulfide Cleavage Buffer.*

CRITICAL STEP This solution must be made fresh every time.

45| Add 100 µL DTT solution (step 2) to the 5 nmoles of lyophilized DNA, wrap in foil, and let stand at room temperature for 2-3 hours. Vortex occasionally.

46|15 minutes prior to the completion of disulfide cleavage, begin flushing Nap-5 column with NANOpure water. At least three column volumes of NANOpure water must flush through before adding DNA.

47| Add the 100 µLs of DNA to the column once all water has run through.

48| Once the 100 µLs flow into the column, add 400 µLs of NANOpure water to the column and allow it to flow through uncollected.

49| Then add 950 µLs NANOpure water to the column and collect the flow through 3-4 drops at a time in 1.5 mL microfuge tubes.

50| Use a UV-spectrophotometer and the absorbance at 260 nm to determine the DNA location and concentration using Beers Law.

$$A=\varepsilon C l$$

ε= molar absorbtivity C= concentration l= cell path length

51| Rinse a 20mL EPA vial with ethanol and then nanopure water, blow dry.

52| Add 1mL 13nm gold nanoparticles synthesized previously.

53| Caluclate the number of moles of oligonucleotide per tube, and add 4 nmoles of the freshly reduced thiolated oligonucleotide to the gold nanoparticles. Record the volume.

54| Wrap in foil and place on orbital shaker overnight at room temperature.

Pause Point: This step goes overnight.

55| Add *Phosphate Adjustment Buffer* to the nanoparticle solution to obtain a final phosphate concentration of 9mM.

Calculation: 1000µL AuNP + XµL DNA = Total Volume in µL

(Total Volume in µL) /10 = YµL *Phosphate Adjustment Buffer* needed

56| Add *Surfactant Solution* to obtain a final SDS concentration of ~ 0.1%. This helps to keep the particles from aggregating, and makes washing them in future steps more efficient.

Calculation: 1000µL AuNP +XµL DNA + YµL Phosphate = Total Vol # 2

SDS to add = (Total Vol # 2 * 0.1)/10

57| Rewrap in foil and place on orbital shaker for 30 minutes.

58| Calculate the volume of *Salting Buffer* needed to obtain a final concentration of 0.3M NaCl.

Calculation: (Total Vol # 2 * 0.3M)/(2M) = µLs *Salting Buffer* needed

# of Additions = 6 amount per addition = salt/6

59| Over the course of 2 days, make six additions of 1/6 of the total *Salting Buffer* needed to reach a final concentration of 0.3M NaCl. Do the additions while shaking gently or on a low vortex speed.

60| After last salt addition, allow particles to equilibrate overnight.

Pause Point: Particles can be stored at room temperature for up to one month in this state.

A.4.4 Bio-Barcode Assay for DNA Detection (for protein detection perform Option C)[9]

61| Determine the number of samples to be tested including one for the negative control (x). Add 20x µL 10mg/mL MMPs to 1.5 mL microfuge tube.

62| Wash the MMPs twice with the *Assay Buffer*. Resuspend MMPs in ½ original volume of *Assay Buffer* to gain 20mg/mL concentration. Omit this step if using the oligo $(dT)_{25}$ kit from Dynal, and follow the kit instructions until the mRNA is isolated.

63| Mix in 1.5mL microfuge tubes

a. 30 µL *Assay Buffer*
b. 10 µL MMP solution
c. 10 µL target solution

64| Shake the reactions at a temperature approximately 15°C below the melting point of the DNA for 45 minutes. A longer incubation period may be needed for samples that are more complex. Shake enough so that the MMPs do not settle.

65| During the incubation, spin 100 µLs of gold nanoparticle probe at 13,000G for 15 minutes. Remove the supernatant and resuspended in 500 µLs *Assay Buffer*. Repeat step 65 4 times.

66| After the final spin/wash in step 65, resuspend the gold particles in *Assay Buffer* to generate a 1 nM solution. Calculate the gold nanoparticle concentration using Beers Law (Step 28) and a molar absorbtivity at 519 nm of 2.7 x 10^8 L/(mole·cm).

67| Wash the magnetic particles with target twice with the *Assay Buffer*, and resuspended in 50 µLs of *Assay Buffer*. Wait 3 minutes between each wash while the magnet isolates the MMPS.

68| Add 10 µLs of gold nanoparticle probes recently spun (step 65).

69| Incubate at the same temperature as in step 64 for 1.5-2 hours with shaking so that the MMPs do not settle.

70| Wash the detections 5 times with 100 µLs *Assay Buffer*. Wait 3 minutes between each wash while the magnet isolates the MMPS. It is critical to remove all unbound gold nanoparticles to be sure that all signal seen is due to specific target binding events.

71| Prepare a 0.5M DTT solution in the *Assay Buffer*.

·This solution must be made fresh each day that the BCA is preformed.

·Increasing the salt concentration in the assay buffer for the remainder of the assay may improve scanometric results depending on barcode sequences.

·DTT is used because it is a less foul smelling reducing agent that 2-mercaptoethanol.

72| Resuspend the MMP-target-Au-NP complexes in 50 µLs DTT buffer from step 71 and vortex.

73| Incubate samples at 50°C for 15 minutes, and 45 minutes 25°C under vortex.

74| Chose appropriate signal readout method protocol…scanometric or fluorescence.

PAUSE POINT The bio-barcode assay can be stopped after the release of the barcodes by DTT. To stop here, remove MMPs and Au-NPs from supernatant and

freeze samples at -20°C. Do not leave the barcodes in solution with the magnetic particles as this will increase noise during the scanometric method.

A.4.5 Scanometric Detection of the Barcodes from DNA and Protein Detection (for Fluorescence detection perform Option D)

75| During the barcode release step, passivate slides with a 0.2% SDS solution made in NANOpure water. Place 40 mLs SDS solution in 50 mL conical tube and add slide. This removes the unreacted NHS groups from the surface of the slides.

76| Incubate at 50°C for 15 minutes, wash in NANOpure water, and spin dry.

77| Assemble the chip in the holder and the hybridization chamber.

78| After barcode release, extract the magnetic particles down on the magnet for 3 minutes and transfer the supernatants to clean microfuge tubes, or remove samples from freezer and thaw.

79| Spin the supernatants for 5 minutes at 13,000g to pellet the aggregated gold particles.

80| Add 15-20 μLs of the supernatant to a freshly re-hydrated/ passivated slide. The volume depends on the slide configuration. One detection per well.

81| Incubate for 15 minutes at 60 °C, 30 minutes at 37 °C and 15minutes at 25°C on the shaker (120 rpm) in a controlled humidity chamber.

82| During the incubation in step 81, spin 100 μLs of universal gold nanoparticle probe at 13,000G for 15 minutes. Remove the supernatant and resuspend in 500μLs *Assay Buffer*. Repeat step 82 four times.

83| Wash the slides twice in 40 mLs of *Assay Buffer* in 50 mL conical tubes for one minute in each.

84| Spin slides nearly dry and reassemble apparatus with a new top gasket. A new gasket is vital, as the one used in step 81 has DTT on it, and can cause the universal probes to aggregate.

85| Add 15-20 µLs of the universal probe solution to each well. 13nm probe solution should be 500 pM 13 nm Au in *Assay Buffer* plus formamide. Again follow step 66 to determine nanoparticle probe concentration.

·Formamide percentage should be determined depending upon the specific system. It is suggested to begin with 10% and work up or down from there.

Formamide is a stringency reagent which lowers the nonspecific interaction between oligonucleotides.

86| Fill each well with 15 µLs universal probe solution from step 85.

87| Allow the probe to associate with the chip for 45 minutes at 37 °C in the controlled humidity chamber shaking at 120rpm.

88| Disassemble apparatus, and wash the slides are individually twice in 40 mLs of *Washing Buffer A* in a conical tube for one minute.

89| Next, wash the slides three times in 40 mLs *Washing Buffer B* for one minute at a time.

90| Finally, quickly immerse the slides in 40mLs cold *Washing Buffer C*, and spin dry.

91| Lay the slide flat on the bench-top on top of a folded over kimwipe.

92| Prepare 2 mLs silver staining solution (1 mL A and 1 mL B) mix well. Be sure not to cross contaminate the stock solutions of A and B.

93| Pipette silver stain on slide ensuring that the lower two-thirds of the slide are completely covered.

94| Develop for 2-4.5 minutes depending on initial target concentration. Once a silver staining time has been determined, all remaining experiments to be compared must use the same times. Do not silver stain so that the spots are visible with the naked eye, as they have become saturated and can no longer be accurately quantified.

95| Wash slide thoroughly with NANOpure water, and spin dry.

96| Image with Verigene-ID or conventional flatbed scanner.

97| Quantify spot intensity using quantification software.

OPTION A

A.4.6 Magnetic Particle Functionalization with Antibodies

i. Remove Tosyl functionalized MMPs from the refrigerator approximately 15 minutes before use. Resuspend with a slow vortex to avoid foaming.

ii. Transfer 100 µLs MMPs into a 1.5 mL microfuge tube, place on magnetic rack, and remove supernatant. (3 µg antibody per 10^7 MMPs, $2x10^9$ MMP/ mL, 100 µL = $2x10^8$ MMP, therefore 60 µg antibody for coupling)

iii. Resuspend the MMPs in 1 mL *Borate Buffer*, and mix by slow tilt for 2-3 minutes. Repeat once.

iv. Extract MMPs from buffer, and resuspend MMPs in 200 µLs *Borate Buffer* containing 60 µgs of antibodies

v. Incubate at 37°C or lower depending on antibody stability for 24 hours with enough mixing to keep the MMPs from settling, but not harsh enough to denature the antibody.

vi. Place the MMPs on magnet and remove supernatant, save the supernatant.

vii. Wash the MMPs twice in the *Washing Buffer* for 5 minutes at 4°C.

viii. Passivate the MMPs in 1mL *Passivation Buffer 2* for 24 hours at 20°C or 4 hours at 37°C.

Pause Point: This step goes overnight

ix. Wash the MMPs in the *Washing Buffer* for 5 minutes at 4°C. Transfer to a new tube.

x. Store the MMPs in 1 mL of the *Washing Buffer* at 4°C, do not freeze.

xi. Calculate the coupling efficiency by measuring change in absorbance at 280 nm before and after the reaction, be sure to adjust for the changes in volume.

Coupling efficiency % = [((A_{280} before)-(A_{280} after))/(A_{280} before))] x 100

OPTION B

A.4.7 Gold Nanoparticle Functionalization with DNA and Antibodies

i) Lyophilize 5 nmoles thiolated oligonucleotide probe.

ii) Prepare 1mL of 0.1M DTT in *Disulfide Cleavage Buffer.*

CRITICAL STEP This solution must be fresh every time.

iii) Add 100 µL DTT solution (step i) to the 5 nmoles of lyophilized DNA, wrap in foil, and let stand at room temperature for 2-3 hours, vortex occasionally.

iv) Pipette 10 mLs 30 nm gold nanoparticles (Au-NPs) into a 15 mL conical vial.

v) Adjust pH to approximately 9.2, and fill seven microfuge tubes (1.5 mL) with 1 mL particles each.

vi) Add one of the following to one of the tubes of Au-NPs: 0 µg, 0.5 µg, 0.75 µg, 1.0 µg, 1.5 µg, 2 µg, 3 µg antibody

·It may be necessary to test antibody amounts higher than this depending on the antibody, but this is a good starting range.

vii) Gently vortex and incubate at room temperature for 30 minutes.

viii) Add 100 µLs 2 M NaCl to each tube and watch for the red-shift indicating aggregation. Line up tubes and select the one where the particles aggregate, but not immediately. This is a rough indicator for how much of the nanoparticle surface is available for thiolated oligonucleotide binding in upcoming steps. (See Figure A.2)

ix) Rinse a 20 mL EPA vial with ethanol and then nanopure water, blow dry.

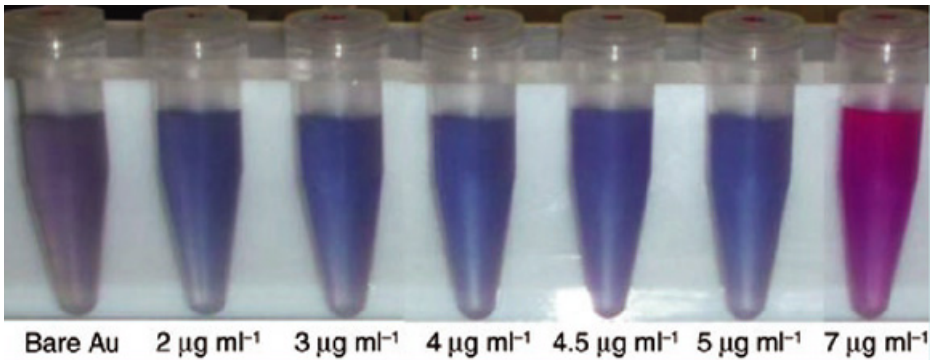

Figure A.2 Testing Antibody Loading. This image shows the gold nanoparticle-antibody loading test using salt to determine reasonable antibody amounts for probe generation. From this data, 6µg/mL would be an appropriate amount of antibody to add as the particles to the left have aggregated, and the ones to the right have not. The lack aggregation indicates they a high level of surface coverage, which would not leave space for the thiolated oligonucleotide barcodes to attach.

x) Place 1 mL of the remaining 30 nm particle at pH 9.2 in the EPA vial and add the amount of antibody as determined above. Vortex gently and incubate 30 minutes in foil.

xi) 15 minutes prior to the end of disulfide cleavage, begin flushing Nap-5 column with NANOpure water. At least three column volumes of NANOpure water must flush through before adding DNA.

xii) Add the 100 µLs of DNA to the column once all water has run through.

xiii) Once the 100 µLs flow into the column, add 400 µLs of NANOpure water to the column and allow it to flow through uncollected.

xiv) Then add 950 µLs NANOpure water to the column and collect the flow through 3-4 drops at a time in 1.5 mL microfuge tubes.

xv) Use a UV-spectrophotometer and the absorbance at 260 nm to determine the DNA location and concentration using Beers Law.

$$A=\varepsilon C l$$

ε= molar absorbtivity C= concentration l= cell path length

xvi) Add 4 nmoles of the freshly cleaved thiolated oligonucleotide to the gold nanoparticle-antibody complex. Rewrap in foil and incubate 4 minutes at 10°C.

xvii) Add *Phosphate Adjustment Buffer* to the nanoparticle solution to obtain a final phosphate concentration of 9mM.

Calculation: 1000µL AuNP + XµL DNA = Total Volume in µL

(Total Volume in µL)/10= YµL *Phosphate Adjustment Buffer* needed

xviii) Rewrap in foil and place on orbital shaker for 30 minutes.

xix) Calculate amount of *Salting Buffer* needed to obtain a final concentration of 0.15M NaCl

Calculation: (Total Vol # 2 * 0.3M)/(2M) = µLs *Salting Buffer* needed

# of Additions = 6 amount per addition = salt/6

xx) Over the course of 3 hours, make six additions of 1/6 of the total *Salting Buffer* needed to reach a final concentration of 0.15M NaCl. Do the additions while shaking gently alternatively, on a low vortex speed.

xxi) Incubate 1 hour.

xxii) Centrifuge the gold particles for 15 minutes at 10,000g at 4°C, remove supernatant. Resuspend in 1 mL of 10mM phosphate 150mM NaCl pH 7.4. Repeat step xxii 2 times.

xxiii) Centrifuge particles for 15 minutes at 10,000g 4°C, remove supernatant. Resuspend in 200 µLs of 10mM phosphate 150mM NaCl pH 7.4 and store at 4°C. Do not freeze.

OPTION C

A.4.8 Bio-Barcode Assay for Protein Detection:[13]

i) Determine the number of samples to be tested including one for the negative control(x). Add 20x µL 10 mg/mL MMPs to 1.5mL microfuge tube.

ii) Wash MMPs twice with the *Assay Buffer*. Redisperse the MMPs in twice their original volume of *Assay Buffer*.

iii) Mix in 1.5 mL microfuge tubes

a. 150 µLs *Assay Buffer*

b. 40 µLs MMP solution

c. 10 µLs target solution

iv) Vortex and incubate for 1.5 hours at 1,400 rpm at 25°C.

v) Place on magnet and remove supernatant, wash twice with 200 µLs *Assay Buffer*.

vi) Prepare tRNA solution 66 mg/mL in NANOpure water (store at 4°C) The tRNA is used to reduce non-specific binding between the antibodies on the gold and magnetic particles.

vii) Add 50 μLs 30 nm Au-NP solution prepared by mixing:

a. 215 μLs *Assay Buffer*

b. 25 μLs tRNA

c. 10 μLs 10nM Au-NP in *Assay Buffer*

viii) Incubate for 1 hour at 1,400 rpm at 25°C.

ix) Add 200 μLs of *Assay Buffer*.

x) Wash 7 times with 200 μLs of assay buffer. Wait 3 minutes between each wash while the magnet isolates the MMPS.

xi) Release barcodes in 50 μLs of DTT solution prepared in the *Assay Buffer*. ·Increasing the salt concentration in the assay buffer for the remainder of the assay may improve results depending on barcode sequences.

xii) Heat the tubes for 15 min at 50°C, and then incubate for 45 min at 25°C under vortex.

xiii) Chose appropriate signal readout method protocol…scanometric or fluorescence.

PAUSE POINT The bio-barcode assay can be stopped after the release of the barcodes by DTT. To stop here, extract MMPs from supernatant and freeze samples at -20°C.

OPTION D

A.4.9 Fluorescence Detection from DNA and Protein Detection

i) After barcode release, extract the magnetic particles down on the magnet for 3 minutes and transfer the supernatants to clean microfuge tubes.

ii) Spin the supernatants for 5 minutes at 13,000g to pellet the aggregated gold particles.

iii) Prepare serial dilution of known concentrations in barcode release buffer to generate a calibration curve.

iv) Remove supernatant from gold pellet and place in new microfuge tube.

v) Adjust the volume of released barcodes to 100 μLs using additional barcode release buffer.

vi) Either: Fill 96 well plate with 100 μL of each sample and standards skipping every other well, filling remaining empty wells with 100 μLs of nanopure water.

Or use cuvette to measure each sample individually.

vii) Measure fluorescence and perform data analysis.

A.5 Troubleshooting

Non-specific binding between gold nanoparticle and magnetic microparticle can be addressed by using varying amounts of formamide during the gold nanoparticle probe hybridization to the target. It is suggested to test a range of concentrations to see which amount of formamide effectively eliminates non-specific binding. Generally, between 5 and 20 percent formamide will solve the problem. The formamide should be stored at 4°C in aliquots to limit degradation. For RNA detection, be sure to purchase RNAse free formamide. Occasionally,

preparation of the antibody functionalized gold probes will fail due to antibody denaturation. Aliquot antibodies upon arrival, and avoid successive freeze/thaws.

Problem	Possible reason	Solution
High negative-control signal	Nonspecific binding between MMPs and Au-NPs	Try various concentrations of formamide during Au-NP hybridization and wash steps to increase stringency (5%–20%). Try increasing the temperature during hybridization steps to increase stringency further. Add 0.1% bovine serum albumin to the assay buffer in order to passivate magnetic microparticles.
		Gold probes are old; remake. Try additional washings after the Au-NP hybridization. Antibodies are denatured and are interacting nonspecifically; remake probe sets.
High negative-control signal	Poor oligonucleotide probe design	MMP sequence and Au-NP sequence could be interacting; check sequences. Then try including formamide to reduce hydrogen bonding if this could be a problem. If formamide does not solve the problem, redesign one of the probes, and be sure to check cross-complementarity.
No signal (expected)	Antibodies denatured	Remake antibody probes.
No signal (expected)	Stringency too high for DNA binding in assay	Lower the temperature at which the assay is run.
No signal (expected)	Old silver stain solution	Use new silver stain.
High slide background	Salt contamination	Wash slides longer in wash buffers before staining.
High slide background	Insufficient passivation	Increase passivation time in 0.2% SDS to 45 min.
Nanoparticles aggregate during salting	Salt additions are too large	Instead of 6 additions, try 10 or 15 over the same time course. Increase the time course if smaller additions do not work. Check that the oligonucleotide sequence does not contain a guanine residue at the end of the strand extending away from the nanoparticle surface. If it does, heat probes to 37 °C.
Nanoparticle aggregate during salting	Antibodies are not compatible with electrostatic attachment to Au-NP	In some cases, antibodies cause the nanoparticles to form an oily film. Attempt to remake the probe once. Also try switching MMP and Au-NP antibodies.
Synthesized Au-NPs appear purple or have wide absorption peak	Reaction not refluxing vigorously enough	Be sure that the reflux of the gold salt is steady and rapid before the addition of the citrate solution. Add citrate solution as quickly, in 15 s or less.
Scanometric intensity levels plateau at higher targets concentrations	Signal saturation	Try diluting the barcodes before adding them to the slides. This should not be a problem for fluorescence detection.

Table A.1 Troubleshooting Steps for the Bio-Barcode Assay

A.6.1 Comments

To perform the bio-barcode assay for RNA detection, it is important that all components be RNAse free. NANOpure water should be treated it with diethyl-pyrocarbonate (DEPC),

autoclaved twice and stirred at room temperature for 1-2 days. This water can then be substituted in all steps of the procedure. Use RNAse free plastic wear, reagents and remember to treat all glassware to remove RNAses.

The most critical steps in the bio-barcode assay are the washing steps. It is vital that none of the magnetic microparticles are accidentally removed. To prevent the loss of magnetic particles/sandwich complexes supernatant needs to be drawn off the particles slowly and carefully. Also during washing it is important not to vortex the microfuge tubes hard as you risk disturbing the hybridization. Additional critical steps are noted in the text with bullets.

A.6.3 Timeline

A.6.3.1 13 nm Gold nanoparticle synthesis

Time: Steps 1-6: 2 hours

Step 7: 3 hours

Steps 8-11: 20 minutes

Total time approximately 5.5 hours

A.6.3.2 Magnetic Particle Functionalization with DNA

Time: Steps 1-8: 45 minutes

Steps 9-12: 4 hours

Steps 13-21: 1.5 hours

Step 22: Overnight

Steps 23-26: 1 hour

Step 27: 1 hour

Steps 28-31: 45 minutes

Total time approximately 21 hours (including overnight = 12 hours)

A.6.3.3 Gold Nanoparticle Functionalization with DNA

Time: Steps 1-11: 3 hours

Step 12: Overnight (12 hours)

Steps 13-14: 10 minutes

Step 15: 30 minutes

Steps 16-18: 2 Days

Total time approximately three days (4 hours active time, remainder incubations)

A.6.3.4 Bio-Barcode assay for DNA detection

Time: Steps 1-3: 20 minutes

Steps 4-6: 45 minutes

Steps 7-8: 15 minutes

Step 9: 2 hours

Steps 10-12: 1.5 hours

Step 13: 1 hour

Total time approximately 5.5 hours

A.6.3.5 Scanometric Detection of the Barcodes from DNA and Protein Detection

Time: Steps 1-6: 1 hour 15 minutes

Step 7-8: 1 hour

Steps 9-12: 15 minutes

Step 13: 45 minutes

Steps 14-23: 45 minutes

Total time approximately 4 hours

OPTION A

Time: Steps 1-4: 30 minutes

Step 5: 24 hours

Steps 6-7: 10 minutes

Step 8: 4-24 hours

Steps 9-11: 30 minutes

Total time minimum approximately 29 hours with one 24-hour incubation, can be as long as 59 hours.

OPTION B

Time: Step 1: 2 hours

Steps 2-3: 2 hours

Steps 4-20: 2 hours

Step 21: 1 hour

Steps 22-23: 1.5 hours

Total time approximately 9 hours

OPTION C

Time: Steps 1-3: 20 minutes

Step 4: 1.5 hours

Steps 5-7: 15 minutes

Step 8: 1 hour

Steps 9-12: 1.5 hours

Total time approximately 4.5 hours

OPTION D

Total Time approximately 1 hour

VITA AND PUBLCATIONS

Haley D. Hill

Haley Diana Hill

EDUCATION

Ph.D.; Chemistry
Northwestern University, Evanston, IL, December 2008, GPA 3.91, Inorganic Division

Bachelor of Arts; Biochemistry
Occidental College, Los Angeles, CA, May 2004, GPA 3.71, Cum Laude, Distinction in Biochemistry

HONORS AND AWARDS

Department of Homeland Security Graduate Fellow 2005-2008
Northwestern University, Evanston, IL

Gelewitz Award, Outstanding 4th Year Chemistry Graduate Student 2008
Northwestern University, Evanston, IL

Delegate, Lindau Meeting of Nobel Laureates selected by the NSF 2007
Lindau, Germany

Washington State Rhodes Scholar Finalist 2003
Seattle, WA

Brantley Award, Outstanding Senior Chem/BioChem Student 2004
Occidental College, Los Angeles, CA

Trustee Scholarship 2000-2004
Occidental College, Los Angeles, CA

Beckman Research Fellowship 2003-2004
Occidental College, Los Angeles, CA

Howard Hughes Medical Institute Fellowship 2002
Occidental College, Los Angeles, CA

Nye Scholarship for Women in Science, 2002-2004
Occidental College, Los Angeles, CA

Occidental College Scholarship, 2002-2004
Occidental College, Los Angeles, CA

Dean's List 2002-2004
Occidental College, Los Angeles, CA

Scholar Athlete Award 2002-2004
Occidental College, Los Angeles, CA

Teaching Assistant of the Year Department of Chemistry 2003
Occidental College, Los Angeles, CA

RESEARCH

Homeland Security Graduate Fellow 2005-2008

- PI: Professor Chad A. Mirkin Ph.D.
- Department of Chemistry, Northwestern University, IL
- Developing ultra-sensitive sensors for biological pathogens using nanoscale materials, And investigating the fundamental properties of DNA functionalized nanoparticles.

Beckman Fellow 2003-2004

- PI: Professor Michael G. Hill Ph.D.

- Department of Chemistry, Occidental College, Los Angeles, CA
- Worked towards the selection of a catalytic RNA molecule through SELEX.
- Presented at Southern California Undergraduate Research Conference.
- Presented findings at Beckman Symposium.

Directed Research 2002-2003
- Department of Chemistry, Occidental College, Los Angeles, CA
- Researched DNA to protein mediated electron transfer.

Howard Hughes Medical Institute Fellow 2002
- Department of Chemistry, Occidental College, Los Angeles, CA
- Began DNA to protein electron transfer project.
- Presented preliminary findings at Summer Undergraduate Research Conference.

PATENTS

(1) Genomic DNA Bio-Barcode Assay, Submitted to US Patent Office 2007
(2) Homogeneous Detection of Gold Nanoparticle Probes, Submitted to US Patent Office 2007
(3) Single Chain Bio-Barcode Assay, (60/706,575) Submitted to US Patent Office 2005

GRADUATE PRESENTATIONS

Oral Presentation, Beckman Foundation Scholars Symposium 2008
Oral Presentation, American Chemical Society National Meeting 2008
Poster, Lawrence Livermore National Laboratory Poster Symposium 2006
Poster, Biosensors, Assays, and Informatics for Homeland Security Conference 2006

TEACHING EXPERIENCE

Science and Engineering Research and Teaching Synthesis Tutor 2005
- Department of Biology, Northwestern University, Evanston, IL
- Developed laboratory experiments about nanotechnology for non-science majors.

Organic Chemistry Laboratory Teaching Assistant 2004-2005
- Department of Chemistry, Northwestern University, Evanston, IL
- Graded laboratory notebooks and exams; supervised and assisted during experiments.

Molecular Biology Laboratory Teaching Assistant 2004
- Department of Chemistry, Occidental College, Los Angeles, CA
- Graded laboratory reports and exams; supervised and assisted during experiments.

General Chemistry Laboratory Teaching Assistant 2002-2003
- Department of Chemistry, Occidental College, Los Angeles, CA
- Graded laboratory notebooks; supervised and assisted during experiments; kept grades.

WORK EXPERIENCE

Telefund Caller 2001-2002
- Occidental College, Los Angeles, CA
- Spoke with Alumni to give college update and to solicit donations.

Doctor's Assistant, 2001
- Issaquah Vision Source, Issaquah, WA

- Preformed patient pre-testing; took retinal photographs; booked appointments.

Ski Instructor 1998-2000
- Powder Pigs Ski School, Snoqualmie Pass, WA
- Taught basic ski techniques to children aged 3 to 6.

LEADERSHIP EXPERIENCE

Vice President, Phi Lambda Epsilon 2007-2008
- Northwestern University, Evanston, IL

Leader, Mirkin Lab Biomaterials Subgroup 2006-2007
- Northwestern University, Evanston, IL
- Chaired weekly meetings to discuss research progress, group business, etc.

Social Chair, Phi Lambda Epsilon 2006-2007
- Northwestern University, Evanston, IL
- Plan and host monthly social gatherings for all members of the chemistry department.

Co-Captain, Varsity Swim Team 2004-2004
- Occidental College, Los Angeles, CA

Co-Founder, Off-Campus Student Coalition 2004-2004
- Occidental College, Los Angeles, CA
- Started group to improve relations between off-campus students and the neighborhood surrounding the college.

Commanding Officer, Issaquah Liberty Naval Junior Reserve Officer's Training Corps 1999-2000
- Issaquah High School, Issaquah, WA
- Created, organized, and executed all activities and outreach for 150 cadets.

PROFESSIONAL AFFILIATIONS AND ACTIVITIES

Chair, Member, Phi Lambda Epsilon, Northwestern University, Evanston, IL 2006-2008
Member, Sigma Xi, National Research Society 2007-2008
Member, American Chemical Society 2007-2008
Member, NSEC Board of Graduate Students & Post Doctoral Associates 2007-2008
Intern, Lawrence Livermore National Laboratory, Livermore, CA 05/06-08/06
Co-Captain, Member, Varsity Swim Team, Occidental College, Los Angeles, CA 09/00-05/04
Senator, Occidental College Student Senate, Occidental College, Los Angeles CA 05/03-05/04
Member, President's Advisory Council, Occidental College, Los Angeles, CA 10/03-05/04
Member, Alumni Ambassador Program, Occidental College, Los Angeles, CA 04/03-05/04
Member, Student Advisory Committee for Dean of Faculty Selection, 09/02
Occidental College, Los Angeles, CA

PUBLICATIONS

(1) Hill, H.D., Hurst, S.J., Mirkin, C.A., "Curvature-Induced Base Pair Slipping Effects in DNA-Nanoparticle Hybridization" *Nano Lett.* **(2008)** accepted.

(2) Hill, H.D., Millstone, J.M., Banholzer, M.J., Mirkin, C.A., "Radius of Curvature: The Key to Estimating the loading of ssDNA on Anisotropic Gold Nanostructues" **(2008)** Submitted *ACS Nano.*

(3) Millstone, J.E., **Hill, H.D.,** Mirkin, C.A., "Hysteresis in Oligonucleotide Gold Nanoparticle Hybridization and Melting," **(2008),** In Preparation.

(4) Hurst, S.J., **Hill, H.D.,** Mirkin, C.A., "The Origins of Hybridization in Apparently Non-Complementary Polyvalent DNA-Au NP Conjugates" *J. Am. Chem. Soc*. **(2008),** 130, *36*, 12192–12200.

(5) ***Hill, H.D., ***Macfarlane, R.J., Senesi, A.J., Lee, B., Park, S.Y., Mirkin, C.A., "Controlling the Lattice Parameters of Gold Nanoparticle FCC Crystals with Duplex DNA Linkers" *Nano Lett.* (**2008**) 8, *8*, 2341–2344.
* These authors contributed equally to this work.

(6) **Hill, H. D.**, Vega, R. A., Mirkin, C. A., "Non-Enzymatic Detection of Bacterial Genomic DNA using the Bio-Barcode Assay" *Anal. Chem.*, **(2007)**, *79*, **23**, 9218-9223.

(7) Seferos, D. S., Giljohann, D. G. **Hill, H. D.**, Prigodich, D. E., Mirkin, C. A., "Nano-Flares: Probes for Transfection and mRNA Detection in Living Cells" *J. Am. Chem. Soc.* **(2007),** *129*, **50**, 15477 -15479.

(8) Xu, X.Y., Georganopoulou, D. G., **Hill, H. D.,** Mirkin, C. A., "*In situ* Detection of Nucleic Acids Based Upon the Light Scattering Properties of Silver-coated Nanoparticle Probes" *Anal. Chem.* **(2007)** *79*, 17, 6650 –6654.

(9) Plomp, M., Leighton, T.J., Wheeler, K. E., **Hill, H. D**., Malkin, A. J., "*In vitro* High-Resolution Structural Dynamics of Single Germinating Bacterial Spores." *PNAS*, (**2007),** 104, **23**, 9644-9649.

(10) Ceres, D. M., Udit, A.K., **Hill, H.D.**, Hill, M.G., Barton, J.K., "The Differential Ionic Permeation of DNA-Modified Electrodes." *J. Phys. Chem. B,* **(2007),** 111, **3**, 663-668.

(11) **Hill, H.D**., Mirkin, C.A., "The Bio-Barcode Assay for the Detection of Protein and Nucleic Acid Targets Utilizing Dithiothreitol Induced Ligand Exchange." *Nat. Protocol,* **(2006),** *1,* **1,** p. 324-336.

(12) Chang, M. M. C., Cuda, G., Bunimovich, Y. L., Gaspari, M., Heath, J. R., **Hill, H. D**., Mirkin, C. A., Nijdam, A. J., Terracciano, R., Thundat, T., Ferrari, M., "Nanotechnologies for Biomolecular Detection and Medical Diagnostics." *Curr. Op. Chem. Bio.,* **(2006),** 10, **1**, p. 11-19.

(13) * Thaxton, C. S., * **Hill, H. D**., Georganopoulou, D. G., Stoeva, S. I., Mirkin, C.A., "A Bio-Bar-Code Assay Based upon Dithiothreitol Induced Oligonucleotide Release." *Anal. Chem.*, **(2005),** *77*, **24**, p. 8174-8178. * These authors contributed equally to this work.

ABOUT THE AUTHOR

Haley Diana Hill was born on November 29th, 1981 in Seattle Washington. Raised and educated in Issaquah Washington, she received her Bachelor of Arts in Biochemistry from Occidental College (Los Angeles, CA) in 2004. She continued her education at Northwestern University (Evanston, IL) performing her Ph.D. work with Dr. Chad Mirkin. While at Northwestern, Haley was selected as a Department of Homeland Security Graduate Fellow and was privileged to attend the 2007 Annual Meeting of Nobel Laureates and Students in Lindau, Germany. She is working as a Consultant for The Boston Consulting Group in Chicago Illinois.